UNIVERSITA' DEGLI STUDI DI SALERNO

Dipartimento di Chimica e Biologia "Adolfo Zambelli"/DCB
Corso di Dottorato di Ricerca in
"SCIENZE CHIMICHE, BIOLOGICHE E AMBIENTALI"-XXXIII Ciclo

Tesi di dottorato in

"Development of eco-sustainable methodologies for innovative materials inspired by cellulose fibers"

Tutor: Prof. **Brigida Bochicchio**

Tutor aziendale: Ing. **Angelo La Spina**

Co-Tutor: Prof. **Antonietta Pepe**

Co-Tutor: RE **Jany Dandurand**

Coordinatore: Prof. **Claudio Pellecchia**   Dottorando: **Nicola Ciarfaglia**

ANNO ACCADEMICO 2019-2020

Abstract

This PhD is an "Industrial-PhD", carried out in collaboration between University of Basilicata and LUCART S.p.A (Porcari, Lucca, Italy), in that case with the plant located at Avigliano (Potenza, Italy). The scholarship was financed by "Regione Basilicata" and the working time was shared between the company and the University.

The goal of the thesis was the development of eco-sustainable methodologies for the production of innovative materials based on cellulose fibers.

As a matter of fact, the aim of the work was to produce cross-linked electrospun hybrid scaffolds composed of gelatin/poly(D,L-lactic) acid (PDLLA), gelatin/PDLLA/cellulose nanocrystals (CNCs), and gelatin/PDLLA/cellulose nanocrystals/elastin as wound dressing materials. Fourier transform infrared spectroscopy, X-ray diffraction, and high-performance liquid chromatography demonstrated the complete embedding of each component in the hybrid scaffolds. The degree of cross-linking was quantified by the 2,4,6-trinitrobenzenesulfonic acid assay, and attenuated total reflectance spectroscopy revealed the effectiveness of the cross-linking reaction. Notably, the interconnected porous structure revealed in un-cross-linked scaffolds persisted even after cross-linking. Scaffolds were characterized in water through their contact angle showing total wettability. We investigated their mechanical properties by uniaxial tensile testing, which showed that even in the dry state, nanocellulose- and elastin-containing scaffolds exhibit higher elongation at rupture compared to those with pure gelatin/PDLLA. Therefore, we succeeded in tuning the toughness of the scaffolds by modulating the composition. In order to use scaffolds as medical devices, we assayed fibroblasts on scaffold extraction

media, indicating that they were noncytotoxic. Finally, the attachment and proliferation of fibroblasts on the surface of different scaffolds were evaluated.

During the six months spent at *Centre inter universitaire des matériaux* (CIRIMAT) of Université Paul Sabatier-Toulouse (France), electrospun scaffolds at different CNCs percentage (w/w) were produced and thermal stability, physical structure and their mechanical behavior were studied. The results suggested that the electrospun scaffolds are characterized by improved thermal and mechanical properties in comparison with bulk materials. We found that the scaffolds containing 3% (w/w) of CNCs showed best hydrophilic and thermo-mechanical properties.

The aim of the collaboration with Lucart SpA was the research of biopolymers and substances of natural origin suitable to be used in the airlaid process in the Avigliano Plant, as cross-linkers in blends or in substitution of the standard vinyl binder. A laboratory-scale binder distribution simulation method was developed. First research efforts were directed to block the development of formaldehyde during the binder crosslinking reaction by adding urea to the standard binder dispersion. A clear decrease in the production of formaldehyde upon the addition of urea was observed. Therefore, an industrial trial was carried out. Although the results were not confirmed in the industrial test. The second path was to collaborate with the Company in the Research and Development of alternative sustainable binders, trying to substitute, partially or totally, the vinyl binder with substances of natural origin, without compromising the final product properties. A laboratory test was performed on an innovative XBS Binder, formaldehyde free free, added with a polyamidoamine-epichlorohydrin based wet strength agent. The results were encouraging because the paper sample with only XBS Binder

showed an important absorbency decrease due to a higher hydrophobicity of the polymer. The study of different poly(vinyl alcohol) dispersions grades was carried out through many laboratory tests. However, they demonstrated that, due to high viscosity values, the stand-alone PVA use is not possible. Finally, a biodegradable and compostable engineered polysaccharide was tested with the aim of increasing the final product compostability. The industrial trial was performed confirming the reduction of wet tensile anticipated by laboratory test.

List of Figures

Figure 64: SEM images of A – B, tissue paper with the vinyl resin, C – D, tissue paper with 30% substitution of EP and E – F, tissue paper with 20% substitution of EP. **P.179**

List of Tables

List of abbreviations

1, 3, 5, 8NGP = 1, 3, 5, 8% (w/w) cellulose nanocrystals/gelatin/poly(lactic acid) scaffold;

1, 3, 5, 8NGPk = 1, 3, 5, 8% (w/w) cellulose nanocrystals/gelatin/poly(lactic acid) cross-linked scaffold;

AFM = Atomic force microscopy;

ANOVA = One-way analysis of variance;

ATR = Attenuated total reflectance spectroscopy;

B2B = Jumbo coils, tissue and airlaid. Papers intended for other paper industries;

BNC = Bacterial nanocellulose;

CD = Circular dichroism;

CNCs = Cellulose nanocrystals;

DMA = Dynamic Mechanical Analysis;

DMTA = Dynamic mechanical thermal analysis;

DSC = Differential Scanning Calorimetry;

DTG = Derivative ThermoGravimetric curves;

ECM = Extracellular matrix;

EDC•HCl = *N*-(3-dimethylaminopropyl)-*N'*-ethyl-carbodiimide hydrochloride;

El = Elastin;

El8NGP = EX15 elastin-like peptide/8% (w/w) cellulose nanocrystals/gelatin/poly(lactic acid) scaffold;

El8NGPk = EX15 elastin-like peptide/8% (w/w) cellulose nanocrystals/gelatin/poly(lactic acid) cross-linked scaffold;

ElNGP = EX15 elastin peptide/cellulose nanocrystals/gelatin/poly(lactic acid) scaffold;

EP = Engineered polysaccharide;

EVAc = Ethylene-vinyl acetate;

EX15 = exon 15 of human tropoelastin gene;

FE-SEM = Field emission scanning electron microscopy;

FTIR = Fourier Transform Infrared Spectroscopy;

GC-MS = Gas Chromatography – Mass Spectroscopy.

GE = Gelatin;

GP = gelatin/poly(lactic acid) scaffold;

GPk = gelatin/poly(lactic acid) cross-linked scaffold;

HFP = 1,1,1,3,3,3 Hexafluoro-2-Propanol;

HPLC = High performance liquid chromatography;

HTE = Human tropoelastin gene;

MFC = Microfibrillated cellulose;

MTS = 3-(4,5-dimethylthiazol-2-yl)-5-(3-carboxymethoxyphenyl)-2-(4-sulfophenyl)-2H-tetrazolium;

MTT = 3-(4,5-dimethylthiazol-2-yl)-2,5-diphenyltetrazolium bromide;

NaOH = Sodium hydroxide;

NCC = Nanocrystalline cellulose;

NGP = cellulose nanocrystals/gelatin/poly(lactic acid) scaffold;

NHS = *N*-hydroxysuccinimide;

NMA = *N*-(Hydroxymethyl)-acrylamide;

PAE = Polyamidoamine-epichlorohydrin binder;

PAN = Polyacrylonitrile;

PCL = poly(-ε-caprolactone);

PDLA = poly(D-lactic acid);

PDLLA = Poly(D,L-lactic) acid;

PEG = poly(ethylene glycol);

PLA = Poly(lactic acid);

PLLA = poly(L-lactide);

PMS = Phenazine methosulfate;

PPII = Poly-L-proline II conformation;

PVA = Poly(vinyl alcohol);

PVDF-HFP = Polyvinylidenefluoride-co-hexafluoropropylene;

SANS = Small angle neutron scattering;

SEM = Scanning Electron Microscopy;

TEM = Transmission electron microscopy;

T_g = Glass transition temperature;

TGA = Thermogravimetric analysis;

T_m = Melting temperature;

TNBS = 2,4,6-trinitrobenzenesulfonic acid;

UTS = Ultimate tensile strength;

VAE = Vinyl acetate-ethylene;

XBS Binder HCHO free = Aqueous dispersion of styrene-butadiene copolymer with 25 - 30% bio polymer content;

XRD = X-Ray diffraction.

List of amino acids

Amino acid	Three letters code	One letter code
Alanine	Ala	A
Arginine	Arg	R
Asparagine	Asn	N
Aspartic acid	Asp	D
Cysteine	Cys	C
Glutamine	Gln	Q
Glutamic acid	Glu	E
Glycine	Gly	G
Histidine	His	H
Isoleucine	Ile	I
Leucine	Leu	L
Lysine	Lys	K
Methionine	Met	M
Phenylalanine	Phe	F
Proline	Pro	P
Serine	Ser	S
Threonine	Thr	T
Tryptophan	Trp	W
Tyrosine	Tyr	Y
Valine	Val	V

Index

Chapter 1: General Introduction

Pollution and environmental sustainability are critical issues worth of attention all over the world in the context of global warming and climate change. In this scenario, scientific research demonstrated that planet poisoning is likely due to human activities. In that framework, politics call for research programs aimed to find alternative energy sources and renewable materials able to feed the circular economy. A new emerging field in that perspective is "Green Chemistry". It is defined as the "design of chemical products and processes to reduce or eliminate the use and generation of hazardous substances"[1,2] and its importance lies in its ability to use chemical research to meet environmental sustainability and economic development simultaneously.[3] These concepts were first formulated in the first half of the 1990s and quickly spread around the world. Green Chemistry is founded on Twelve Principles, that were proposed in 1998 by Paul Anastas and John Warner; these Principles are listed below:[4]

1. **Prevention**. It is better to prevent waste than treat or clean up waste after is formed;

2. **Atom economy**. Synthetic methods should be designed to maximize the incorporation of all materials used in the process into the final product;

3. **Less Hazardous Chemical Synthesis**. Wherever practicable, synthetic methodologies should be designed to use and generate substances that possess little or no toxicity to human health and the environment;

4. **Designing Safer Chemicals**. Chemical products should be designed to reduce toxicity;

5. **Safer Solvents and Auxiliaries**. The use of solvents should be made unnecessary wherever possible;

6. **Design for Energy Efficiency**. Energy requirements should be minimized. Synthetic methods should be conducted at low temperature and pressure;

7. **Use of Renewable Feedstocks**. A raw material or feedstock should be renewable;

8. **Reduce Derivatives**. Unnecessary derivatization (blocking group, protection/deprotection) should be avoided whenever possible;

9. **Catalysis**. Catalytic reagents (as selective as possible) are superior to stoichiometric reagents;

10. **Design for degradation**. Chemical products should be designed so that at the end of their function they do not persist in the environment and break down into degradation products;

11. **Real-Time Analysis for Pollution Prevention**. Analytical methodologies need to be further developed to control the formation of hazardous substances;

12. **Inherently Safer Chemistry for Accident Prevention**. Substances and the form of a substance used in a chemical process should be chosen in order to minimize the occurrence of chemical accidents, including releases, explosions, and fires.

These Twelve Principles are a guide for the design of new chemical processes and products, with particular attention to all aspects, from the raw materials used to the biodegradability or toxicity of reagents and products obtained. Moreover, efficiency and safety of the transformation play a key role in the vision of Green Chemistry. The first principle expresses the intention to protect the environment from pollution. The remaining ones concern atom economy, reduction of the toxicity of chemical syntheses and of chemical products, solvents, energy consumption, and use of renewable raw materials.

It is worth of note that, after few years, many fields of Chemistry decided to adopt Green Chemistry principles as their working philosophy. As matter of fact, nowadays these concepts are usually used, for example, in organic compounds synthesis,[5] design of nanomaterials,[6] catalysis,[7] analytical chemistry,[8] polymer production technology,[9] green dry cleaning of clothes,[10] even for understanding organic reactions mechanism on asteroids,[11] and at industrial scale. Biodegradability and compostability are properties required for materials of interest for Green Chemistry, in terms of reducing waste products and disposal.

A **biodegradable** material is capable of undergoing decomposition into carbon dioxide, methane, water, inorganic compounds, or biomass thanks to the action of biological agents such as bacteria, plants, animals and other physical components including the sun and water. The standard test known as ISO 14855 measures the biodegradability. According to this regulation, the test is passed if the material degrades by 90% in less than six months. A material can be defined as **compostable** if it is biologically degradable, producing carbon dioxide, methane, water, inorganic compounds and biomass in a controlled period of time and in compliance with certain conditions. The criteria to establish if a material is compostable in an industrial compostable plant are defined by the European legislation called UNI-EN 13432 and compostability is measured with EN 14045 test. For example, compostable plastic must disintegrate in less than three months and no longer be visible. Therefore, biodegradability is *conditio sine qua non* for compostability. Nowadays, researchers are joining their forces in order to find biodegradable and compostable polymers alternative to conventional plastics and packaging materials.[12,13] Analyzing their origin, **compostable polymers** can derive from petrochemical or renewable resources. Poly(vinyl alcohol),[14]poly(ε-

caprolactone),[15] polyesteramides, aliphatic polyesters and copolyesters are some examples together with poly(butylene succinate), poly(butylene succinate adipate) and aromatic copolyesters, such as poly(butylene adipate terephthalate).[16] **Biodegradable polymers,** deriving from renewable resources, include poly(lactic acid),[17] cellulose, proteins, polyhydroxyalkanoates,[18] thermoplastic starch[19] and chitosan.[20] The first three will be discussed in Chapter 2. Some of these polymers are also biocompatible[21]. They form three-dimensional matrices, called scaffolds, suitable in drug delivery and tissue engineering and able to mimic the complexity and three-dimensional size of the extracellular matrix (ECM)[22,23]. Furthermore, they act as physical support for anchoring cells that would regenerate new tissue after injury and damage. Hereafter, the scaffold would degrade to by-products in the form of metabolites, according to a property called **bioresorbability**.[24] Electrospinning is a relatively novel technology used to produce scaffolds made up of nonwoven tissue organized in nano- and micro-fibers. The present PhD work is inspired by the principles of green chemistry and by the concepts of biodegradability and biocompatibility. The goal is the development of eco-sustainable methodologies for the production of innovative materials based on cellulose fibers. The present PhD project is an "Industrial-PhD", an industrially focused research project and education carried out in collaboration between University of Basilicata and LUCART S.p.A (Porcari, Lucca, Italy). The collaboration was carried out in the plant located at Avigliano (Potenza, Italy) specialized in Airlaid production made with a special nonwoven technology which helps to form cellulose fibers into wet bonded webs. Thanks to its strength and very good absorption Airlaid is suitable for household use. The scholarship

1.1 Aim of the work

The main aim of this work was to design and produce electrospun scaffolds by using nature-inspired and biodegradable polymers. The working hypothesis was the modulation of the final scaffolds characteristics such as fibers dimension, wettability, elasticity and resistance to rupture through the choice of the polymers to be electrospun. The rationale was to combine biopolymers (proteins) and green polymers with complementary properties in terms of hydrophobicity, mechanical properties, and biocompatibility. Gelatin (GE) and poly(D,L-lactic) acid (PDLLA) were carefully chosen for their bioactivity and bioresorbability, respectively. Additionally, in order to counterbalance their strong hydrophobicity and to tune the resistance to rupture of the hybrid electrospun scaffolds, cellulose nanocrystals (CNCs) and an elastin inspired peptide, encoded by exon 15 (EX15) of human tropoelastin gene were added. To the best of our knowledge, herein for the first time GE and PDLLA were blended together and along with CNCs and the elastin-inspired peptide for electrospun scaffolds production. Therefore, hybrid scaffolds composed of gelatin/poly(-D,L-lactide), gelatin/poly(-D,L-lactide)/cellulose nanocrystals and gelatin/poly(-D,L-lactide)/ cellulose nanocrystals /elastin were prepared via electrospinning. Due to the presence of gelatin, water soluble component, a cross-linking reaction was carried out, using *N*-(3-dimethylaminopropyl)-*N'*-ethyl-carbodiimide hydrochloride (EDC•HCl) as cross-linker. The produced matrices were characterized by studying the embedding of each component in the hybrid scaffolds, the degree of cross-linking,

the effectiveness of cross-linking reaction, the morphology, hydrophilicity, Young's modulus, Ultimate Tensile Strength and elongation at rupture of the scaffolds. In order to use them as medical devices, mitochondrial activity of murine fibroblasts on scaffolds extraction media using MTS assay according to EN ISO 10993-5 and cell attachment and proliferation onto the surface of scaffolds were evaluated. Cellulose nanocrystals played a plasticizer effect on the scaffolds, therefore electrospun scaffolds at different CNCs percentage (w/w) were produced and analyzed in terms of thermal and mechanical properties at *Centre inter universitaire des matérieux* (CIRIMAT) CIRIMAT of Universitè Paul Sabatier-Toulouse (France), during the six months spent abroad.

During the time shared with the industrial partner, "green" cross-linkers to use in blends or in substitution of the standard vinyl binder used in the airlaid process at Lucart S.p.A in Avigliano Plant, were characterized. On that basis, the more promising blends were tested through industrial trials.

On summarizing, this work was carried out is in accordance with 1, 4, 5, 6, 7 and 12 Green principles of Green Chemistry. The thesis is organized in three parts. The first section (chapter 2) describes, the production and the characterization of electrospun matrices containing 8.0% (w/w) of CNCs (expressed on the total mass of the remaining components in polymer solutions).

The second part (Chapter 3) concerns the thermal and mechanical properties of electrospun scaffolds at 1, 3, 5, 8% (w/w) CNCs percentages.

The third part (Chapter 4) deals with the work carried out at LUCART S.p.A in Avigliano Plant.

Chapter 2: Production and characterization of electrospun scaffolds containing 8.0% (w/w) of CNCs

2.1.1 State of the Art

Electrospinning has been employed for the production of materials composed of nano- and micro-structured nonwoven tissues, with applications ranging from electrode production[25] and catalysis[26,27] to drug delivery, tissue engineering,[28–31] and biosensing.[32,33] Pore connectivity and the high ratio between the surface and the area of fibers mark electrospun polymers as high performing materials,[28] especially in drug delivery and tissue engineering applications as they mimic the complexity and three-dimensional size of the extracellular matrix (ECM) acting as a physical support for anchoring cells that would regenerate new tissues after injury and damage.[34–36]Afterwards, the scaffold would degrade to byproducts in the form of metabolites according to a property called bioresorbability.[37] Synthetic polyesters have been widely electrospun into fibrous scaffolds,[38] with poly(-ε-caprolactone) (PCL) and poly(glycolic acid) as well-known examples. Besides, poly(lactic acid) (PLA) is one of the most used polymers in biomedical applications because of its biocompatibility and biodegradability.[39,40] It degrades to lactic acid, its monomeric unit, a metabolite produced in mammalian muscles during glycogenolysis.[41] It can be commercially produced either from petrochemical feedstock or from bacterial sources affording a racemic and enantiomerically pure polymer.[42–49] However, the main disadvantages in the use of PLA are related to its slow degradation rate, hydrophobicity, and brittleness.[50] Enantiomeric pure forms of PLA[51,52] are semicrystalline polymers, whereas the

raceme poly(D,L-lactide) (PDLLA) has a lower crystalline degree and shows a faster degradation rate.

Notably, the degradation rate is a function of molecular weight and crystallinity degree: the higher the crystallinity, the higher the degradation times.[50] On this basis, PDLLA has been preferred to poly(L-lactide) (PLLA) for electrospun matrices in bone regeneration.[53] However, one of the main weaknesses in the use of PDLLA is its strong hydrophobicity.[54] In order to overcome these drawbacks, hydrophilic and natural polymers were added as complementary components to PDLLA. Gelatin (GE), for example, is highly biocompatible and biodegradable and has the ability to promote cell adhesion and accelerate the wound-healing process.[55] The use of GE fulfills a double issue: increasing the hydrophilicity of the scaffolds and inserting bioactive sequences. Besides GE, other proteins are blended with synthetic polymers. Human recombinant tropoelastin, for example, has been successfully electrospun with poly(ethylene glycol) (PEG).[56] Elastin (El) is a crosslinked polymer whose insolubility hampers the study of its molecular structure in solution. Short El peptides encoded by single exons of human tropoelastin gene (HTE) were easily investigated, revealing the structure–function relationship of the entire protein. One of the most appealing peptides was the sequence encoded by exon 15 (EX15) of HTE, which is considered bioactive (data not shown) and having GVGPQAAAAAAAKAAAKF as the primary structure.[57] To overcome the unfit performances of PLA-based scaffolds' mechanical trials and improve their biomedical applications, nanoparticle composites with metallic[58,59] and cellulose nanofillers have been developed.[60] Cellulose nanocrystals (CNCs) are gaining increasing interest as nanofillers in the perspective of employing renewable resources which are preferable to oil-based polymers in terms of

sustainability.[61] They are mainly produced by acid hydrolysis of cellulose, with dimensions dependent on the sources and hydrolysis conditions employed[62,63] and exhibit estimated Young's modulus and tensile strength of 138 GPa and 7500 MPa, respectively, in the crystalline region.[64] The use of CNCs allowed tuning the tensile strength, strain, Young's modulus, and toughness in PLA/CNCs/PEG composites[65] as well as they are reported for polyvinyl alcohol films in the presence of 1,2,3,4-butane tetracarboxylic acid as a crosslinking agent.[66] In the present work, we have combined for the first time El peptides, CNCs, GE, and PDLLA for the production of electrospun membranes obtaining noncytotoxic scaffolds with fiber diameters and mechanical properties appealing for the development of new wound-dressing materials. The problems common to conventional dressings are that they do not ensure a moist environment, and moreover, they adhere to desiccated wound surfaces causing trauma upon removal. Besides, severe wound dehydration would disturb the ideal moist healing environment and delay wound healing.[67] The aim of the present work was to obtain hydrophilic wound dressings by modulating the scaffold composition through the addition of biopolymers that are able to maintain a moist environment at the wound interface. PDLLA and GE alone are ineffective as dressing materials; therefore, both polymers were blended together and along with elastin (El) and CNCs serve as a suitable wound dressing material from mechanical and biological points of view.

2.1.2 Electrospinning technique

Electrospinning is a technique which allows to produce scaffolds composed of nonwoven tissue organized in nano- and micro-fibers using a strong voltage, in the order of thousands of Volts applied to the opposite ends of the system. The main advantage of electrospinning consists in the possibility of easily tuning fibers diameter and porosity, i.e. the ratio between the volume of voids called pores and the total volume of the material considered, together with the surface-to-volume ratio as well.[68] The first recorded observation of electrospraying was described by William Gilbert in the late 1500s, when, studying the behavior of magnetic and electrostatic phenomena, he noted an ejection of small droplets of water from the cone formed when a suitably charged piece of amber was brought near a droplet of water.[69] However, only in 1902 J. F. Cooley filed a United States patent entitled "Apparatus for electrically dispersing fluids"[70] in which there was the first description of a process recognizable as electrospinning. Studied in the following years, the technique was developed and used for commercial purposes by Anton Formhals in 1934, when he patented his first invention relating to the process and instrument for the production of artificial filaments by exploiting electrical charges.[71] In the following years many patents were issued, but was between 1964 and 1969 that Sir Geoffrey Ingram Taylor produced a series of works in whom the theoretical description of the electrospinning process was present.[72-74] He demonstrated that the shape of the fluid droplet produced at the tip of the needle following the application of an electric field was conic and the jets were ejected from the vertices of the cone. This characteristic cone shape now takes the name of Taylor cone.

The term "electrospinning" was instead used for the first time in 1995 by Doshi and Reneker, when they rediscovered this technique as a potential source of nanostructured materials.[75]

Electrospinning is usually conducted at atmospheric pressure and at room temperature. A typical experimental set up is made up of the following devices:

• A high voltage power supply;

• A syringe and needle assembling that in needles type it is collectively called spinneret;

• A pump, to dose the outgoing fluid;

• A grounded collecting plate, usually a metal plate, screen or rotating mandrel.

Some classifications of electrospinning equipment are based on the nature and number of axial units, such as mono-axial, co-axial and multi-axial electrospinning and on the number of nozzles, for example single nozzle and multi-nozzle electrospinning.[76]

A basic set-up for electrospinning, similar to the one used in this PhD work, is shown in Fig. 1.[77]
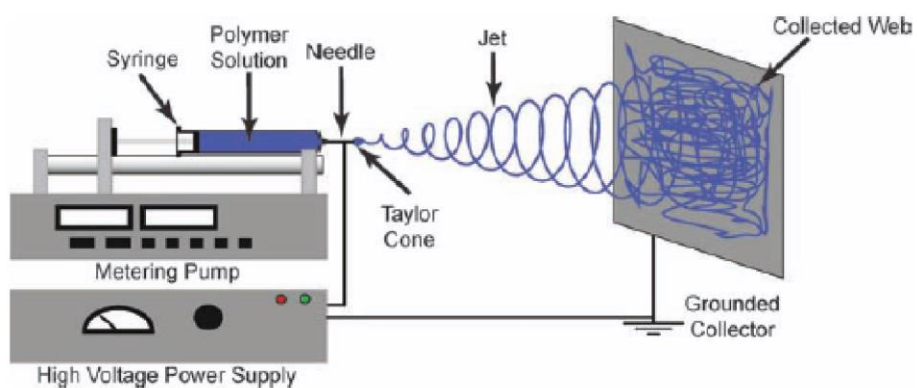
Figure 1: Typical electrospinning set-up showing high voltage power supply, syringe and needle assembling, pump and collecting plate.[77]

Essentially, a high voltage is applied to a polymer solution or melt in order to create an electrically charged jet. This jet undergoes stretching before it reaches the collector where, by the evaporation of the solvent, solidifies in the form of nano- or micro-fibers.[78,79] The polymer solution or melt is subjected to the electric field at the end of the capillary. On increasing the intensity of the electric field, and consequently of the superficial charge density (due to the repulsion of the electric charges) the hemispherical surface of the solution at the tip of the capillary elongates and forms a conical shape known as Taylor cone. When the electric field reaches a critical value, in which the force linked to electrical charges overcomes the force linked to the surface tension and viscosity of the solution neglecting the force of gravity and inertial forces, the ejection of a charged jet of polymer solution from the tip of the Taylor cone occurs. The jet travels in air and therefore there is evaporation of the solvent and the deposition of the charged polymer fiber on the collector.[80]

Generally, theoretical models indicate four different regions involved in electrospinning process (Fig. 2). They are the ***base region*** at the nozzle end where the charged surface of the solutions is present, the ***jet region*** where the polymer solution travels along a straight line, the ***splay region*** where the jets split into many fibers and the ***collector region*** where there is the deposition of the fibers.
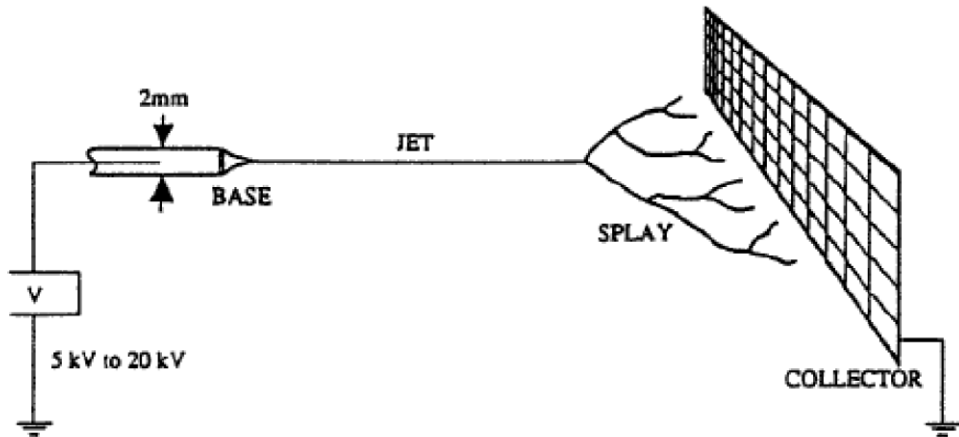
Figure 2: Image of the four different regions of the electrospinning process.[81]

Three main steps describe the behavior of the fluid. The first one is the formation of Taylor cone, the second one is the ejection of the straight jet while the third one is the unstable whipping jet region. The jetting mode takes the name of electrohydrodynamic cone-jet.[82] After the formation of the Taylor cone and the ejection of the solution from it, the ejected liquid travels straight path and then becomes unstable. As suggested by Yarin et al.,[83] due to the repulsive forces present in the fluid and originated from the charged species, the jet takes on a chaotic motion during its travel toward the collector. At first, it was thought that this instability was linked to the phenomenon called splaying,[75] i.e. the division of the jet into many smaller filaments that occurs due to electrostatic repulsion.[84] In reality the splaying, even if it happens, is not responsible for this phenomenon.

Shin and coworkers proposed the possibility of three different instabilities, linked to the fluid parameters and the operating conditions:[85]

1) *Rayleigh instability* or non-conductive axisymmetric or varicose instability;

2) *Axial symmetric conductive instability*;

13

3) **Whipping motion**, non-axisymmetric, also known as kink instability.

Rayleigh instability prevails at low flows and weak electric fields and depends mainly on the surface tension. The other two instabilities appear with the increase of the electric field and, therefore, of the surface charge. It was observed that the whipping mode instability prevails in presence of high charge density in the jets, while the axisymmetric instability is dominant at lower charge density.[85] **Whipping motion** depends on the formation of small curvatures in the jet (bending) which cause the formation of a dipolar moment perpendicular to the jet itself. The jet thus assumes a spiral motion with an overall path cone-shaped. The torsion thus imparted, together with the acceleration of the electric field and the electrostatic repulsion, are responsible for stretching the fiber. The last step of the path of the jet is the impact of the fibers on the collector, with consequent closure of the electrical circuit.

2.1.3 Parameters affecting the electrospinning process

There are many parameters that influence the electrospinning process, and they can be classified into **solution parameters, process parameters, and ambient parameters**.[68] All these variables can have a major impact on fibers morphology of the obtained scaffolds and by changing these parameters it is possible to modify the morphology and the diameter of the fibers.

The **solution parameters** are:

✔*Polymer solution concentration*;

✔*Polymer Molecular Weight* ;

✔*Viscosity*;

✔*Conductivity*;

✔*Surface tension*.

2.1.3.1 Polymer solution concentration

In order to form fibers through electrospinning process, a minimum solution concentration is necessary. When the solution concentration is low a mixture of beads and fibers is obtained. The increase of the solution concentration triggers the change in the shape of the fibers from spherical to spindle-like, the higher viscosity resistance producing fibers having larger diameters.[86] However, the relationship between the solution concentration and the fiber diameter is usually non-linear because also between the polymer solution concentration and the solution viscosity there is a non-linear relationship, with a considerable increase of viscosity after a specific value of the concentration is reached.[87] Therefore, the concentration of the polymer solution must be neither too low, because defects would form, nor too high, because large diameter fibers would be formed due to the inability to maintain stable the flow of the solution on the needle tip.

2.1.3.2 Molecular weight of polymer

Rheological and electrical properties such as viscosity, surface tension, conductivity and dielectric strength are significantly influenced by the molecular weight of the polymer and this parameter affects the morphology of electrospun fibers. Generally, high molecular weight polymers are preferred in order to obtain an acceptable viscosity value. Low molecular weight polymers prompts the formation of beads instead of fibers while high molecular weight polymers stimulates the formation of fibers with larger average diameters. Given the

importance of the concentration of polymer solution, it is crucial to choose polymers having proper molecular weight.

2.1.3.3 Viscosity

Viscosity will be treated in Chapter 4. The role of solution viscosity in determining properties of the fibers such as size and morphology is fundamental. Viscosity is strongly related to the molecular weight and to the polymer solution concentration and therefore changing it, it is possible to vary also the viscosity.[88] Furthermore, viscosity depends also on the temperature of the working environment, on the electrospinning process, and on the presence of impurities in the solution. Optimal viscosity is necessary in order to start electrospinning process.[68] If the solution has low viscosities, surface tension prevails and just beads or beaded fibers are formed, because the chain entanglements present in the polymer are too limited to favor the spinning process leading to the formation of drops.

Above a critical concentration, it is possible to obtain a continuous fibrous structure, while at higher concentrations the drop of solution dries before the jet begins to drag the fibers accelerated by the electric field towards the collector. Moreover, the magnitude of the viscoelastic forces that oppose the splaying of the jet and which are closely related to the structure (linear, branched or cross-linked) of the polymer and to its molecular weight depends on viscosity value. A longer stress relaxation times is usually present at very high viscosity and this property could block the splaying of the jet, leading to a higher fiber diameter.

2.1.3.4 Conductivity

Conductivity is the ability of a solution, a metal or a gas to conduct an electric current. In solutions the current is carried by charged species, mainly cations and anions, whereas in metals it is carried by electrons. Solution conductivity depends mainly on the polymer type, solvent used, the availability of ionisable salts and temperature. Conductivity is the ratio between the current density and the electrical field strength or the inverse of resistivity and it is measured in Siemens per centimeter (Scm^{-1}).

Regarding electrospun matrices, with the increase of the electrical conductivity of the solution, a significant decrease in the diameter of the electrospun nanofibers was observed whereas with low conductivity of the solution it is possible to obtain beads, because the elongation of a jet by electrical force results insufficient to produce uniform fibers. It is possible to obtain fibers devoid of beads and with small diameter by adding ionic salts such as KH_2PO_4, NaH_2PO_4, and $NaCl$, as shown by Zong et al.[89]

2.1.3.5 Surface tension

Surface tension is defined as the force exerted in the plane of the surface per unit length,[90] and it is a function of the solvent. It is important that the applied voltage is high enough in order to overcome the surface tension of the polymer solution and to produce scaffolds.[77] Generally, the electrospinning process is inhibited by a high surface tension of the solution because jets becomes instable and sprayed droplets can be generated. Their formation is influenced by the surface tension of solution and a lower surface tension of the spinning solution leads to a better electrospinning process at a lower electric field.[86]

The process parameters that influence electrospinning process are the following:

• **_Applied voltage_**;

• **_Flow rate_**;

• **_Type of collector_**;

• **_Tip to collector distance_**.

2.1.3.6 Applied voltage

The applied voltage to the polymeric solution plays a key role in the electrospinning process, because it is possible to obtain the formation of the fibers only if a threshold value of the voltage is reached. Nowadays several research groups have demonstrated that fiber diameter is influenced by the applied voltage.[91,92] It is worth of note that there are different theories about the behavior of the voltage on fiber diameter. Some scientists found a bigger polymer ejection with higher voltages, with consequent formation of a higher diameter of fibers, but other groups demonstrated that the electrostatic repulsive force on the jet increases with an increase in the applied voltage, leading to a smaller fiber diameter. Anyway, the applied voltage has not a great influence on the diameter of the fibers, if compared to the other process parameters.

2.1.3.7 Flow rate

The flow rate of the polymer influences the jet velocity and the material transfer rate. Analogously to other parameters, a minimum value of the flow rate is required in order to be able to electrospun the polymer solution. In order to

consent solvent evaporation, it is better to work with a lower flow rate. As a matter of fact, with higher flow rate the solvent does not have enough time for drying with consequent formation of beads in the fibers.

2.1.3.8 Type of collector

The type of collector used is important, because in electrospinning process it serves as a conductive substrate collecting fibers. Usually, the most used is an aluminium foil but other typologies of collector are common. The collector, in addition to being on a static plane (horizontal or vertical)[93] can have different configurations. In the case of static and planar collectors, the resulting membrane presents a random orientation of the fibers.[94] With rotating collectors (disc or cylinder), uniaxially aligned fibers can be obtained. The speed of fiber deposition is influenced by the rotating speed of the disc and the cylinder. Actually, with slow rotating rates, the alignment of the fibers is reduced while if the speed is too high, they can break into small fragments.[95] A coaxial collector, on the other hand, is useful for producing core-shell fibers. Thanks to this technique, the thickness of the shell and the mechanical strength can be controlled.[96]

2.1.3.9 Tip to collector distance

An additional parameter that influences fiber diameter and scaffold morphology is the distance between the tip and the collector, even if not as much as other process parameters. Fibers formation needs of enough time to let solvent evaporation before reaching the collector. Therefore some studies found that a

minimum tip to collector distance is necessary. Otherwise, the formation of beads could occur if the distance is too small or too big.[97,98]

Additional parameters affecting the electrospinning process are the following:

• *Humidity*;

• *Temperature*;

• *Solvent*.

2.1.3.10 Humidity

Humidity is the concentration of water vapor present in the air. It affects each solution differently, depending on the solvent used and on the hydrophilicity of the polymer solution. As humidity being a measure of the vapor pressure of the solvent in the atmosphere, aqueous solutions are obviously the most affected and it can be expected that the water in solution and in the atmosphere interact between each other. Humidity influences the volatility and therefore the evaporation rate of the solvent affecting the porosity and the final size of the pores present in electrospun material. It has been demonstrated that low humidity favors solvent evaporation, however it becomes higher than the extrusion speed from the needle tip, making the electrospinning process impossible for the potential obstruction of the needle. On the other hand, at high values of humidity small circular pores on the surface of the fibers could be present, while a further increase can produce pore coalescence.[99] Finally, humidity affects the charge and surface tension by promoting the discharge of the fiber extruded.

2.1.3.11 Temperature

Another parameter that has an effect on fibers characteristics is the temperature.[100] Wang and coworkers studied the effects of heating from 25 to 100°C a polyacrylonitrile (PAN) solution. They observed viscosity and surface tension reduction with concomitant conductivity increase. The final result was the production of smaller fiber diameters.[101] At high temperature the increase of kinetic energy of the polymer molecules provokes the reduction of the voltage required for the electrospinning process.[102] The increase in temperature, with the consequent faster evaporation of the solvent, can also lead to fibers flattening. Collector temperature influences fibers morphology too.[77] Kim et al demonstrated that the size and the number of the pores present on the electrospun fibers was slightly related to the temperature of the collector.[103]

2.1.3.12 Solvent

In order to produce a polymeric blend with good properties capable of being electrospun, the optimal dissolution of the polymers is required with accurate selection of the solvent. Volatility, vapor pressure, and boiling point are some of the properties to take into account before choosing the solvent for electrospinning (Table 1).

Table 1: Properties of the most common solvents used in electrospinning.[68]

Solvent	Surface tension (mN/m)	Dielectric Constant	Boiling point (°C)	Density (g/ml)
Chloroform	26.5	4.8	61.6	1.498
Dimethyl formamide	37.1	38.3	153.0	0.994

Hexafluoro isopropanol	16.1	16.7	58.2	1.596
Tetrahydrofuran	26.4	7.5	66.0	0.886
Trifluoro ethanol	21.1	27.0	78.0	1.393
Acetone	25.2	21.0	56.1	0.786
Water	72.8	80.0	100.0	1.000
Methanol	22.3	33.0	64.5	0.791
Acetic acid	26.9	6.2	118.1	1.049
Formic acid	37.0	58.0	100.0	1.21
Dichloro methane	27.2	9.1	40.0	1.326
Ethanol	21.9	24.0	78.3	0.789
Tri fluoro acetic acid	13.5	8.4	72.4	1.525

Solvent vapor pressure is important in determining the evaporation rate and the drying time and in the formation of nanostructures, because it influences the phase separation process. Solvents affect also properties such as surface tension, influencing the morphology and the size of the fibers. Substantially, the solvent plays two fundamental roles in electrospinning: at first, to dissolve the polymer for forming the blend to electrospun and secondly to carry the jet towards the collector.[104]

In this PhD work the solvent chosen for electrospun matrices production was 1,1,1,3,3,3 Hexafluoro-2-Propanol (HFP).

2.1.4 Applications of electrospinning

Electrospinning gives the possibility to produces matrices with tunable fibers diameter and porosity and with high surface-to-volume ratio. These characteristics make it suitable for many applications in many fields.[77] Some of these applications can be found in the field of biomedicine, chemistry, defense and environmental protection (Fig. 3).
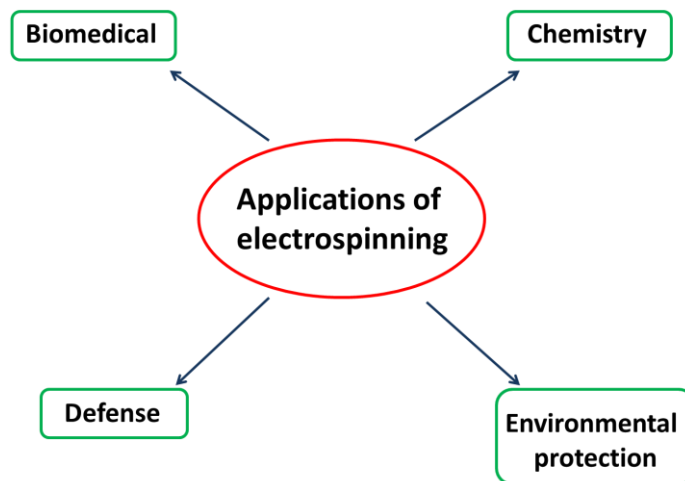
Figure 3: Scheme of the main applications of electrospinning.

2.1.5 Electrospun polymer materials

2.1.5.1 Poly(lactic) acid

Poly(lactic) acid, (PLA) also named polylactide, is an aliphatic polyester derived from lactic acid (2-hydroxy propionic acid) and it is widely used thanks to its properties of biocompatibility, recyclability and compostability. In Fig. 4 chemical formula of PLA is shown.
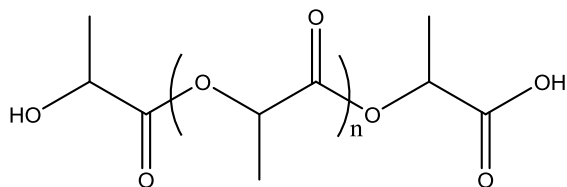
Figure 4: chemical formula od PLA.

Lactic acid is present in the form of two stereo-isomers, L-lactic acid and D-lactic acid. The corresponding polymers can be enantiomerically pure as poly(L-lactic acid) (PLLA) and poly(D-lactic acid) (PDLA) or racemic as poly(D,L-lactic acid) (PDLLA). It is possible to modify the stereochemical structure by polymerizing a controlled mixture of L and D isomers in order to obtain high molecular weight polymers with amorphous (PDLLA) or semi-crystalline (PLA) characteristics. In Table 2 some physical properties of poly(lactic) polymers are shown.

Table 2: Physical properties of different Poly(lactic) acids.[105]

Lactic acid polymer	Glass Transition Temperature T_g (°C)	Melting Temperature T_m (°C)	Density (g/cm³)
PLLA	55 – 80	173 – 178	1.290
PDLLA	43 – 53	120 – 170	1.250
PDLA	40 – 50	120 – 150	1.248

2.1.5.1.2 Properties of poly(lactic) acid

Polylactide is clear, colorless, it is similar in many aspects to polystyrene and it can be processed like most thermoplastic polymers into fibers and films. Analogously to other polymers, the molecular characteristics influence the structural properties of poly(lactic) acid such as crystallinity. Lactic acid presents a stereocenter. Therefore, it exists as L, D, and DL isomer able to polymerize in PLLA, PDLA and PDLLA polymers. The stereochemical composition strongly affects its molecular structure affecting physical and mechanical properties, and degradation rates. It was demonstrated that poly(lactic) acids containing more than 93% of L-lactic acid are semi-crystalline. If the percentage of L-isomer is in between 50-93%, the polymer presents an amorphous structure.[106-108] As a consequence, PDLA[109] and PLLA[110] are semicrystalline polymers while PDLLA is amorphous. Indeed, meso- and D-lactide induce twists in the regular poly(L-lactide) molecular architecture, resulting in a decrease of cristallinity.[111] The preparation conditions affect the crystalline structure of PLLA. It is possible to obtain three different forms of this polymer: α, β and γ. The α-form exhibits a well-defined diffraction pattern,[112] and a melting temperature (T_m) of 185 °C. The β-form can be obtained at a high draw ratio and a high drawing temperature and presents melting temperature of 175 °C and therefore it is less stable than the α-form. The γ-form of PLLA derives from epitaxial crystallization.

In Table 2, the physical properties of different PLA are shown. Due to the changes in polymer chain mobility, glass transition temperature (T_g) is one the most important factors for amorphous PLA, while for the semicrystalline form, both T_g and T_m are important physical parameters for predicting its behavior.[112]

Additionally, the molar mass, thermal history and purity of the polymer affect characteristics such as melting temperature and degree of crystallinity.

PLA presents a typical T_g between 50°C and 80°C, while T_m ranges from 130°C to 180°C. For example, semi-crystalline PLA presents a T_g of 55°C and a T_m of 180°C. For this kind of PLA, the melting temperature is connected to the different processing parameters and to the initial PLA structure. It was demonstrated that a blend containing PLLA and PDLA in equal ratio leads to the formation of a stereocomplex (racemic crystallite) of both polymers. This stereocomplex presents higher melting temperature and improved mechanical properties in comparison to both PLAs.

The most used solvent for PLA is chloroform. Other solvents are chlorinated or fluorinated organic compounds: dioxolane, dioxane and furan. Poly(rac-lactide) and poly(meso-lactide) are soluble in many other organic solvents as acetone, pyridine, tetrahydrofuran, ethyl lactate, xylene, dimethylformamide, ethyl acetate, methyl ethyl ketone. Furthermore, we also count alcohols (*e.g.* methanol, and ethanol) and alkanes (*e.g.* hexane and heptane). Regarding to PLA degradation, it occurs by hydrolysis after several months of exposure to moisture. Thereafter, two stages take place. The first one is a random, non-enzymatic ester hydrolysis with resulting reduction in molecular weight. In the second one, microorganisms metabolize lactic acid and low molecular weight oligomers, producing carbon dioxide and water. Raceme PDLLA shows a faster degradation rate than PLLA.

2.1.5.2 Cellulose nanocrystals

2.1.5.2.1 Cellulose

Cellulose is the most abundant polymer in the world, it is found mainly in plants, in several marine animals and less in invertebrates, fungi, bacteria and algae. Cellulose is a linear syndiotactic homopolymer consisting of D-anhydroglucopyranose units, covalently linked through *O*-glucopyranosyl-(1→4) bonds. Each monomeric unit is corkscrewed 180° with respect to its neighbors. The atoms involved in these bonds are C-1 and C-4 of adjacent glucose units, leading to the formation of a cellobiose unit, a dimer of the glucose. The hydroxyl groups occupy the equatorial position in the ring while the hydrogen atoms are axial.[62] The reactivity of the cellulose polymer is determined by the three free hydroxyl groups of the anhydroglucopyranose units, situated on C-2, C-3 and C-6. The terminal hydroxyl groups present at the ends of the cellulose chains, on C-1 and C-4, are not chemically equivalent. The properties of cellulose, as the high hydrophilicity and the high surface energy, the biodegradability and its chemical reactivity associated with the three OH groups present on C-2, C-3 and C-6 of each anhydroglucopyranose units are a consequence of this structure. Furthermore, the presence of intra- and inter-molecular hydrogen bonded OH groups gives to cellulose a higher tendency to crystallize in a regular network.[113,114] Cellulose exists in six different polymorphs named cellulose I, II, III, and IV. Cellulose I occurs in two allomorphs, I_α and I_β.[115] Cellulose fibers are constituted of microfibrils deriving from the assembly of elemental fibrils, the protofibrils (Fig. 5). Inside the cellulose fibrils amorphous regions and crystalline regions are present. Cellulose nanocrystals (CNCs) derives from crystalline region.
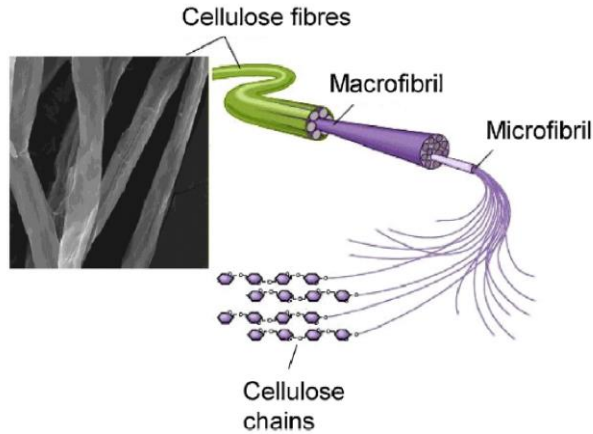
Figure 5: Structure of cellulose fibers.[114]

2.1.5.2.2 Cellulose nanocrystals production

The term ***nanocellulose*** indicates cellulosic material with one dimension in the nanometer range. These materials can be divided in three main subcategories, depending on the dimensions, methods of production and function[116]. They are cellulose nanocrystals (CNCs) (also named nanocrystalline cellulose, NCC), microfibrillated cellulose (MFC) and bacterial nanocellulose (BNC), synthesized from glucose by a family of bacteria, named *Gluconoacetobacter xylinius*. CNCs are formed by rigid rod-like particles with widths ranging between 5 and 100 nm and lengths of several micrometres. They are 100% cellulose made up and present highly crystallinity, between 54 and 88% and derive from a variety of cellulosic sources, such as plants, animals (tunicates), bacteria, algae and from MCC. Obviously, wood is the main source for CNCs production due to its abundance and high presence of cellulose. On the other hand, cellulose nanocrystals derived from

tunicate present high crystallinity, however the cost of gathering is high. In order to produce CNCs from cellulose source materials, two passages are needed.

The first passage is a pre-treatment of the source material which leads to the isolation of the cellulosic fibers and to the elimination of other materials present in wood and plants such as hemicelluloses and lignin. The second step is the removal of the amorphous regions of the fibers and it takes place through a controlled chemical treatment, generally hydrolysis. Hydrolysis usually induces the formation of rod-like cellulose nanocrystals. The most used acids for CNCs production are sulfuric and hydrochloric acid. In the last case, nanocrystals present a limited ability to disperse and their aqueous suspensions tend to flocculate. Conversely, sulfuric acid promotes a better dispersion of CNCs in water through the reaction with the surface hydroxyl groups of cellulose giving rise to charged surface sulfate esters. The presence of charged sulfate groups can get worse the thermostability of the nanocrystals acting as flame retardant.[117]A method to increase thermal stability of CNCs consists in neutralizing sulfate groups by using NaOH solution, as suggested by Wang et coworkers.[118]A way to introduce, in a controlled way, sulfate moieties on CNCs, is a pre-treatment with hydrochloric acid followed by the use of sulfuric acid while a mix of these two acids during hydrolysis steps under ultrasonic treatment can produce spherical nanocrystals.[119]

2.1.5.2.3 Properties of cellulose nanocrystals

Geometrical (length, diameter and thickness) and morphological properties of CNCs depend on the cellulosic source and on the methodology used for its

extraction. Generally, morphology and geometry of the nanocrystals are observed by using microscopy techniques, such as field emission scanning electron microscopy (FE-SEM), transmission electron microscopy (TEM), atomic force microscopy (AFM) and light scattering techniques, for example small angle neutron scattering (SANS). It was observed that CNCs with rod-like morphology derived from wood, cotton, ramie, flax, sisal, present length ranging from 100 nm to 700 nm, and diameter from 5 nm to 30 nm, while bacterial cellulose shows length ranging from 100 nm to several mm, and diameter about 5 nm to 50 nm.[120] The presence of crystalline regions in cellulose is due to the formation of hydrogen bonds between hydroxyl groups and oxygen atoms of the polysaccharide and of Van Der Waals bonds. CNCs derives from these crystalline regions and therefore it should present a degree of cristallinity of 100%; however this does not happen. The reason is that the removal of the amorphous regions is not complete, resulting in lower degrees of cristallinity ranging from 54 to 88%. Regarding the elastic modulus of cellulose nanocrystals, it depends on the source and on the technique used for the measure and it can reach a value of 250 ± 50 GPa. By using thermogravimetric analysis (TGA) it is possible to measure the degradation temperature of CNCs, usually in between 200 and 300 °C. Due to the presence of the three hydroxyl groups for each glucose unit, chemists have carried out chemical modifications on CNCs surface, in order to bind hydrophilic CNCs with hydrophobic matrices. These strategies consist of esterification, silylation, etherification, polymer grafting, polymer coating and the use of adsorbing surfactant.[121]

2.1.5.3 Gelatin

Gelatin is composed of proteins for 85-92%, the remaining part being mineral salts and water. It derives mostly from pig skin and in minor percentages from bovine hides, pig and cattle bones, and fish. It is produced by partial hydrolysis of collagen. Collagen is a protein present in the skin, tendons, bones, membranes and connective tissue. Until now, twenty-eight types of collagen have been detected with high specificity as function of tissues. Skin, for example, is composed mostly by type I and to a lesser extent by type III collagen. It is structured in a triple-helix conformation composed of three different chains called α-chain. Every α-chain consists of the (Gly-X-Y) repeated motif with proline and hydroxyproline as guest residues. The latter amino acid depends on the type of collagen.[122] In Fig. 6 the structure of the collagen is shown.
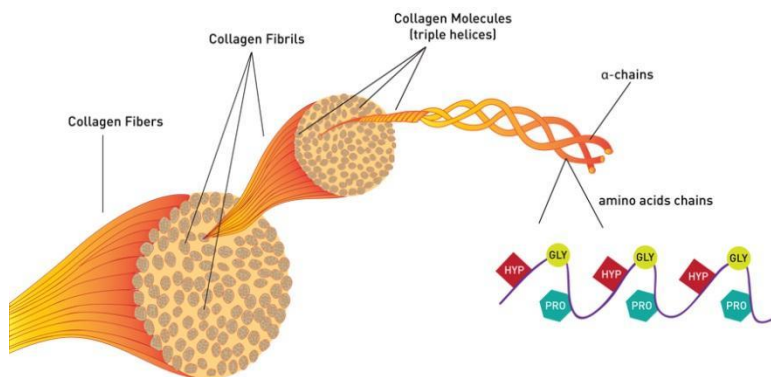
Figure 6: structure of the collagen.[123]

The α-chain adopts a left-handed helix type conformation called poly-L-proline II conformation (PPII) strongly favored by the presence of proline and hydroxyproline residues. The triple helix is right-handed and formed by the union

of three chains. It is stabilized by intra and inter-chain hydrogen bonds with glycine residues oriented in the center and the side chains of the X and Y residues exposed to the solvent. Gelatin production process consists of two steps. At first, collagen denaturation occurs followed by cooling with consequent entrapment of water molecules in the chain and formation of a hydrogel. During gel formation, helix structures of collagen are partially reformed. Amino acidic composition plays a key role in gelatin chemistry, in particular in the formation of hydrogen bonds and in the reactivity of the side chain groups, such as $-NH_2$ and -COOH. Hydrogen bonds are important because they stabilize the collagen structure and are involved in the gel-forming process. This gel is a network of polypeptide chains with junction zones. During the gelatin production, in the gelation process, there is a partial reformation of collagen triple helix structure, with inter-chain hydrogen bonds, similar to those found in native collagen, that stabilize the junction zones.

The content of lysine usually increases gelatin reactivity, because the ε-amino group can react as a traditional amine, while the amino groups from histidine residues, also present in collagen with arginine, usually play a less important role than lysine. The highly basic guanidinium group of arginine is active only under some conditions, because at neutral pH it is protonated. ε-amino group from lysine residues are involved in hydrogen bonds and in nucleophilic substitutions, in particular, cross-linking reactions. The other reactive group of gelatin is the carboxylic function of aspartic and glutamic acid. This functional group is involved, for example, in the process named chromium tanning used in leather industry. Other reactions involving COOH groups are cross-linking reactions with carbodiimide.[124]

2.1.5.3.2 Properties of gelatin

Gelatin is an amphoteric protein, due to the presence of the amino and of carboxylic groups. Physical properties of gelatin are gel strength or ***Bloom strength***, solubility, viscosity, melting point and setting point. The gel strength is a function of the molecular weight, concentration, pH, thermal history and ionic content of the protein. Finally, the presence of α- and β-chain in the gelatin influences this property. The Bloom strength is important to understand the behavior of the gel and for this reason it is a primary property in the food industry. The gel Bloom is defined as "the weight required to push a cylindrical plunger, of 13 mm diameter, 4 mm into a previously prepared gel of 6⅔% (w/w) concentration matured at 10 °C for 16-18 h".[125] For commercial products, gelatin is usually divided in three categories:

- *Low Bloom gelatin*, with a Bloom less than 125;

- *Medium Bloom gelatin*, Bloom between 150 and 200;

- *High Bloom gelatin*, with a Bloom above 220.

Gelatin is very soluble in cold water and it is non-soluble in ethanol and apolar solvents, such as mannitol and glycerine. Parameters as molecular weight, temperature and concentration affect the viscosity of gelatin solutions usually showing low viscosity and a Newtonian fluid behavior above 40 °C.

2.1.5.4 Elastin

Elastin is a protein of connective tissue whose primary function is to confer elasticity to organs and tissues. It is found in all tissues that need to extend and then return to their original state in order to exert their physiological functions. It is most abundant in skin where also plays a key role in cutaneous homeostasis, lungs, bladder, intestines, and arteries.[126] Concerning the amino acidic composition, elastin is rich in hydrophobic residues as glycine (Gly), proline (Pro), alanine (Ala), leucine (Leu) and valine (Val) present in about 75%. It is rich of repeated motifs, organized in flexible and highly dynamic chains.[127] Human elastin is a cross-linked, water-insoluble protein and it is synthesized by a variety of cells such as fibroblasts, smooth muscle cells, endothelial cells, and chondrocytes, starting from a water-soluble precursor, called tropoelastin, which has molecular weight of about 72 kDa, 760 amino acids encoded by 35 exons. Elastin insolubility is due to the presence of inter-chain cross-links and it is encoded by a single gene located on human chromosome 7, which produced tropoelastin.[128] In Fig. 7 human tropoelastin sequence is shown.

```
        -EX1                              -EX2            -EX3        -EX4
  1 MAGLTAAAPRPGVLLLLLSILHPSRPGGVPGAIPGGVPGGVFYPGAGLGALGGGALGPGG
           -EX5          -EX6                            -EX7
 61 KPLKPVPPGGLAGAGLGAGLGAFPAVTFPGALVPGGVADAAAAYKAAKAGAGLGGVPGVGG
        -EX8                 -EX9              -EX10
121 LGVSAGAVVPQPGAGVKPGKVPGVGLPGVYPGGVRPGARFPGVGVLPGVPTGAGVKPKAP
    -EX11      -EX12                      -EX13        -EX14
181 GVGGAFAGIPGVGPFGGPQPGVPLGYPICAPKLPGGYGLPYTTGKLPYGYGPGGVAGAAG
              -EX15              -EX16                         -EX17
241 KAGYPTGTGVGPQAAAAAAAKAAAKFGAGAAGVLPGVGGAGVPGVPGAIPGIGGIAGVGT
                    -EX18
301 PAAAAAAAAAAAKAAKYGAAAGLVPGGPGFPGPVVGVPGAGVPGVGVPGAGIPVVPGAGIP
        -EX19            -EX20
361 GAAVPGVVSPEAAAKAAAKAAKYGARPGVGVGGIPTGVGAGGFPGFGVGVGGIPGVAGV
           -EX21            -EX22
421 PSVGGVPGVGGVPGVGISPEAQAAAAAKAAKYGAAGAGVLGGLVPGPQAAVPGVPGTGGV
    -EX23                 -EX24
481 PGVGTPAAAAAKAAAKAAQFGLVPGVGVAPGVGVAPGVGAGVGLAPGVGVAPGVGVAP
         -EX25                 -EX26
541 GVGVAPGIGPGGVAAAAKSAKVAAKAQLRAAAGLGAGIPGLGVGVGVPGLGVGAGVPGL
             -EX26A                        -EX27            -EX28
601 GVGAGVPGFGAGADEGVRRSLSPELRGDPSSSQHLPSTPSSPRVPGALAAAKAAKYGAA
                       -EX29                  -EX30
661 VPGVLGGLGALGGVGIPGGVVGAGPAAAAAAAKAAAKAAQFGLVGAAGLGGLGVGGLGVP
          -EX31         -EX32              -EX33        -EX36
721 GVGGLGGIPPAAAAKAAKYGAAGLGGVLGGAGQFPLGGVAARPGFGLSSPIFPGGACLGKA

781 CGRKRK
```

Figure 7: Human tropoelastin protein sequence (Swiss Prot. Accession number P15502). The yellow text indicates the KP-crosslinking domains; the green text indicates the KA-crosslinking domains, the black text belongs to glycine-rich hydrophobic domains, while the bleu text indicates typical domains (EX1, signal peptide; EX26A, rarely expressed hydrophilic domain; EX36, C-terminal domain).[129]

In tropoelastin molecule hydrophobic and hydrophilic domains coexist. The first ones, composed of Gly, Val, Ala and Pro residues are organized in repeats such as (Gly-Val-Gly-Val-Pro), (Gly-Val-Pro-Gly-Val) and (Gly-Val-Gly-Val-Ala-Pro), responsible for the elastic properties of the protein. The hydrophilic domains containing Lys and Ala residues are involved in cross-linking. Intervals of Ala residues are often placed between Lys residues and the latter are involved in the formation of tetrafunctional crosslinks.[130]

Figure 8: Cross-linking reaction of tropoelastin.[131]

For this reason they are also called "cross-link domains". These domains can be divided in two types, Lys-Ala-type and Lys-Pro-type (Fig. 9).

Figure 9: Domain structure of human tropoeleastin.[132]

Lys-Ala-type domains are those mentioned above, with stretches of alanine residues interspersed with two or three lysines. Lys-Pro-type cross-linking domains are rich of proline residues and they are fewer in number in mammalian, avian, and reptilian tropoelastins and abundant in amphibian and teleost tropoelastin.[133]

2.1.5.4.2 Properties of elastin

The water content of elastin influences its glass transition temperature (T_g). Actually, T_g is about 200 °C in the dehydrated state and 30 °C at 30 % hydration level.[134] The phenomenon present in tropoelastin and in elastin-based materials is coacervation. It is classified as "a process during which a homogeneous solution of charged macromolecules undergoes liquid–liquid phase separation, giving rise to a polymer-rich dense phase at the bottom and a transparent solution above".[135] Tropoelastin is water-soluble at ambient temperature. However, on increasing temperature, the self-aggregation of the molecules due to interactions between hydrophobic domains occurs, resulting in a cloudy solution. The physical properties of elastin prevent an in-depth analysis of its secondary structure, because mature elastin does not crystallize and is not soluble in common solvents used in spectroscopy. Therefore, X-ray diffraction study and the use of classical spectroscopic techniques are impossible to perform. The availability of the entire tropoelastin obtained by recombinant DNA technology allowed circular dichroism (CD) spectroscopy.[136] The CD analysis showed that the secondary structure consists of 3% in α-helices, derived from the cross-linking regions of poly-alanine, 41% in β-sheets, 21% in β-turns and 33% in other minor conformations.[137] Raman spectroscopy studies, on the other hand, have shown the presence of about 10%

of α-helices, 35% of β sheets and 55% of "unordered" conformations.[138] Tamburro and coworkers studied the conformational features of the protein by the investigation of the short elastin peptides encoded by each exon of human tropoelastin gene, because each exon encodes an independent structure.[57] On that basis, herein the elastin peptide encoded by exon 15 of human tropoelastin gene was added in the polymeric mixtures and then electrospun. Its sequence is: GVGPQAAAAAAA**K**AAA**K**F.

2.2 Materials and methods

In this chapter materials used for scaffolds production and techniques employed for their characterization are described.

2.2.1 Materials

GE from bovine skin (type B powder, Bloom strength: 225, isoelectric point: 3.8–5.5 at 25 °C) was purchased from Sigma-Aldrich (St. Louis, Missouri, USA). PDLLA (EasyFil PLA, transparent pellets, molecular weight: 126,000 g/mol, density: 1240 kg/m^3) was purchased from FormFutura (Nijmegen, Netherlands). CNCs (from wood, spray-dried powder, particle size: 1–50 µm, particle length: 44–108 nm, particle diameter: 2.3–4.5 nm, pH: 6–7, crystalline fraction: 88%) were bought from CelluForce (Montreal, Quebec, Canada). El peptide was synthesized as reported previously.[57]

2.2.2 Electrospinning procedure

All the polymers were dissolved in 3 ml of 1,1,1,3,3,3 Hexafluoro-2-Propanol (HFP) (Iris Biotech GMBH, Marktredwitz, Germany). Polymer solutions composition produced at University of Basilicata is listed in Table 3. NGP contains 8.0% (w/w) of CNCs (expressed on the total mass of the remaining components in polymer solutions).

Table 3: Composition of polymeric blends used for scaffolds fabrication. GP = gelatin/poly(lactic acid), NGP = cellulose nanocrystals/gelatin/poly(lactic acid) and ElNGP = EX15 elastin peptide/cellulose nanocrystals/gelatin/poly(lactic acid).

Sample name	Gelatin (GE) mass (g)	Poly(DL-Lactic Acid) (PDLLA) mass (g)	Cellulose nanocrystals (CNCs) mass (g)	Elastin peptide (EX15) mass (g)	Solvent (HFP) volume (ml)
GP	0.090	0.27	/	/	3.0
NGP	0.090	0.27	0.030	/	3.0
ElNGP	0.090	0.27	0.030	0.0039	3.0

All mixtures were prepared at 37 °C by dissolving GE in HFP. The solution was kept under magnetic stirring for 2 hours. Afterwards, PDLLA was added and the mixture was kept under magnetic stirring for 3 hours. The polymer mixture containing CNCs was prepared by adding CNCs previously dispersed in HFP at room temperature and kept under magnetic stirring for 24 hours. CNCs dispersion underwent different sonication cycles. The polymer mixtures were loaded into a 5 mL plastic syringe with an 18 G stainless-steel needle and then electrospun at 19 kV (Gamma High-Voltage generator), with a flow rate of 1.6 mL/hours of the pump for a single syringe BSP-99 mM (Linari Engineering, Pisa, Italy). The target was a round copper plate having 9 mm diameter coated with aluminum foils and the distance between the collector and the needle was set to 19 cm.
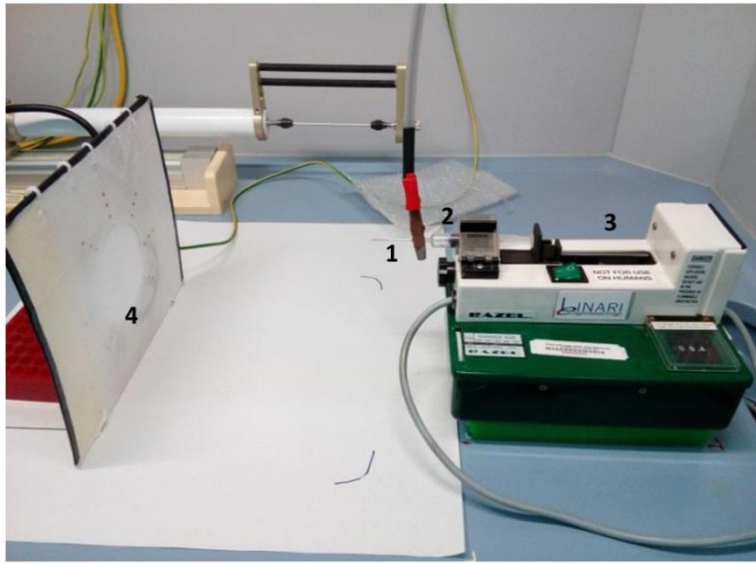
Figure 10: Electrospinning apparatus used for scaffold production. Needle (1), plastic syringe (2), pump (3)and, scaffold (4).

2.2.3 Cross-linking procedure

Cross-linking reaction is mandatory when scaffolds containing gelatin are used in aqueous solutions because GE is a water-soluble component. In this work the cross-linking agents used were *N*-hydroxysuccinimide and *N*-(3-dimethylaminopropyl)-*N'*-ethyl-carbodiimide hydrochloride. The cross-linking reaction mechanism is shown in Fig. 11.
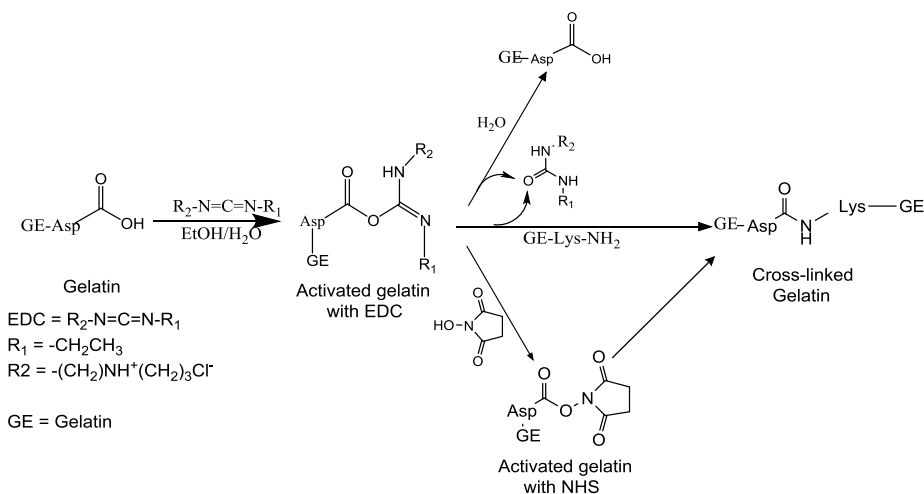
Figure 11: Scheme of the cross-linking reaction of gelatin.

In the first step, EDC reacts with carboxylic moiety of L-aspartic or L-glutamic acid present in GE to form an active *O*-acylisourea intermediate. Through NHS addition there is the formation of a molecule that is easily displaced by nucleophilic attack from ε-amino group of lysine in GE to give new stable amide bonds. The use of two cross-linking agents is justified by the fact that if only EDC was used, the cross-linked bonds that would form could be hydrolyzed in an aqueous environment with the restoration of the starting reagents and consequent decrease in the yield of the reaction.

N-Hydroxysuccinimide (NHS) and *N*-(3-dimethylaminopropyl)-*N'*-ethyl-carbodiimide hydrochloride (EDC·HCl) were used as cross-linking reagents and purchased from Sigma-Aldrich (St. Louis, Missouri, USA) and Novabiochem (Darmstadt, Germany), respectively. Cross-linkers were solubilized in an 85.5% ethanolic solution (Carlo Erba Reagents, Cornaredo, Italy) in an equimolar ratio, both at the concentration of 45.0 mM. Electrospun scaffolds were immersed in a cross-linking solution at room temperature. Subsequently, they were shaken at 60

rpm using an orbital shaker (PSU-10i, Biosan, Riga, Latvia) for 24 hours. The electrospun materials were gently dried by using a filter paper and washed with ultrapure water (20 mL × 3 times) to remove any residual trace of cross-linkers. Finally, they were immersed in 95.0% ethanol, shaken again for 1 hour at 60 rpm, and air-dried at room temperature. Ultrapure water was produced by a Milli-Q Water Purification System (Merck, Darmstadt, Germany). Water is first pumped through the reverse osmosis cartridge; thereafter, the permeate water is pumped from the reservoir through the Quantum cartridge by the recirculation pump in order to produce high resistivity product water, which is delivered at a flow rate of 0.6 L/min through a 0.22 μm filter.

2.2.4 Amine group content and degree of cross-linking

The content of free primary amine groups present in the uncross-linked scaffolds and that in cross-linked were determined using the 2,4,6-trinitrobenzenesulfonic acid (TNBS) assay with a protocol similar to those reported by Davidenko[139] and Ofner.[140] To each sample (4–6 mg), 0.5 mL of a 4% (w/v) NaHCO$_3$ solution and 0.5 mL of a freshly prepared solution of 0.05% (w/v) TNBS were added. After 2 hours at 40°C, 1.5 mL of 6 M HCl was added and the samples were hydrolyzed at 60 °C for 90 minutes. The reaction mixture was diluted with distilled water (2.5 mL) and cooled to room temperature, and absorbance at $\lambda = 346$ nm was measured using a Cary 60 UV–Vis spectrometer (Agilent, Santa Clara, USA). Controls (blank samples) were prepared using the same procedure, except that HCl was added, prior to the introduction of TNBS solution, to prohibit any reaction of TNBS with the amine groups. The blank sample value was subtracted from each sample absorbance. Three replicates on three pieces of each scaffold were used for each

determination. The uncross-linked sample was assumed to contain 100% of the available free amine groups and this value was used to calculate the percentage of remaining free amine groups after the cross-linking treatment using the following equation (eq. 1):

$$\frac{n(NH_2)}{g(scaffold)} = \frac{(Abs\ x\ V)}{(14,600\ Lmol^{-1}cm^{-1}\ x\ W\ x\ l)}$$

In the above formula used for the calculation of the amine group content, 14,600 L mol^{-1} cm^{-1} is the molar extinction constant at λ = 346 nm of TNBS-Lys, while V is the volume (L), W is the mass sample (g), and l is the cell path length (cm). The degree of cross-linking was evaluated as the difference between the chemically determined number of free amine groups before and after cross-linking, relative to the initial free amine content.

2.2.5 X-Ray diffraction analysis (XRD)

CNCs powder was analyzed by X-Ray Diffraction and used as standard to characterize electrospun scaffolds containing CNCs. This technique is widely used in the study of crystalline structures, because by using it is possible to identify and characterize compounds analyzing their diffraction pattern.[141] As a matter of fact, it is possible to determine the structural arrangement of a crystal by making it interact with a coherent beam of electromagnetic waves, such as, in this case, X-rays. The interaction of the X-ray beams with the crystalline structure of the sample occurs through the so-called "scattering" phenomenon, i.e. the diffusion of electromagnetic radiation (in the physical phenomenon known as diffusion there is a variation in the trajectory of the waves following the interaction with

other waves or particles). In the case of X-rays the term used is "coherent" scattering where all identical atoms interact with the incident monochromatic beams in an identical way. Naming E(i) the energy of the incident beam and E(s) the energy of the beam after scattering, there is an elastic scattering if the following relationship is satisfied (eq. 2):

$$\Delta E = E(s) - E(i) = 0$$

i.e. the wavelength (and therefore the energy) of the radiation remains unchanged during the interaction with the crystal structure.

The waves diffused by the crystal lattice can give rise to interference phenomena of a destructive type, with the consequent zeroing of the resulting beam intensity, or constructive, according to Bragg's law (eq. 3):

$$2dsen(\Theta) = n\lambda$$

where **n** is a natural number representing the order of diffraction, **λ** is the wavelength of the incident radiation, **d** is the distance between two adjacent crystalline planes and **Θ** is the angle of incidence between the beam and the crystalline plane. By varying the angle of incidence of the X-rays with the sample, a diffractogram is obtained. XRD analysis was carried out on a Siemens D5000 diffractometer (Munich, Germany). The current generator and the voltage generator adjusted at 32 mA and 40 kV, respectively, and the step size was kept at 0.042, with a total duration of analysis equal to 75 minutes.

2.2.6 High Performance Liquid Chromatography

Chromatography is a widely used tecnique for the separation, identification and determination of chemical components in complex mixtures. In particular, high performance liquid chromatography (HPLC) allows the separation and purification of compounds present in a mixture as a function of the different affinity that each chemical species has towards the mobile phase and the stationary phase.

The conventional columns used for HPLC are made of stainless steel and built to withstand very high pressures, up to 5.5×10^7 Pa. Since the amount of material analyzed through an HPLC column is often very small, the sensitivity of the detection system used for the analysis must be sufficiently high and stable to respond to the low concentration of analyte present in the eluate. The most used detectors are UV-Vis detectors with variable wavelengths, which are based on UV-Vis spectrophotometry and allow to measure the signal in the form of a chromatogram. The chromatogram is the graphic representation of the detector response as a function of the retention time (t_R), the time required for the injected substance to be eluted from the beginning to the exit of the column. A typical chromatogram consists of a series of peaks, ideally of symmetrical shape, which represent the elution of the individual analytes. HPLC was used in order to verify if the elastin peptide was embedded into the electrospun scaffolds. Small pieces of uncross-linked and cross-linked ElNGP (EX15/CNCs/GE/PDLLA) hybrid scaffolds (1 cm × 1 cm) were immersed in 85.5% ethanol solution and shaken at 60 rpm using an orbital shaker (PSU-10i, Biosan, Riga, Latvia) for 24 hours. Afterwards, the solution was transferred into a round-bottom flask. The solvent was evaporated under nitrogen flow, and freeze-dried after the dilution with ultrapure water. After lyophilization, the sample was solubilized in H_2O (0.1% TFA)

and analyzed by reverse-phase HPLC on a Jupiter 300 Å C18 analytical column (250 × 4.60 μm 5 Å) (Phenomenex, Bologna, Italy). H_2O (0.1% TFA) and CH_3CN (0.1% TFA) in a 95:5 ratio, respectively, were used as mobile phases in the binary gradient. The uncross-linked ElNGP scaffold was immersed in 85.5% ethanol solution of EDC/NHS (45 mM). The solution was shaken at 60 rpm for 24 hours, treated as previously described, and analyzed by HPLC. EX15 El-inspired peptide was used as standard and analyzed by HPLC in both aqueous and cross-linking solutions.

2.2.7 Fourier Transform Infrared Spectroscopy (FTIR)

FTIR spectroscopy was used in order to track the presence of pure components into the hybrid scaffolds. This analysis was performed in the solid state in KBr pellets using a Jasco FTIR 460 plus (JASCO, Easton, MD, USA) spectrometer in order to analyze electrospun scaffolds. Contextually, pure polymers GE, CNCs, and PDLLA were processed and used as reference. Each electrospun scaffold was cut into small pieces and added to KBr powder previously dried under vacuum at 180 °C for 12 hours. Spectra were acquired in the region from 4000 to 500 cm^{-1} using 256 scans and a resolution of 2 cm^{-1}. The KBr pellet spectrum was recorded before each measurement and then subtracted from the sample spectrum.

2.2.8 Attenuated Total Reflectance (ATR)

Attenuated total reflectance spectroscopy (ATR) is usually used in order to obtain absorption spectra of thin films and opaque materials and to reveal the effectiveness of cross-linking reaction. Attenuated total reflectance (ATR) spectra were obtained out on electrospun scaffolds before and after the cross-linking reaction. Measurements were carried out on a Nicolet 5700 (Thermo Fisher Scientific, Waltham, MA, USA) equipped with an ATR accessory, Smart Orbit with a type II A diamond crystal, of refractive index 2.4, with a KBr beam splitter and an MCT/B detector. Spectra were acquired in the region from 4000 to 450 cm^{-1} with a spectral resolution of 2 cm^{-1} and 32 scans. Background spectra were recorded each time and then subtracted from the sample spectra.

2.2.9 Scanning Electron Microscopy (SEM)

The morphology of electrospun scaffolds was investigated by Scanning Electron Microscopy (SEM). SEM analyses are generally conducted by collecting secondary electrons which are identified by a special detector and converted into electrical pulses. A black and white image is produced relating to the intensity of the electrons detected by the detector for each region analyzed, which can be interpreted as representative of the morphology of the sample. However, in order to be analyzed, the sample must be conductive and, therefore, it is metallized before analysis. The morphology of the electrospun scaffolds was investigated on a Philips, FEI ESEM XL30 instrument. SEM images were acquired with a voltage of 20 kV and different magnifications, after gold sputter-coating. The diameter of the fibers and scaffold porosity were evaluated using ImageJ (National Institute of

Health, USA, http://rsbweb.nih.gov/ij) software supplied with the DiameterJ plug-in (n > 1000).

2.2.10 Swelling test analysis

With swelling test a measure of the hydrophilicity of the scaffolds is possible. The swelling process is one of the most relevant phenomena characterizing polymers with a high molecular weight, when immersed in a specific solvent. As a matter of fact, the liquid molecules penetrate inside the matrix, spreading inside its pores and giving rise to the swelling process.[142] For each sample, four pieces from four different cross-linked scaffolds (a total of 16 samples) were investigated. Each sample was immersed in 10 mL of ddH$_2$O at room temperature (r.t.) for 60 minutes and shaken at 60 rpm on an orbital shaker. Thereafter, they were gently dried on a filter paper to remove the excess of water and weighed on a balance (Precisa Instruments AG, Model, XR 205 SM-DR, 8953 Dietikon, Switzerland, 2005) having a sensitivity of ± 0.00001 g. The water absorbed by each scaffold was calculated according to the following equation (eq. 4):

$$\textbf{Swelling \%} = \frac{W_w - W_d}{W_d} \ x \ \textbf{100}$$

W_w and W_d are the masses (g) of wet and dry scaffolds, respectively.

2.2.11 Contact angle measurements

The measurement of the contact angle (indicated with θ) indicates the ability of a liquid to distribute itself over a given surface. Thanks to it, it is possible to establish the wettability of a surface by measuring the angle that is formed

between the tangent to the profile of a drop, deposited on the surface of the sample, and the surface itself (Figure 12). This technique, in addition to the wettability of the surface, gives additional information on the characteristics of the examined surface such as surface tension and homogeneity (by measuring the hysteresis between the angle of advance and the retreat angle of a drop moving on the sample surface).
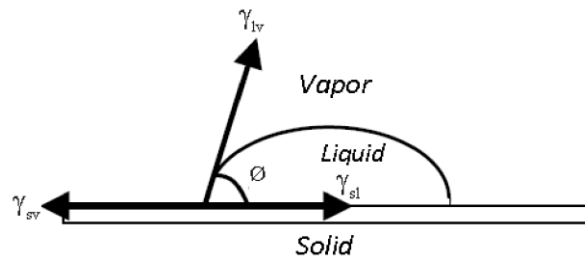
Figure 12: Image of the contact angle and interfacial tension of the three surfaces at the three-phase boundary.[143]

Analyzing the phenomenon from a thermodynamic point of view, the contact angle value depends on the solid-vapor (γ_{SV}), solid-liquid (γ_{SL}) and liquid-vapor (γ_{LV}) surface tensions according to Young's equation (eq. 5):

$$\gamma_{SV} - \gamma_{SL} - \gamma_{LV} \cos(\theta) = 0$$

If we indicate the contact angle with **θ**, it is possible to describe three different situations:

- $90° < \theta < 180°$: the surface is hydrophobic;

- $0° < \theta < 90°$: the surface is partially hydrophilic;

- $\theta = 0°$: the surface is super hydrophilic.

An indirect evaluation of the hydrophilicity scaffold was assessed by the contact angle on an OCA 40 device (DataPhysics Instruments GmbH, Filderstadt, Germany) instrument. The final result is calculated from 16 measurements obtained from four different pieces for each cross-linked scaffold. A water drop having 2 µL of volume was placed onto the sample and after 10 s the contact angle was measured using a video setup and SCA20 software (DataPhysics Instruments).

2.2.12 Uniaxial tensile testing

The uniaxial tensile test is one of the most commonly used tests to determine important material parameters such as Young's modulus, yield strength, Ultimate Strength, elongation at break, Poisson's ratio, and Lankford coefficients (r-values). By subjecting a sample to a controlled tensile or compressive displacement along a single axis, the change in dimensions and resulting load can be recorded to calculate a stress-strain profile. The elastic and plastic material properties can then be calculated from the obtained curve.

In a typical uniaxial tensile test, the displacement is usually held at a constant rate, and displacement and resulting load are recorded. In order to make direct comparisons between materials, normalization against sample geometry and therefore, against the dimension of each sample, of loading responses is necessary. Thus, a stress-strain curve can be built, as shown in Fig. 13.
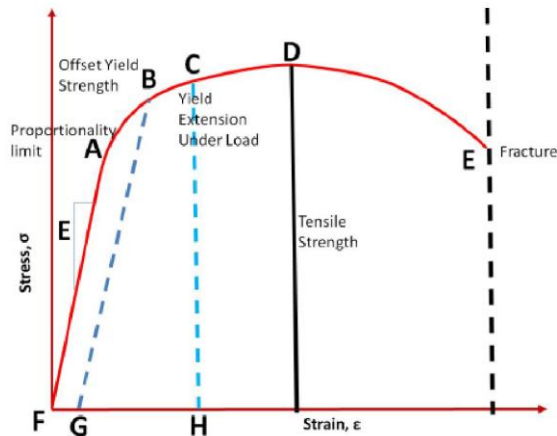
Figure 13: Typical stress-strain curve for a metal specimen.[144]

Observing Fig. 13, it is possible to note that initially stress and strain are linearly related, the material behaves in a linear elastic manner and the deformation is recoverable. The slope of this linear elastic portion is Young's modulus and it is given by the following equation (eq. 6):

$$E = (\sigma_2 - \sigma_1)/(\varepsilon_2 - \varepsilon_1)$$

E characterizes the stiffness of a material and it has the dimension of a pressure.

After the linear region, at larger strains, material deformation becomes irrecoverable and non-linear, or plastic. In this region, the material also exhibits its ultimate tensile stress, indicated by the letter D in Fig. 13, or the maximum load divided by the initial cross-sectional area (eq. 7):

$$\sigma_{ult} = P_{max}/A_0$$

Where P_{max} is the maximum load and A_0 is the initial cross sectional area of the sample normal to the loading direction. Instead, the point indicated by the letter E on graph in Fig. 11 represents the break of the sample. Uniaxial tensile tests were carried out. For each sample, four rectangular pieces from four different cross-linked scaffolds were obtained (10 mm × 20 mm). They were clamped to the uniaxial tensile testing device (ElectroForce 5500, ElectroForce Systems Group, Bose Corporation, Minnesota, USA). They were pulled to failure after applying a stretch of 0.025 mms^{-1}. Then, Young's modulus and the ultimate tensile strength were calculated. For each measurement, E modulus was calculated using the initial linear slope of the stress versus strain curve.

2.2.13 Cytotoxicity assay

MTS assay is a colorimetric assay used in order to measure cell metabolic activity. It is similar to MTT, another test used for the same purpose. It is based on the bioreduction of 3-(4,5-dimethylthiazol-2-yl)-5-(3-carboxymethoxyphenyl)-2-(4-sulfophenyl)-2H-tetrazolium (MTS), in the presence of phenazine methosulfate (PMS), while MTT on the bioreduction of 3-(4,5-dimethylthiazol-2-yl)-2,5-diphenyltetrazolium bromide into a formazan product which is soluble in culture media, as shown in Fig. 14:
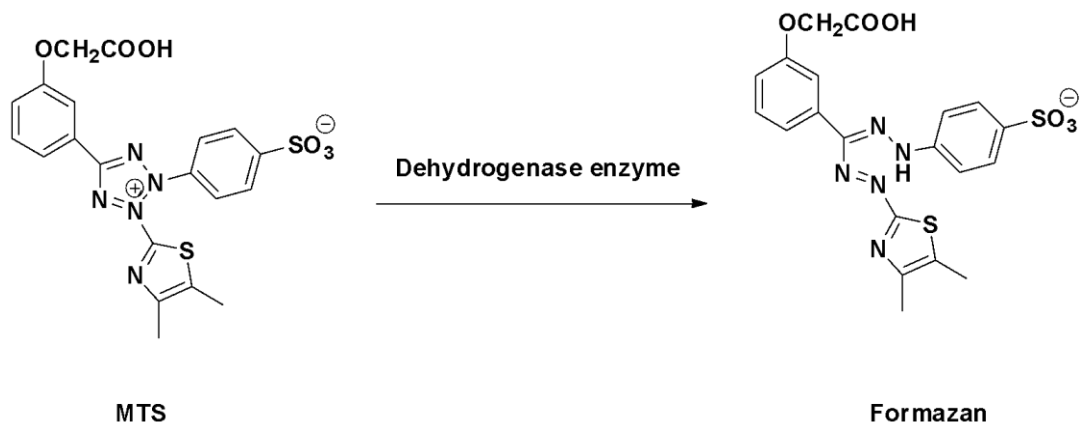
Figure 14: Enzymatic reduction of MTS to formazan.[145]

This reduction is carried out by NADPH-dependent dehydrogenase enzymes in metabolically active cells and the formazan dye produced is then quantified by measuring the absorbance at 490 – 500 nm.[146]

Prior to cell culture experiments, the fabricated scaffolds were tested for biocompatibility. For this purpose, a cytotoxicity test according to EN ISO 10993-5 has been performed using the MTS assay CellTiter 96 AQueous OneSolution Cell Proliferation Assay (G3582, Promega, Madison, USA). Each polymer was incubated for 72 hours at 37 °C and 5% CO_2 in Dulbecco's modified Eagle's medium (21063-029, Thermo Fisher Scientific, Waltham, USA) and 1% penicillin–streptomycin (15070-063, Thermo Fisher Scientific) in an extraction ratio of 0.1 g/mL. NIH/3T3 cells (ATCC CRL-1658TM, ATCC, Manassas, USA) were then cultured for 24 hours with the sterile filtered extraction medium supplemented with 10% fetal bovine serum (10270-106, Thermo Fisher Scientific). The medium without polymer extract served as a negative control. The cells incubated with 1% SDS were used as a positive control. Subsequently, the MTS assay was performed according to the

manufacturer's protocol. The absorbance of the soluble formazan produced by the cellular reduction of MTS was measured at 490 nm (n = 3). The cell viability was determined by the absorption of the samples relative to the control.

2.2.14 Cell Seeding and Culture

In order to investigate cell attachment and proliferation, L929 cells (ACC2, Leibniz Institute DSMZ, Braunschweig, Germany) were cultured onto the scaffolds for 1, 3, and 5 days (n = 3). Briefly, scaffolds with a diameter of 6 mm were placed in a 96-well plate and 5000 cells/mL were seeded in 150 µL of modified Eagle's medium (11090081, Thermo Fisher Scientific) supplemented with 4 mM Lglutamine (A2916801, Thermo Fisher Scientific), 1% penicillin–streptomycin, and 10% fetal bovine serum. Cells were cultured at 37 °C and 5% CO_2. The medium was changed every 2 days. After cell culture, the cell-seeded scaffolds were washed once with PBS and fixed with 4% paraformaldehyde (P6148, Sigma-Aldrich). The cell membrane was permeabilized with 0.1% Triton X-100 (3051.3, Carl Roth, Karlsruhe, Germany) for 20 minutes. F-actin was stained for 30 minutes in the dark using Alexa Fluor 647 (1:500, A22287, Thermo Fisher Scientific). For cell number analysis, the cells were stained with 4',6-diamidino-2-phenylindole (DAPI) (1:50, 10236276001, Roche Diagnostics, Mannheim, Germany) for 20 minutes. Images were obtained using a fluorescence microscope (Cell Observer, Carl Zeiss AG, Oberkochen, Germany). The cell number was quantified by counting the DAPI-stained cell nuclei per area using ImageJ.

2.2.15 Statistical analysis

The graphs were plotted using Origin Data Graph software (OriginLab Corporation, Northampton, MA, USA) and Microsoft Excel. Data are reported as mean ± standard deviation. Fiber diameter and swelling test statistical analyses were carried out using the one-way analysis of variance (ANOVA) method, Tukey's test, and Student's t-test. A p value ≤ 0.01 (*) was considered as statistically significant. For the porosity and mechanical analysis, two way analysis of variance and Tukey's test were used, with a p value ≤ 0.05 (*) defined as statistically significant, while for the cytotoxicity assay ANOVA was performed and the mean value of the samples was compared with the mean value of the negative control using Fisher's least significant difference test. For cell number analysis, a two-way ANOVA and Tukey's multiple comparison test were performed with GraphPad PRISM (GraphPad Software, San Diego, USA).

2.3 Results and discussion

In this PhD work, bioinspired electrospun scaffolds were produced using green polymers and biomaterials. GE and PDLLA were blended together with CNCs and EX15. CNCs and EX15 were added to the GE/PDLLA blending up to 8 % and 1% (w/w) final concentration, respectively (expressed on the total mass of the remaining components in polymer solutions). The aim was to confer strength and biocompatibility to electrospun scaffolds. Furthermore, electrospun hybrid scaffolds were cross-linked by EDC/NHS chemistry in ethanol. They showed insolubility in aqueous solution and porous interconnected structure with appealing characteristics as biomedical devices. The topic of this chapter, will be the production, the electrospinning and the molecular and morphological characterization of electrospun matrices. HPLC, FTIR, ATR, UV and SEM analyses were carried out at University of Basilicata (Potenza, Italy). Mechanical tests and biological assays were performed in the Laboratory of Professor Schenke-Layland at the University of Tubingen (Germany).

2.3.1 Production of electrospun scaffolds

Starting from the first application in vascular prosthesis[147] nowadays electrospinning has gained even more diffusion for the production of scaffolds in tissue engineering.[148,149] Our work aimed to produce electrospun scaffolds made of natural polymers such as cellulose, protein-based materials, and PDLLA. Recently, recombinant HTE has been electrospun with collagen to improve biocompatibility.[150] Herein, an elastin (El) derived peptide with a bioactive sequence was added to the polymer mixture. CNCs are generally used to reinforce scaffolds electrospun from different polymers, such as polyvinylidenefluoride-co-hexafluoropropylene (PVDF-HFP),[151] PCL,[152] polyacrylonitrile (PAN),[153] and PLA.[154] CNCs were added to counterbalance the strong hydrophobicity of PDLLA and improve the mechanical properties of hybrid scaffolds. Polymer solutions described in Table 3 (Paragraph 2.2.2) were electrospun using process parameters recently published elsewhere.[155] HFP, known for its low nucleophilicity and strong hydrogen bond-donating ability,[156,157] was chosen as solvent because of its ability to solubilize proteins, PLA polymer,[155] GE, El, and CNCs, even if in the final form of a dispersion. The GP blend was prepared by mixing GE and PDLLA to a final concentration of 3.0 and 9.0% (w/v) of GE and PDLLA, respectively. GP blend at a concentration of 12.0% (w/v) in HFP showed good miscibility with resulting stable electrospinning process. The preliminary result consisted of an electrospun scaffold with uniform structure at macroscopic level. In order to increase the hydrophilicity and wettability of electrospun scaffolds,[158] CNCs were added as a filler to the GP blend in the amount of 1.0% (w/v) corresponding to 8% (w/w). As a matter of fact, surface wettability, which is a crucial property for the interaction with cells, is affected by the scaffold hydrophilicity.[159] Moreover, the El peptide

(0.1% w/v) was employed as a filler in CNCs/GE/PDLLA blend (NGP). The scope was not only mimic ECM composition but also enable cell incorporation.[56,57] The addition of CNCs and El gave rise to polymer solutions in HFP of 13.0 and 13.1% (w/v), respectively.

2.3.2 XRD analysis

Diffractograms of cross-linked NGP and uncross-linked GP, NGP, and ElNGP scaffolds were recorded. XRD curves were matched with CNCs powder spectra used as positive standard for the assessment of CNCs presence. *Viceversa*, GP XRD spectra represented the negative control (Fig. 15). The CNCs powder diffractogram shows two peaks at 2θ = 22.6 and 34.6°, corresponding, respectively, to (2 0 0) and (0 0 4) reflections of crystallinity.[160] In the diffractograms of uncross-linked NGP and cross-linked NGP and ElNGP, a shoulder at 2θ = 22.6° appeared as a contribution from the CNC component (black line). Accordingly, the GP scaffold diffractogram that is devoid of CNCs, and therefore used as a negative control, did not show any shoulder or peak. Summarizing, XRD measurements demonstrated that CNCs retained their crystallinity when added as a coadjuvant in polymer mixtures. On that basis, we infer that the CNCs were successfully dispersed in polymer mixtures.
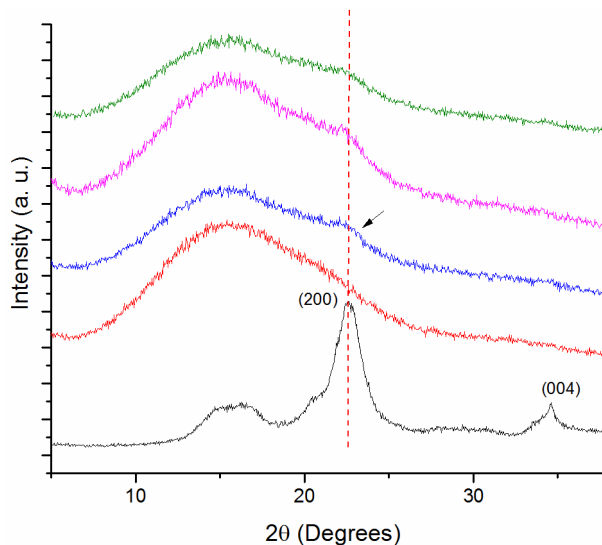
Figure 15: Diffractograms of electrospun scaffolds: CNCs powder (black); GP (red); NGP (blue); ElNGP (purple); and cross-linked NGP (green).

2.3.3 HPLC analysis

The chromatograms obtained after treatment of the uncross-linked ElNGP scaffold in 85.5% ethanolic solution are shown in Fig. 16. The uncross-linked ElNGP scaffold chromatogram (black curve in Fig. 16A) shows the presence of a peak with a retention time (Rt) of 29.0 min that could be ascribed to the EX15 peptide by comparison with the chromatogram of peptide alone used as the reference (blue curve of Fig. 16A). In contrast, the peak was not present in the chromatogram of the cross-linked ElNGP scaffold treated under the same conditions (data not shown). The rationale for the experimental findings could be that the EX15 peptide escaped from the scaffold into the reaction solution during the cross-linking reaction while it was constrained into the scaffold upon cross-linking reaction. In order to confirm the embedding of the EX15 peptide in the ElNGP scaffold during the cross-linking reaction, the uncross-linked ElNGP scaffold

was treated in 45 mM EDC/NHS, as described before. The chromatogram (black curve of Fig. 16B) did not show the peak assigned to the EX15 peptide under the cross-linking reaction conditions (Rt = 25.6 min) (blue curve in Fig. 16B), proving on this basis that the EX15 peptide was fully embedded.
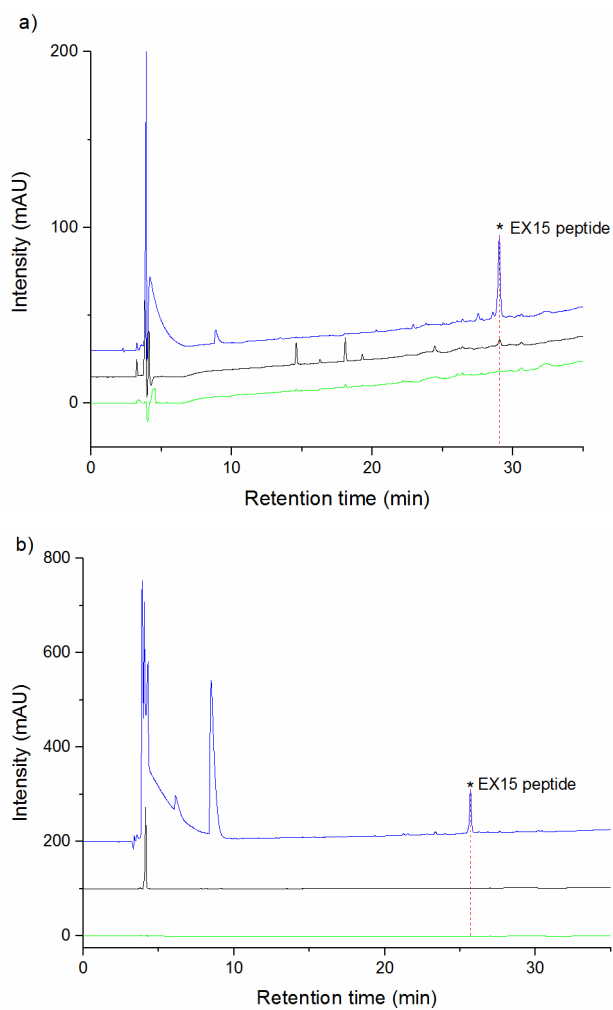
Figure 16: HPLC chromatograms in: (a) aqueous solution and (b) EDC/NHS 45 mM of blank (green); uncross-linked ElNGP scaffold (black), EX15 peptide (blue).

2.3.4 FT-IR spectroscopy

FT-IR spectroscopy was used in order to analyze scaffolds at a molecular level. First, functional groups were assigned to pure polymers, and then they were used as a fingerprint for tracking the presence of a pure component in the hybrid scaffold spectra. From top to down, the first three FT-IR spectra in Fig. 17 are ascribed to pure GE, CNCs, and PDLLA, while the remaining are related to GP, NGP, and ElNGP electrospun hybrid scaffolds.
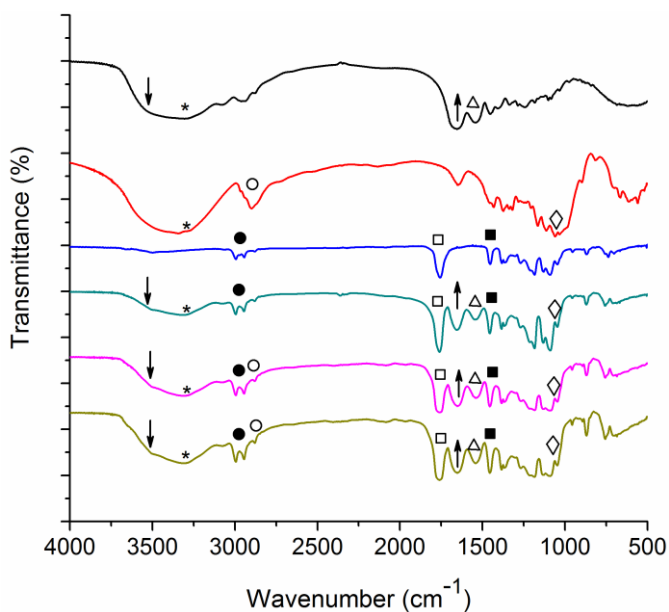
Figure 17: FT-IR spectra of GE (black); CNCs (red); PDLLA (blue); GP scaffold (dark cyan); NGP scaffold (purple), and ElNGP scaffold (dark yellow).

The FT-IR spectrum of GE showed at about 3521 cm^{-1} the amide A band (downward arrow) assigned to N−H stretching. At approximately 3316 cm^{-1}, a broad band originated from O−H stretching (asterisk) of 4-hydroxyproline residues. At shorter wavenumbers, the amide I band at 1665 cm^{-1} (upward arrow) derived from peptide C=O stretching and the amide II band situated at 1551 cm^{-1} due to N−H bending (triangle), as hallmarks of proteins, were visible.[161] Regarding the CNCs' FT-IR spectrum (red curve), a broad band can be noted from 3700 to 3100 cm^{-1} which is assigned to the stretching vibrations of carbohydrates' O−H groups (asterisk). Furthermore, bands due to aliphatic C−H stretching at about 2900 cm^{-1} (empty circle) and due to C−O stretching (diamond), typical of carbohydrates, were visible in the region ranging from 1200 to 1100 cm^{-1}.[153] The PDLLA FT-IR spectrum showed the aliphatic C−H stretching bands (filled circle) at 2995 and 2945 cm^{-1}, the ester C=O stretching (empty square) at 1760 cm^{-1}, and the C−H$_3$ bending (filled square) at 1454 cm^{-1}.[162] The FT-IR spectra of electrospun scaffolds are shown in Fig. 15 as dark cyan, purple, and dark yellow curves. Accordingly, the GP electrospun scaffold contains amide I (upward arrow), amide II (triangles), and A bands (downward arrow) from GE and aliphatic C−H (filled circle), C−H$_3$, (filled square), and ester C=O bands (empty square) from PDLLA. In NGP electrospun scaffolds, the band due to O−H (asterisks) is also visible, together with aliphatic C−H stretching bands (filled and empty circles), derived from PDLLA and CNCs. In order to check if CNCs were successfully embedded in electrospun scaffolds, the bands' absorbance values from OH stretching and amide A were rated and the arithmetic ratio was calculated. The ratio values were equal to 1.1, 1.4, and 1.2 for GP, NGP, and ElNGP scaffolds, respectively. The data infer that in the NGP scaffold, a stronger contribution has been found from the stretching of

the −OH groups. The smaller value found for ElNGP compared to NGP, even though CNCs are present in both scaffolds, is probably due to the contribution of additional N−H stretchings derived from the El peptide that is absent in NGP. The results demonstrate the successful incorporation of CNCs in the polymer mixture, confirming the efficiency of the electrospinning process.

2.3.5 Amine group content and degree of cross-linking

The values of cross-linking degrees, calculated from the free amino group content after each treatment, indicated that the percentage of cross-linking of GP, NGP, and ElNGP is 91 ± 9, 100 ± 1, and 91 ± 1%, respectively. The results are expressed as mean values of three parallel measurements ± standard errors (n = 9).

2.3.6 Cross-linking assessment: ATR spectroscopy

In order to estimate the progression of the cross-linking reaction, we investigated GP electrospun scaffolds before and after the cross-linking reaction using ATR spectroscopy. In Fig. 18, ATR spectra are shown in the region of interest comprised between 2000 and 1000 cm^{-1}.
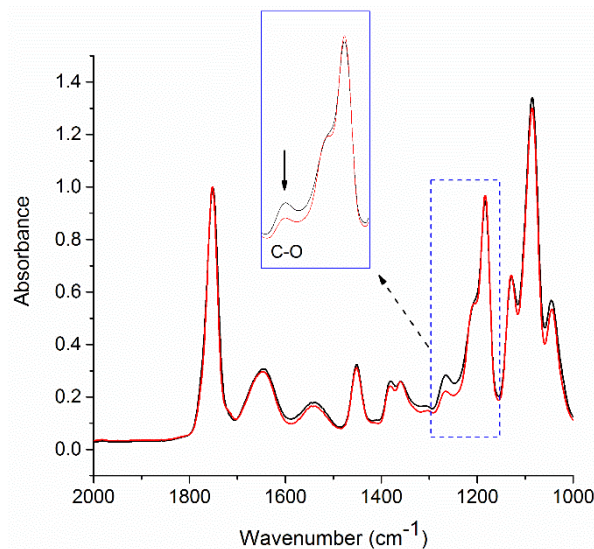
Figure 18: ATR spectra of GP electrospun scaffolds: before (black) and after cross-linking (red).

ATR spectra are shown in the region of interest comprised between 2000 and 1000 cm^{-1}. The presence of amide I and amide II bands from GE is evident in both samples. Our attention focused on the bands at 1266 and 1541 cm^{-1}. The first band is assigned to the C−O stretching of carboxylic acid present in the side chains of Asp and Glu residues. The second band is attributed to N−H$_2$ bending from free ε-amine groups of lysine residues, both present in GE. In the spectrum of the cross-linked scaffolds of GP (red curve), the intensity of the band at 1266 cm^{-1} was considerably reduced and this feature was found in all three kinds of electrospun scaffolds: GP, NGP, and ElNGP (data not shown). The intensity of the band at 1541 cm^{-1} was slightly lower too. These findings indicated the decrease in the number of carboxylic and free primary amine groups after the cross-linking reaction due to the formation of amide bonds according to the reaction scheme (Fig. 9).[163,164] ATR

spectra of uncross-linked and cross-linked GP electrospun scaffolds were slightly different, demonstrating that the reaction was successfully carried out.

2.3.7 SEM: morphology, fibers diameter and porosity evaluation

SEM was used to evaluate the electrospun scaffold morphology, as shown in Fig. 19, with particular attention to the assessment of any defect (beads), investigating the fiber orientation and diameter distribution before and after the cross-linking reaction.
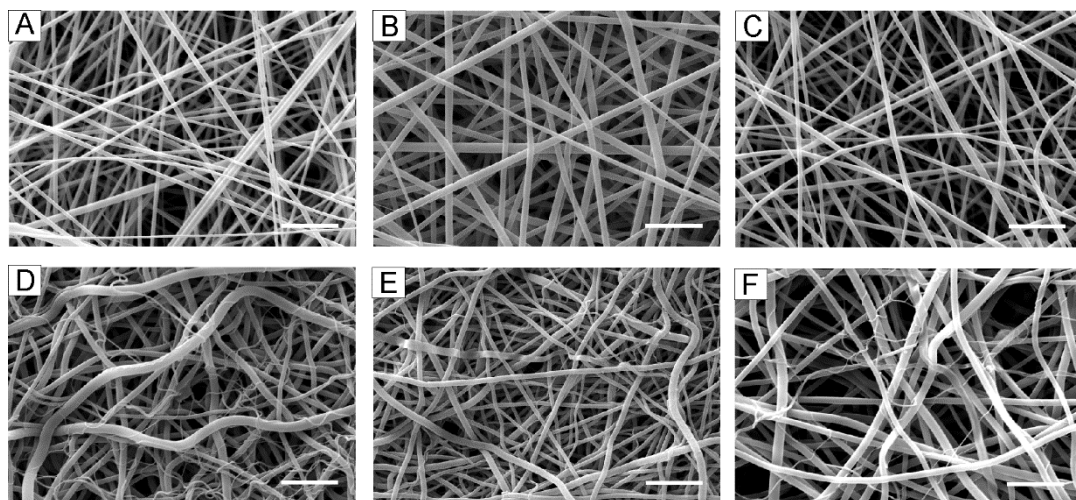
Figure 19: SEM images of electrospun scaffolds. Uncross-linked: GP (A), NGP (B), and ElNGP (C). Cross-linked: GP (D), NGP (E), and ElNGP (F); (bar: 10 μm).

The SEM image of the uncross-linked electrospun GP scaffold (Fig. 19A) showed a well-defined three-dimensional fibrillar microstructure enriched with interconnected pores. It is worth noting that the interconnection was

permanently visible even in the cross-linked sample (Fig. 19D). The fibers appeared linear in the uncross-linked scaffold and curvilinear in the cross-linked one. In both cases, no traces of solvent and beads were detected, suggesting a good degree of dispersion of the polymers in the solvent.[165] Herein, EDC was used as a GE cross-linker[166–168] and is preferred to others, as vapor-phase glutaraldehyde could be potentially cytotoxic at certain concentrations,[169] and aqueous phase genipin or glyceraldehyde gave rise to fused fibers.
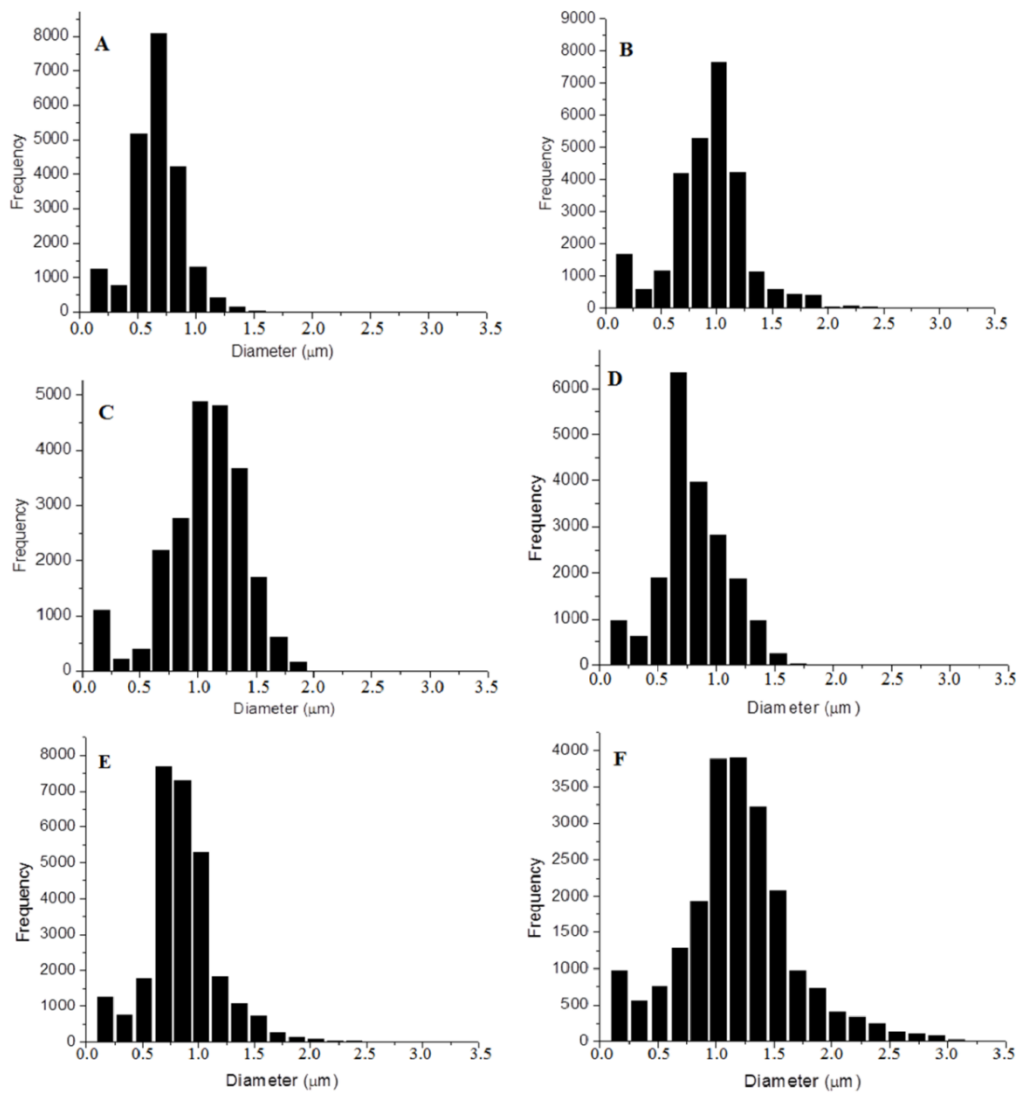
Figure 20: A-F. Histograms of the frequency as a function of the diameter of the fibers for uncross-linked (left column, A,C,E) and cross-linked electrospun scaffolds (right column, B,D,F): GP (A, B), NGP (C,D), ElNGP (E,F).

The average diameters of GP fibers as a frequency function are represented as a histogram (Fig. 20A,B), showing a normal distribution around a mean value of 683

± 174 nm and after the cross-linking reaction, the average diameter of the fibers increased from 683 ± 174 to 955 ± 240 nm (Table 4).

Table 4: Average fibers diameter, wettability and porosity with standard deviation. (For the fibers diameter, n > 1000 from three different images, for wettability n = 16, while for porosity n = 3).

Scaffold	Average fibers diameter (nm)	Wettability (%)	Porosity (%)
GP	683 ± 174	n. d.	68 ± 2
GP cross-linked	955 ± 240	374 ± 28	59.5 ± 0.6
NGP	1116 ± 290	n. d.	66.1 ± 0.7
NGP cross-linked	828 ± 280	449 ± 26	62 ± 1
ElNGP	823 ± 216	n. d.	63 ± 1
ElNGP cross-linked	1176 ± 344	607 ± 52	51 ± 3

The SEM image of the uncross-linked NGP scaffold (Fig. 19B) showed fibrillar and interconnected porous microstructures presenting randomly oriented fibers forming a nonwoven matrix with a normal distribution around a mean value of 1116 ± 290 nm (Fig. 20C,D). The striking analogy with the uncross-linked GP electrospun scaffold is an indirect inspection of the homogeneousness of dispersion and the efficiency of the electrospinning process, despite the presence of CNCs. Interestingly, unpromising results were obtained from cellulose microcrystals (CMCs) when added to a polymer blend. Indeed, in related SEM images, the presence of CMCs induced the excessive enlargement of the fibers probably due to the scale dimension of CMCs, micro-instead of nano-, as reported

by Jia et al.[170] After the cross-linking reaction, the NGP scaffold presented a change in the orientation of the fibers assuming a curvilinear shape (Fig. 19E). Diverse to previous results, the cross-linking reaction performed on the CNC hybrid scaffold induced the decrease of the average diameter of the fibers from 1116 ± 290 to 828 ± 290 nm (Table 4). Concerning the ElNGP electrospun hybrid scaffold obtained after the addition of the EX15 peptide, neither the fibrillar nor the interconnected porous microstructures were affected (Fig. 19C).[166,171] Analogous to GP, the cross-linking reaction triggered the curling of fibers (Fig. 19F) with the average diameter growing from 823 ± 216 to 1176 ± 344 nm (Fig. 20E,F). To evaluate if the average diameter values found were statistically different from each other, statistical analyses were performed using the one-way ANOVA method and Tukey's test (Fig. 21).
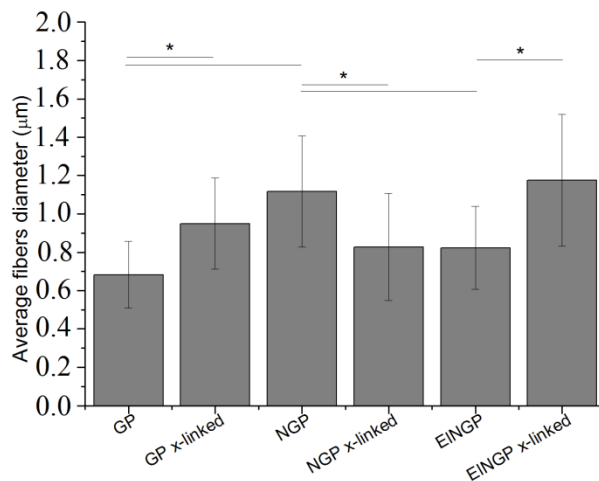
Figure 21: Fiber diameter comparison among the hybrid electrospun scaffolds. (*p ≤ 0.01).

The results showed that the average diameters of the fibers of uncross-linked scaffolds are statistically different from those of cross-linked samples. The different morphology of cross-linked fibers, different in orientation and size, is an indirect proof of the accomplishment of the cross-linking reaction. The persistence of porous interconnected structures could make these scaffolds appealing as biomedical devices able to assure oxygen and vapor permeation. Furthermore, the fibrillar organization mimics the natural ECM matrix hierarchically organized in fibrillar structures of different sizes from El, collagen, and polysaccharides. These features could make the produced scaffolds appealing for wound dressing. As a matter of fact, wound dressings are required to absorb exudates and at the same time to ensure oxygen permeation. MacLellan and co-workers reported that scaffolds presenting ~880 nm fiber diameter might be optimal for soft tissue engineering applications,[172] even if the assessment of the best fibril size is difficult to claim from the perspective of the wide pool of potential polymers to use, while antibacterial dressings with fiber diameters ranging from 0.2 to 3 µm showed healing efficacy.[173] Furthermore, the addition of CNCs to GP led to a significant increase of the average diameter of the fibers, with p* ≤ 0.01 (from 683 ± 174 to 1116 ± 290 nm, Table 5). This finding is probably due to an increase in the polymer solution viscosity,[174] in agreement with literature data on electrospun blends made of PLGA[175] at different percentages of CNCs; however, CNCs have also been suggested to induce the opposite effect on the fiber diameter through their reduction.[176,177] This behavior could be explained by an increase of electric conductivity of the polymer solutions. As a matter of fact, CNCs are usually produced through acid hydrolysis of cellulose, generally through H_2SO_4,[62] leaving sulfate groups on them, causing an increase of the electrical charge and,

consequently, the electrical conductivity of the electrospun solution and a decrease in the average diameter of the fibers. These two different effects act in opposition to each other: in the case of NGP, the increase in the polymer solution viscosity prevailed on enhanced electrical conductivity. On the contrary, the addition of EX-15 peptide led to a significant decrease of the average diameter of fibers according to Swindle-Reilly et al.,[178] who reported electrospun scaffolds composed of a PCL/El blend in HFP having a diameter of fibers that is significantly smaller than that of neat PCL ones, due to peptide incorporation into the fiber network. Generally, porosity dictates cellular infiltration and tissue ingrowth into the scaffolds.[179] Looking at literature, Ameer et al. have presented many strategies to tune electrospun scaffold porosity to enhance the cell response in tissue engineering.[180] The porosity of scaffolds studied in this work has been evaluated, and the results summarized in Table 5 together with statistical analysis in Fig.22.
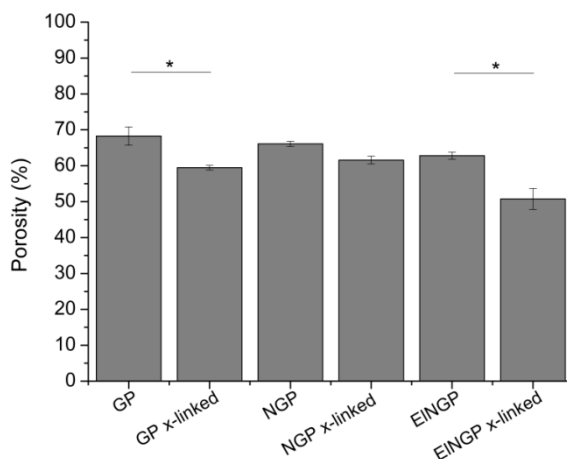
Figure 22: Histogram of porosity values found for electrospun scaffolds. (*p ≤ 0.05).

Uncross-linked and cross-linked scaffolds showed similar porosity: GP, NGP, and ElNGP displayed calculated values of 68 ± 2, 66.1 ± 0.7, and 63 ± 1%, respectively, with a decrease for their cross-linked scaffolds (59.5 ± 0.6, 62 ± 1, and 51 ± 3% for GP, NGP, and ElNGP, respectively). Statistical analysis showed that the decrease was significant only for GP and ElNGP scaffolds, and that the cross-linking reaction induced a slight decrease of porosity in all electrospun scaffolds. Cross-linking of the scaffolds by the EDC/NHS protocol performed in ethanol/water solution determined a variation in fiber diameters and porosity due to a macroscopically evident shrinkage. Fig. 23 exhibits a scaffold showing a shrinkage of the diameter from 9 to 4.5 cm after cross-linking. Other authors observed similar findings, which are particularly evident in scaffolds containing a high content of GE.[154,181] GE hydrogels in ethanol concentrations >40% (v/v) exhibited a volume shrinkage that can be extended to values of 25–50%.[182] Plausibly, the cross-linking reaction performed at a high ethanol concentration (85%, v/v) determined a shrinking effect on GE, ascribed to deswelling. In the case of microfiber shrinkage, a decrease in the fiber length translated into an increase in the fiber diameter,[182] a reduction of porosity, and a higher density of the scaffold.

Figure 23: Shrinkage of the electrospun scaffold after the cross-linking reaction (NHS and EDC·HCl = 45.0 mM in 85.5% ethanolic solution, RT, overnight).

2.3.8 Swelling Test and Contact Angle Measurements

The swelling test was carried out on the cross-linked scaffolds to evaluate their capacity to absorb water, thereby indirectly testing their hydrophobicity degree. The average swelling of the scaffolds, expressed in terms of percentages and calculated according to eq. 4, afforded values of 374 ± 28, 449 ± 26, and 607 ± 52% for GP, NGP, and ElNGP scaffolds, respectively (Table 5), thus demonstrating the progressive increase of wettability with CNCs and El contents. Statistical analysis was performed on these values using Student's t-test (Fig. 24), displaying a statistical difference (*p ≤ 0.01).
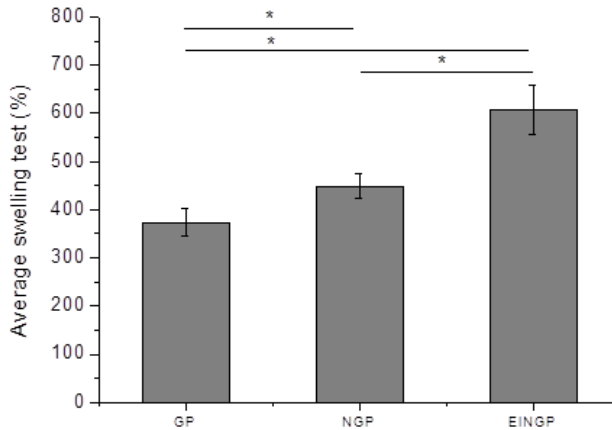
Figure 24: Histogram of the average swelling test (%) for the various types of cross-linked electrospun scaffolds (*p ≤ 0.01).

Even if in a speculative way, the rationale for the observed increase of wettability with CNCs and EX15 is the onset of hydrogen bonding network between water, cellulose hydroxyl moieties, and peptide polyamide groups. Nevertheless, all electrospun scaffolds showed strong hydrophilicity due to their swift water drop absorption (less than 2 s), during contact angle measurements. That finding is worth noting if we consider that PDLLA, similar to PLA, is usually considered highly hydrophobic. Therefore, we successfully modified the physical characteristics of hybrid electrospun scaffolds by mixing polymers having complementary properties: the highly hydrophilic polymers GE, CNCs, and EI mitigated the hydrophobicity of PLA. In summary, even if with some differences, all scaffolds showed total wettability, suggesting their employment as a wound dressing material, as a low degree of hydrophobicity is the best for biomedical devices. Highly hydrophilic wound dressing, indeed, prevents scab formation and dehydration of the wound bed.[184]

2.3.9 Uniaxial Tensile Testing

In order to evaluate the mechanical properties, uniaxial tensile testing on cross-linked GP, NGP, and ElNGP scaffolds was conducted. Young's modulus and ultimate tensile strength calculations were carried out on dry and swollen scaffolds (Table 5).

Table 5: Values of the Young's modulus, ultimate tensile strength and elongation at break calculated for the electrospun scaffolds before and after the swelling test (n = 16).

Scaffold	Young's modulus (MPa)	Ultimate tensile strength (MPa)	Elongation at break (%)
GP	87 ± 13	6.5 ± 0.6	57.2 ± 32.6
GP after swelling	24 ± 4	4.0 ± 0.3	> 120%
NGP	75 ±14	6.2 ± 0.4	104.0 ± 18.1
NGP after swelling	27 ± 3	4.1 ± 0.3	> 120%
ElNGP	75 ± 15	6.3 ± 0.3	113.8 ± 8.3
ElNGP after swelling	23 ± 4	4.0 ± 0.2	> 120%

Young's moduli were calculated from the linear elastic portions of stress versus strain curves (see for example Fig. 27), in particular between 1 and 5% of strain in the dry state and from 3 to 7% of strain in the swollen state. They were 87 ± 13, 75 ± 14, and 75 ± 15 MPa for dry GP, NGP, and ElNGP, respectively. Moreover, statistical analysis (Fig. 25A) evidenced that for NGP and ElNGP, Young's modulus is significantly different from GP (p* ≤ 0.05), inferring an influence of CNCs.
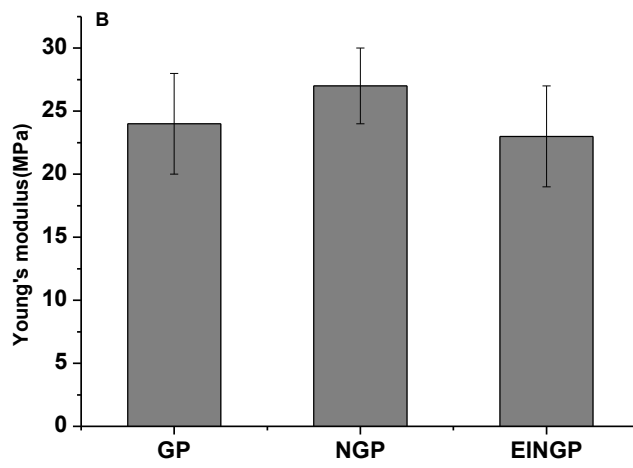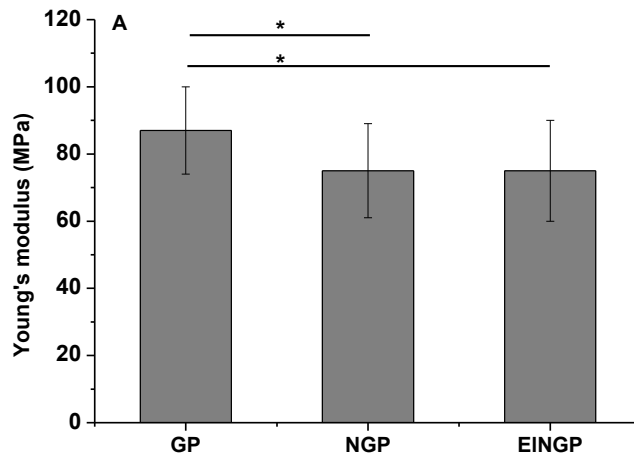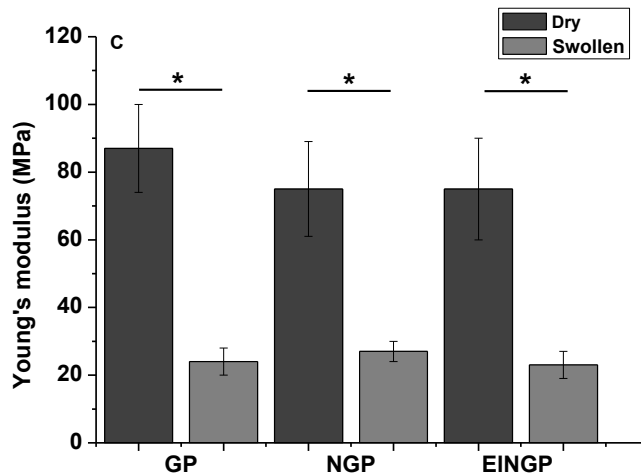
Figure 25: A-C. Young's modulus values: (A) dry scaffolds; (B) swollen scaffolds; (C) comparison of Young's modules of dry and swollen scaffolds. (*p ≤ 0.05).

As recently reported,[185,186] the addition of small percentages of CNCs to PLA (5% based on the weight) led to an increase of the Young's modulus and tensile properties as well. Conversely, for values higher than 5%, a decrease in the Young's modulus has been observed, probably because of the self-aggregation of CNCs in electrospun fibers being responsible for the weakening of the cohesion among them.[186] It is well known that the source of CNCs and their production should be taken into account, as they affect the rheology of the electrospun solution and then the mechanical properties of the final fibers. In the present study, commercial CNCs employed presented a low aspect ratio, with shear thinning behavior. The increase of the viscosity in comparison with neat PLA, as reported by Hamad and co-workers,[187] generally affects the fiber diameter of electrospun scaffolds. It, in turn, influences the mechanical properties. CNCs were

added at a final concentration of 8.3% (w/w) in the NGP scaffold and 8.2% (w/w) in the ElNGP scaffold expressed on the total mass of the remaining components in polymer solutions inducing the decrease of Young's modulus. That finding is important because we suggested that it is possible to modify the scaffold elasticity and optimize the mechanical properties of PLA-based scaffolds. After swelling the scaffolds in water, a dramatic change in the Young's modulus value was observed, affording 24 ± 4, 27 ± 3, and 23 ± 4 MPa for GP, NGP, and ElNGP scaffolds, respectively. The values observed by comparing the dry state with the swollen ones were significantly different ($p* \leq 0.05$) (Fig. 25B, C), and swollen scaffolds appear more elastic. Young's modulus values are compatible with those found for scaffolds with applications in soft tissue engineering, such as, for example, of natural skin showing a tensile modulus of 15–150 MPa compatible with our scaffolds having Young's modulus within this range.[188] Ultimate tensile strength (UTS values), calculated from the maximum points of the stress versus strain curves in the plastic region, in the dry state were 6.5 ± 0.6, 6.2 ± 0.4, and 6.3 ± 0.3 MPa for GP, NGP, and ElNGP scaffolds, respectively. The corresponding swollen scaffolds showed UTS values of 4.0 ± 0.3, 4.1 ± 0.3, and 4.0 ± 0.2 MPa, respectively. However, also in that case, changes were not significant ($p > 0.05$) (Fig. 26A,B). On the contrary and analogous to Young's modulus, UTS values of dry scaffolds significantly differ from swollen samples ($p* \leq 0.05$) (Fig. 26C).
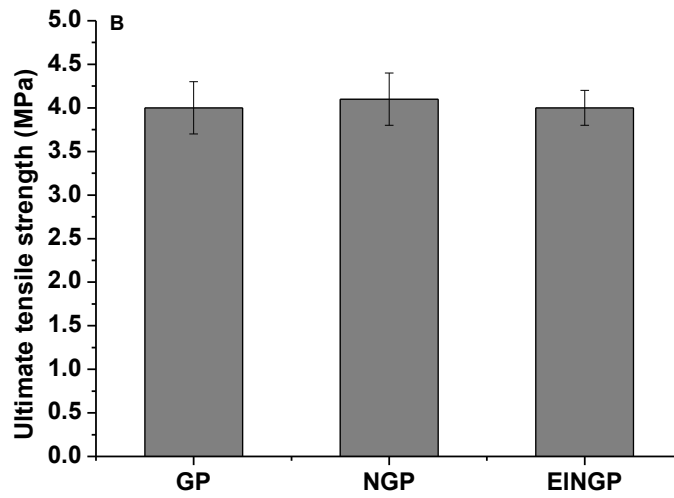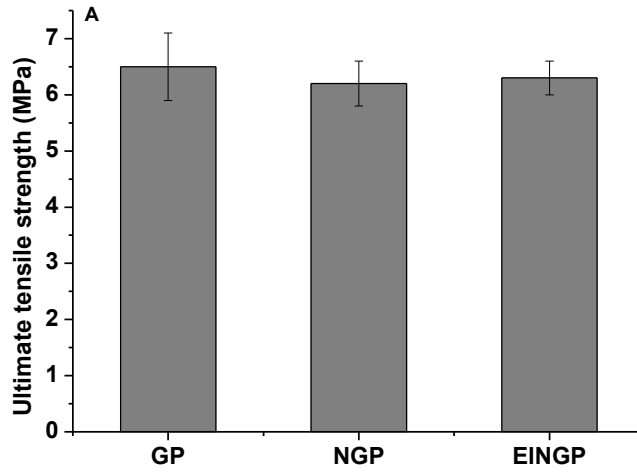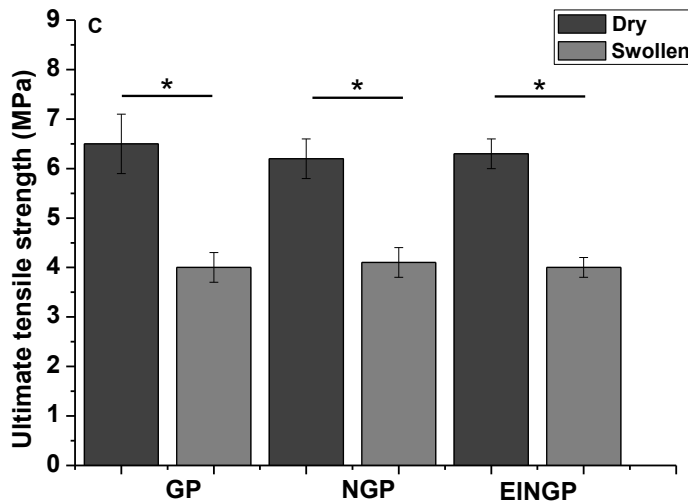
Figure 26: A-C. Ultimate tensile strength (UTS) values of: (A) dry scaffolds; (B) swollen scaffolds; (C) comparison of Ultimate tensile strength of dry and swollen scaffolds; (*p ≤ 0.05).

Once the breaking load is reached, the stress versus strain curve undergoes a sharp downward descent until it reaches the sample breaking, identified, in the dry state, from the point where the curve begins to flatten (Fig 27A, C, E). In this way the elongation at break of the samples was calculated. It is interesting to note that NGP and ElNGP scaffolds show the greatest elongation at break in the dry state [elongation (%) = 57 ± 33, 104 ± 18, and 114 ± 8% for GP, NGP, and ElNGP], respectively, as shown in Table 5 and Fig. 27C,E in comparison to GP (Fig. 27A). In the swollen state the three scaffolds display maximum elongation at break [elongation (%) > 100 for GP, NGP, and ElNGP] (Fig. 27B,D,F).
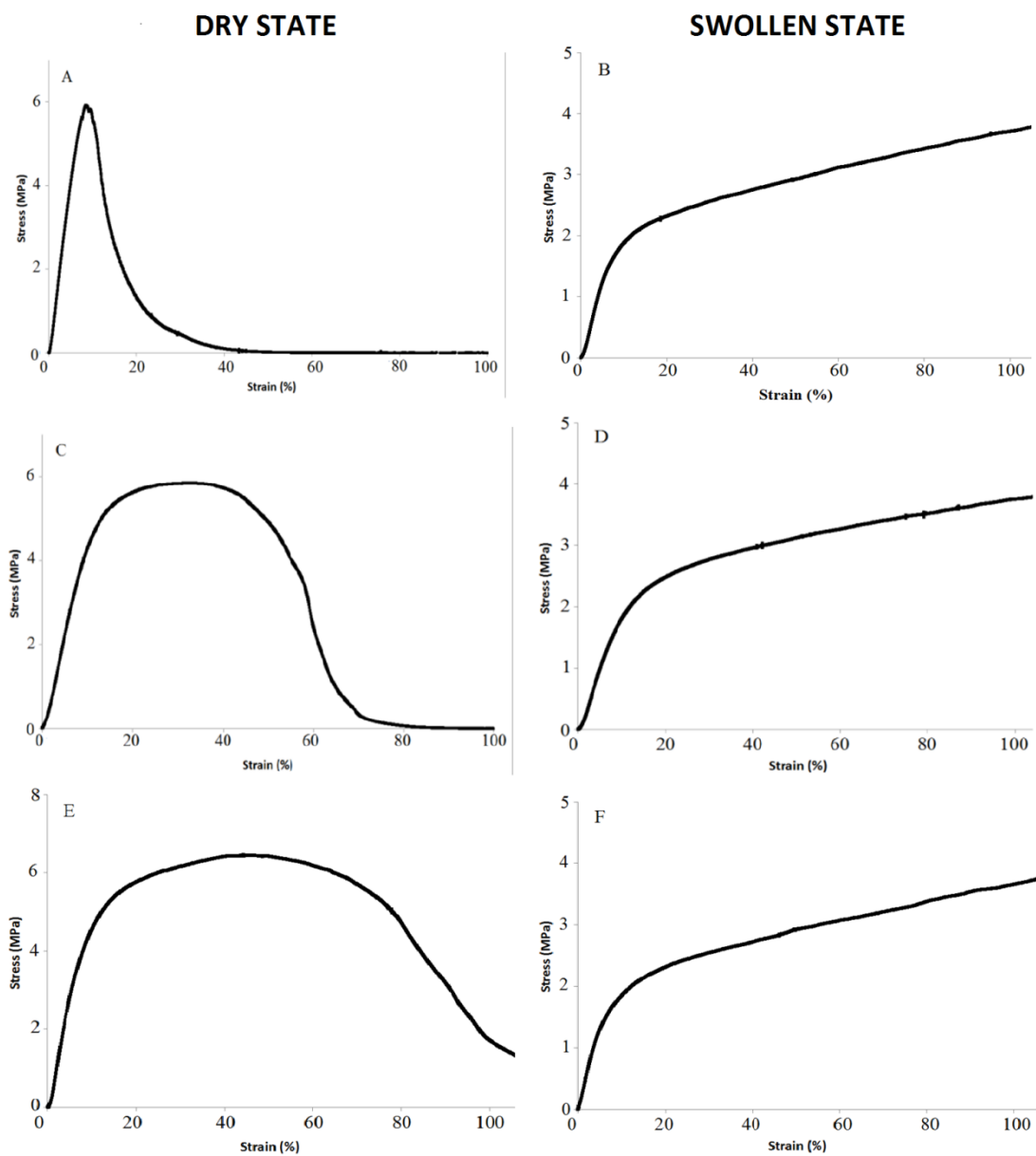
Figure 27: Representative stress-strain curves for electrospun scaffolds before swelling (left column) and after swelling (right column): GP (A,B), NGP (C,D), ElNGP (E,F).

Studies of MacLellan and co-workers, in the production of electrospun PCL-composite scaffolds for soft tissue engineering,[172] reported that electrospun GE scaffolds presented, in the dry state, correspondingly higher tensile strength and lower brittleness than those containing collagen and El. Our scaffolds in the dry state, as well, showed UTS values along the same lines varying from ~6 to ~4 MPa after swelling. Plasticizers can increase the free volume between the polymer chains leading to greater chain mobility and film flexibility. Generally, El exerts its elastic function in a solid- although in a swollen state-when immersed in water. The aqueous solvent interacts with the amorphous regions of the protein. Actually, water and polar solvents such as dimethylsulfoxide exert a plasticizer effect on El, that is, they facilitate the localized movements of the polypeptide chains.[189] In our case, the polar solvent destructures the β-sheet of EX15.[57] The consequence is the increase of the entropy of the system and the onset of the entropic elastomeric force. The addition of a plasticizer would increase the elongation. NGP and ElNGP, indeed, exhibit higher elongation at rupture than that of the GP hybrid scaffold in the dry state (Fig. 27A,C,E). Moreover, a plasticized polymer would be less resilient and would deform at a lower force than without the plasticizer. The Young's modulus is the slope of the linear section on the stress–strain curve where a polymer undergoes elastic deformation, and because there is greater chain mobility with the addition of a plasticizer, there is less resistance to deformation, hence a lower Young's modulus is expected.[190] These considerations explain why CNCs and El hybrid scaffolds are less brittle in the swollen state. Nevertheless, our data are in good agreement with data inferred for microfibrillated cellulose incorporating materials acting as a plasticizer.[191] Water instead acts as a sort of normalizer for the different typologies of scaffolds

because all swollen electrospun scaffolds reach a plateau with an elongation (%) > 100% at break (Fig. 27B,D,F). This behavior is in accordance with previous data.[155]

2.3.10 Cytotoxicity Assay

The results of the cytotoxicity assay showed no negative influence of the polymer extracts on the metabolic activity of NIH/3T3 cells (Fig. 28).
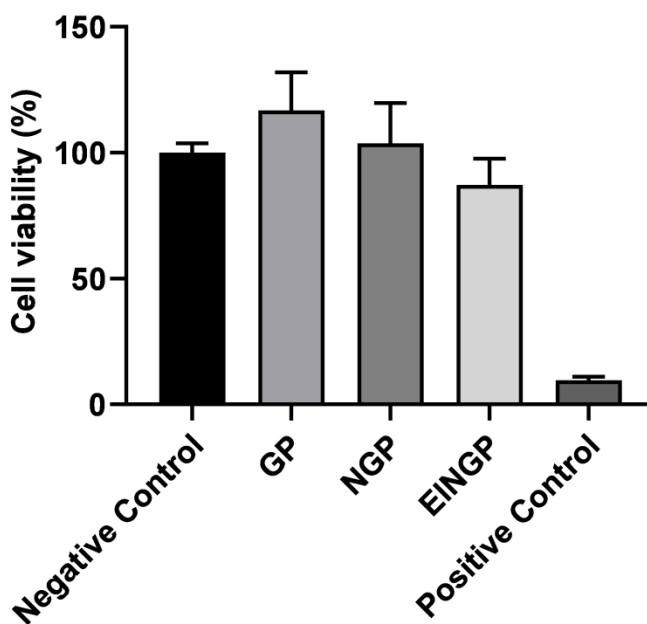
Figure 28: Cytotoxic assay of different cross-linked electrospun microfibers on the metabolic activity of NIH/3T3 cells (n = 3).

The cells in the extraction medium of GP and NGP showed an even higher metabolic activity (117 and 104%, respectively) than the negative control. However, the difference was not significant. Only the metabolic activity of cells in

the ElNGP-extracted medium was slightly lower than that in the negative control (87%). According to ISO 10993-5:2009, the extract shows no cytotoxic potential if the relative viability is not reduced below 70%. This condition was met in this cytotoxicity test for all three polymers. The scaffolds were spun out of polymers, which were previously described as mostly biocompatible. Even if PLA, which is approved by the FDA for use in medical devices, is highly biocompatible,[192] to the best of our knowledge, only data regarding the cytotoxicity of poly(D/Llactide-co-L-lactide) have been reported;[193] that finding required a cytotoxic assay on PDLLA, which shows faster degradation than the semicrystalline PLA. In combination with GE, no cytotoxic effects on human skin fibroblasts were observed.[155] The influence of CNCs on cells is described rather controversially. No cytotoxicity on fibroblast cells was observed for CNCs with PLGA,[194] PLA, and PBS matrices.[195] Nanofibers based on PLA and CNCs proved to be biocompatible.[196,197] However, the cytotoxic effect at high- CNC concentrations was described as well.[198] Electrospun El in combination with silk[199] and collagen[150] showed the absence of cytotoxicity.

2.3.11 Cell Attachment and Proliferation

The cell culture on different scaffold types showed the attachment and proliferation of L929 cells for different time points (Fig. 29).
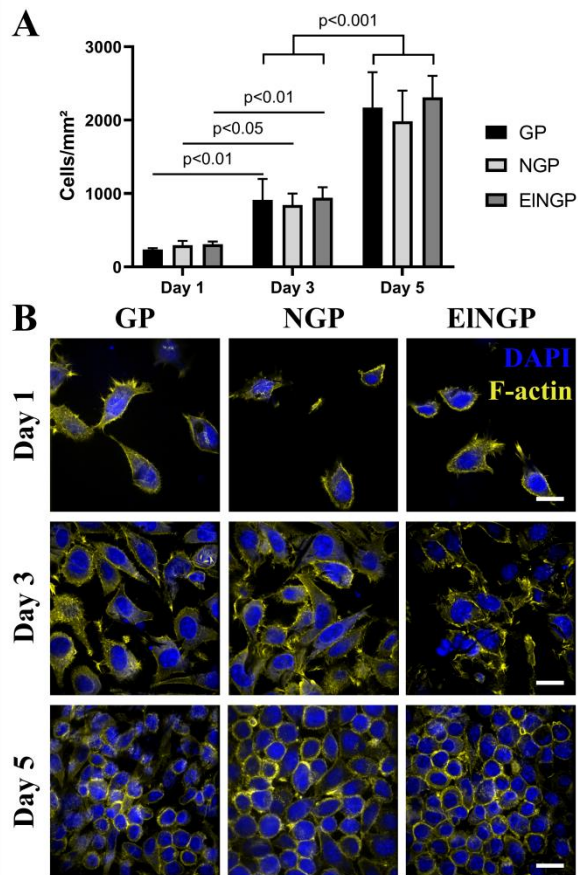
Figure 29: Attachment and proliferation of L929 cells on different scaffold types GP, NGP, and ElNGP. (A) Quantification of attached L929 cells after 1, 3, and 5 days. Two-way ANOVA, n = 3. (B) Nucleus and F-actin staining of L929 cells. Scale bar equals 20 μm.

It turns out that the cells adhered to and spread on the surface of all scaffold types from day 1 to day 5. There was a significant increase in cell densities for all scaffold types over the entire culture period (Fig. 29A, Table 6).

Table 6: Statistical analysis of the cell count on the scaffolds. Comparison between the different scaffold types and between the different time points using a Two-way ANOVA. P-values are shown.

Scaffold comparison	Day 1	Day 3	Day 5
GP vs. NGP	0.8013	0.7271	0.1557
GP vs. ElNGP	0.7229	0.9530	0.3080
NGP vs. ElNGP	0.9896	0.5512	**0.0106**
Time comparison	**GP**	**NGP**	**ElNGP**
Day 1 vs. Day 3	0.0057	0.0216	0.0090
Day 1 vs. Day 5	<0.0001	<0.0001	<0.0001
Day 3 vs. Day 5	<0.0001	<0.0001	<0.0001

Whereas at day 1, only few cells were observed on the scaffold surface, at day 5, the cells reached confluence on all scaffold types. It should be noted that the cells do not detach, even at a high cell density. Besides, it shows no significant different number of adherent cells between the scaffold types except on day 5 NGP versus ElNGP (1986 ± 415 cells/mm^2 vs 2312 ± 290 mm^2, $p < 0.05$). The F-actin staining of L929 showed a stretched morphology of the cells at day 1 and day 3, whereas the cells at day 5 form a roundish morphology (Fig. 29B). The change in the cell morphology corresponds to the behavior of L929 cells, as shown by Hong et al.[200] and Koegler et al.[201] In conclusion, this work confirmed the findings from previous studies, which showed that electrospun scaffolds made of materials such as GE, El, and CNCs have good biocompatibility in terms of cell attachment and proliferation.[150,155,202]

Chapter 3: Thermal and mechanical characterization at Université Paul Sabatier-Toulouse.

3.1 Aim of the work

The results obtained by uniaxial tensile test on NGP and ElNGP electrospun scaffolds containing 8.0% (w/w) of CNCs (expressed on the total mass of the remaining components in polymer solutions) inferred for the crucial role played by CNCs on the mechanical properties of the scaffolds. Actually, Young's modulus decreased after the addition of CNCs making less brittle and more plastic the scaffolds. According to Shi[185] and Zhou,[186] CNCs amount in hybrid scaffolds strongly affects the properties of matrices as a function of CNCs percentage with 5 % (w/w) as threshold value. Generally, percentages of 1, 2 and 5 % (w/w) trigger the increase of Young's modulus and tensile properties as well. Probably, at percentages higher than 5 % (w/w), self-aggregation of CNCs in PLA electrospun fibers occurs, leading to the weakening of the cohesion among them and therefore to the decrease of Young's modulus.[185] On that basis, we prepared electrospun scaffolds at variable percentages of CNCs. Polymer mixtures at 1, 3, 5% of CNCs were prepared, electrospun and cross-linked (Table 7).

The thermal and mechanical properties of matrices were studied at CIRIMAT, Universitè Paul Sabatier, Toulouse (France) during the six months spent abroad.

ThermoGravimetric Analysis (TGA) investigated thermal properties and the hydrophilic degree of the electrospun scaffolds, while Differential Scanning Calorimetry (DSC) assessed the physico-chemical changes as a function of

warming and cooling. Finally, Dynamic Mechanical Analysis (DMA) was used in order to investigate mechanical properties of the samples.

In this chapter, the results obtained by using TGA, DSC and DMA techniques are described.

Table 7: Composition of polymeric blends used for scaffolds fabrication at different percentages of CNCs. GP = gelatin/poly(lactic acid), 1, 3, 5, 8NGP = 1, 3, 5, 8% (w/w) cellulose nanocrystals/gelatin/poly(lactic acid) and El8NGP = EX15 elastin-like peptide/8% (w/w) cellulose nanocrystals/gelatin/poly(lactic acid). The suffix k was used in order to indicate the cross-linked scaffolds.

Sample name Uncross-linked/cross-linked	Gelatin (GE) mass (g)	Poly(DL-Lactic Acid) (PDLLA) mass (g)	Cellulose nanocrystals (CNCs) mass (g)	Elastin peptide (EX15) mass (g)	Solvent (HFP) volume (ml)
GP/GPk	0.090	0.27	/	/	3.0
1NGP/1NGPk	0.090	0.27	0.0036	/	3.0
3NGP/3NGPk	0.090	0.27	0.0108	/	3.0
5NGP/5NGPk	0.090	0.27	0.018	/	3.0
8NGP/8NGPk	0.090	0.27	0.030	/	3.0
El8NGP/El8NGPk	0.090	0.27	0.030	0.0039	3.0

3.2 Materials and Methods

3.2.1 ThermoGravimetric analysis

ThermoGravimetric analysis (TGA) follows the evolution of the sample during a linear temperature ramp in temperature under controlled atmosphere. This method tells us about the thermal stability of materials and it is used for example to determine the percentage of hydration of the sample.

In a classic thermogram, the percentage of mass as well as the derivative of the mass with respect to the temperature are represented as a function of the temperature. Depending on the samples, we can observe on these thermograms a departure of water, a decomposition or a degradation and they are unique for each compound. These phenomena are observed in the form of a sigmoid on the signal of the mass percentage, and a peak on the signal of the derivative. In general, generic thermogram can be divided in sections:[203]

• below 150 °C there is the release of physisorbed water, low molecular weight volatile compounds, solvents and trapped gases;

• between 150 °C - 250 °C, a mass loss happens because chemisorbed water and low molecular weight compounds like additives and volatile decomposition products leave from the sample;

• at temperature above 250 °C, compounds begin to decompose between the onset and endset temperature. Multiple onset and endset temperatures are possible for multi-component systems and for reactions with intermediate steps;

• non-volatile inorganic ashes and metals are included in the remaining material above the endset temperature;

• if you are working in an oxidizing environment, metallic compounds increase their oxidation state and gain mass.

TGA is often coupled with FTIR spectroscopy, because in this way it is possible to identify the gaseous effluents in real time when the temperature rises.

In Fig. 30 an example of a thermogram is shown:
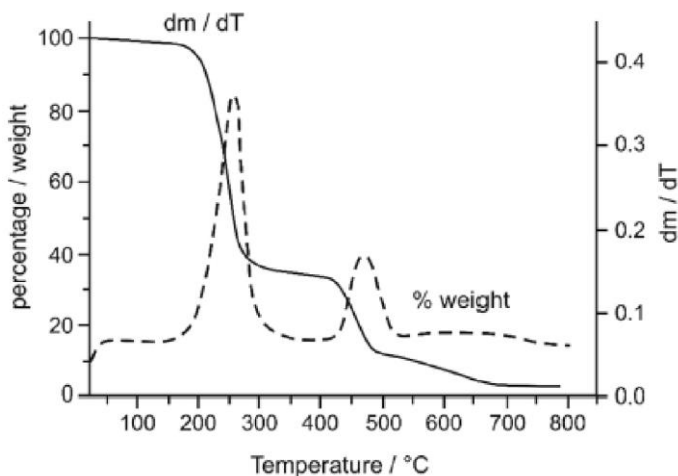
Figure 30: Thermogram derived from TGA of cashew nutshell liquid.[204]

Thermal stability of the electrospun scaffolds were carried out by ThermoGravimetric Analysis using a Q50 device (TA Instruments, New Castle, DE, USA). Samples with a mass between 5 mg and 7 mg were cut from the board of the scaffolds and placed into the instrument under a synthetic air flow of 10 mlmin^{-1} (oxidizing atmosphere). They were heated from room temperature to 700 °C at 10 °Cmin^{-1}. Three samples were analyzed for each electrospun scaffold.

3.2.2 Differential Scanning Calorimetry

For the study of phase transitions, a differential calorimeter was used. The studied and reference samples are heated at constant rate in order to maintain both temperature identically. On DSC thermogram the necessary heat flow dH/dt is recorded versus temperature T. The heat variation dH exchanged by the sample during the transition induced by the temperature variation dT is given by (eq. 8):

$$dH/dT = mCp$$

where m is sample mass and Cp the heat capacity. The first order transitions melting/crystallization appear on DSC thermograms as endo/exothermic peaks. This process is defined as a first order transition, because it presents a discontinuity in the first order derivative of the Gibbs free energy equations. The pseudo second order transitions (glass transitions) are associated with a step on base line. The glass transition temperature was determined as the temperature position midpoint of the heat capacity increment (inflection point).

The phase transition thermograms were recorded with a Perkin Elmer DSC7 (Waltham, MA, USA). The temperature and energy scales were calibrated using the manufacturer's instructions with Indium and Tin as standards. Samples with a mass ranging between 4 mg and 7 mg were cut from the board of the scaffolds and were sealed in aluminum pans under Nitrogen. Empty pans were used as references. Investigations were performed on two heating scans between 30 °C and 200 °C at a rate of 20 °Cmin^{-1}, and two cooling scans from 200 °C to 30 °C at a rate of -20 °Cmin^{-1}. DSC was conducted also after the swelling test at low temperatures. The instrument used was a Diamond DSC of Perkin Elmer (Waltham, MA, USA). Samples were placed into the pans and then, 30 μl of ultrapure water were put into them for 60 minutes in order to reproduce the

swelling test. After, samples were placed in the DSC instrument under Helium flow. Two cooling rates has been performed, the first one between 25 °C and -120 °C, the second one between 80 °C and -120 °C at a rate of 10 °Cmin^{-1} and two heating scans from -120 °C to 80 °C and from -120 °C to 85 °C at a rate of 10 °Cmin^{-1}.

3.2.3 Dynamic Mechanical Analysis (DMA)

In Dynamic Mechanical Analysis (DMA) a small deformation is applied to a sample in a cyclic manner, with a response of the materials to stress, temperature, frequency and other values to be studied. This technique is often referred to as dynamic mechanical thermal analysis (DMTA), dynamic mechanical spectroscopy, or dynamic thermomechanical analysis. Furthermore, it is estimated to have a sensitivity to the glass transition 100 times higher than DSC and it can resolve other more localized transitions such as side chain movements that are not detected in the DSC.

In Dynamic Mechanical Analysis, a constant, sinusoidal load is applied on a sample: the consequent deformation will be sinusoidal and reproducible if the material is deformed within its linear viscoelastic region. For any point of the curve, the applied stress can be described by (eq. 9):

$$\sigma = \sigma_o \sin \omega t$$

in which σ is the stress at time t, σ_o is the maximum stress, ω is the frequency of oscillation, and t is the time. The resulting strain wave shape will depend with both viscous and elastic behavior of the sample.

In the linear region σ (the stress) and ε (the strain at any time t) are related by the modulus E and the relationship is (eq. 10):

$$\varepsilon(t) = \varepsilon_o \sin(\omega t)$$

where ω is the frequence, ε_o is the strain at the maximum stress and t is the time. The difference between the applied stress and the resulting strain is an angle δ, resulting in a change of the previous equation (eq. 11):

$$\varepsilon(t) = \varepsilon_o \sin(\omega t + \delta)$$

Using trigonometry, this equation can be separate in two parts, the first one representing the in-phase strain while the second one is the out-of-phase strain.

Also the modulus can be express as the in-phase component, the storage modulus E' or G', which is the measure of the sample's elastic behavior and the out-of-phase component, the loss modulus E'' or G'', characteristic of the sample's plastic behavior. The ratio between the loss and the storage is the tan delta, also known as damping and it is a measure of the energy dissipation of a material.[205]

It is possible to conduct DMA experiments also at different temperatures, in order to have the values of E' and E'' also as a function of the temperature, thus obtaining thermograms.

In Fig 31 an example of a DMA thermogram is shown:
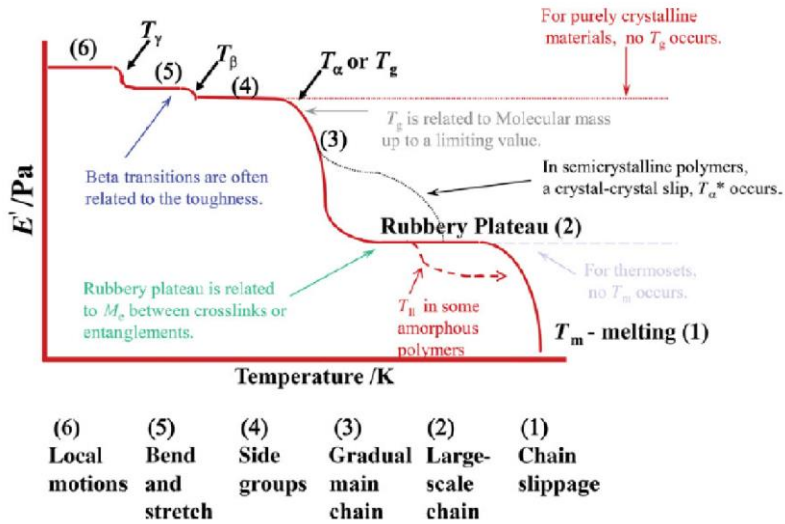
Figure 31: Extracted of idealized DMA thermogram.[206]

In a typical DMA thermogram, it is possible to note, at low temperatures, the so-called gamma transition Tγ, associated with localized bond movements (bending and stretching) and side chain movements. With the increase of the temperature, starts to be enough space for the motions for the whole side chains and localized groups of four to eight backbone atoms and the material starts to develop some toughness. This transition, called the beta transition Tβ, can be affect by the water content. As heating continues, the chains in the amorphous regions begin to coordinate in large-scale motions and therefore mechanical manifestation of glass transition Tα appears. Increase of temperature drives the material through the Tα* and T$_{ll}$. The first one occurs in crystalline or semicrystalline polymer and is a slippage of the crystallites past each other, while the second one is a movement of

coordinated segments in the amorphous phase that relates to reduced viscosity. Finally, there is the melting of the sample (T_m).[206]

Dynamic Mechanical Analysis was conducted on electrospun scaffolds using an ARES G2 strain-controlled rheometer (TA Instruments, New Castle, DE, USA). Samples dimensions were of 35 mm × 12.5 mm with a thickness of 0.3 mm for the non-cross-linked scaffolds and of 0.7 mm for those cross-linked. The scaffolds were analysed in tensile geometry mode and the temperature range of the heating scans was from 0 °C to 80 °C at a heating rate of 3 °Cmin^{-1}. The strain and the frequency were fixed at 0.03 % and 1 Hz respectively within the material linearity range. $E'\omega(T)$ (elongational storage modulus) and $E''\omega(T)$ (elongational loss modulus) were determined.

3.3 Results and discussion

In this chapter, the results obtained by using TGA, DSC and DMA techniques are described.

3.3.1 Thermal stability

In order to analyze the thermal stability of the samples, ThermoGravimetric Analysis was carried out under oxidative atmosphere (synthetic air flow). For each electrospun scaffolds, three analysis were done.

In fig. 32 a comparison between TGA thermograms of respectively GP, 8NGP and El8NGP scaffolds is presented.
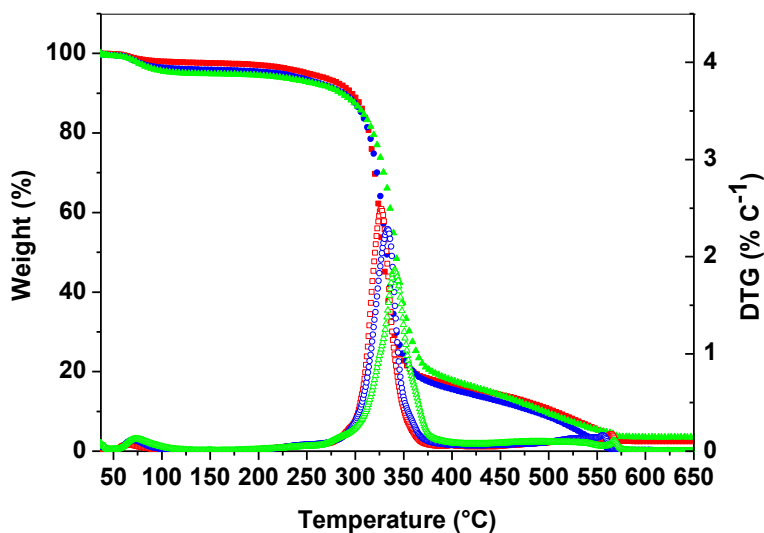
Figure 32: Comparison of thermal behavior by TGA thermograms of the three typologies of the electrospun scaffolds. Loss mass and derivated loss mass are reported (10 °Cmin^{-1}). Square (red), circle (blue) and up triangle (green), represents GP, 8NGP and El8NGP

samples respectively. Loss mass is reported as filled symbols, while derivated loss mass is reported as empty symbols.

This graph shows the normalized weight and the Derivative ThermoGravimetric (DTG) curves in function of the temperature. On GP scaffold (Fig. 32), three main thermal phenomena were noted. The first one was observed at a maximum of intensity at about 63 °C due to the loss of the water present in the matrix. In fact, despite PDLLA is essentially a hydrophobic polymer, the presence of the hydrophilic regions of gelatin increased the ability of the electrospun scaffold to bind water. In literature this desorption phenomenon was observed when gelatin was electrospun.[207] The main degradation started at temperature around 250 °C and reached a maximum of intensity at 327.1 ± 0.3 °C, (Table 8) with the loss of about 80 % of the scaffold mass.

Table 8: Degradation temperature, calculated using derivated loss mass curves, and percentage of water lost calculated on the TGA thermograms (n = 3).

Scaffold	Degradation temperature (°C)	Lost water (%)
GP	327.1 ± 0.3	- 2.2
GPk	327.4 ± 0.7	~ 0
1NGP	332.6 ± 0.5	- 4.3
1NGPk	333 ± 2	- 1.8
3NGP	338 ± 2	- 5.1
3NGPk	330 ± 6	- 1.7
5NGP	329 ± 4	- 4.4

5NGPk	326.1 ± 0.3	- 2.2
8NGP	331 ± 4	- 3.7
8NGPk	330 ± 5	∼ 0
El8NGP	335.8 ± 0.8	- 4.6
El8NGPk	334.1 ± 0.8	∼ 0

Subsequently, a high temperature degradation phenomenon (deriving from the oxidation of the first degradation residue) with a lower slope of the normalized weight curve, was present and led to the total decomposition of the sample, at a temperature around 560 °C. The same trend for 8NGP and El8NGP scaffolds can be noted, with an increase of the degradation temperature with the presence of elastin peptide (335.8 ± 0.8 °C).

CNCs have been used as nanofiller even in the case of electrospun scaffolds made up of gelatin.[208]

Electrospun scaffolds at different CNCs percentage were tested. The scaffolds named 1NGP, 3NGP and 5NGP, which contain a percentage of CNCs of 1%, 3% and 5% (w/w) respectively, presented thermograms very similar (data not shown). Table 9 shows the values of thermal degradation. For the first two typologies of mats, an increase of degradation temperature, which reached the maximum value of 338 ± 2 °C for the 3NGP scaffold was observed. This increased temperature with the presence of CNCs is in agreement with the works of Shi et al,[185] and Zhou et al,[186] on electrospun blends of PLA with different amounts of CNCs. When the amount of added CNCs became higher (scaffolds 5NGP and 8NGP) a decrease of the degradation temperature was observed.

Therefore, the presence of the CNCs, up to 3% (w/w) seems to improve the thermal stability of our matrices, probably due to char formation from CNCs before the thermal decomposition of GP scaffold, inhibiting the thermal conductivity and then leading to a decrease of the degradation temperature of these scaffolds.[209] In literature this behavior is described to be a threshold of thermal properties.[210]

Also the peptide effect seems to improve the thermal stability of the samples. As a matter of fact, if we compare 8NGP and El8NGP, we note an increase of 5°C for degradation temperature.

Fig. 33 shows the TGA thermograms before and after cross-linking reaction for 8NGP scaffold.
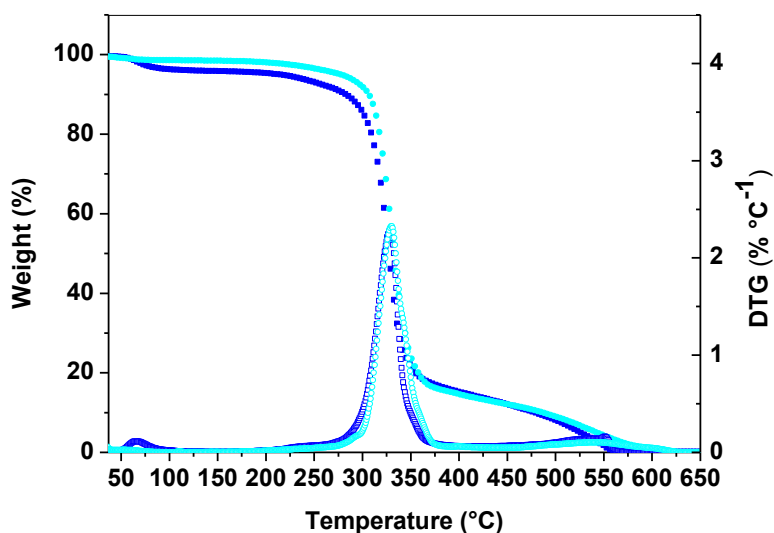
Figure 33: Comparison between the TGA thermograms of 8NGP electrospun scaffolds before (square/blue) and after (circle/cyan) cross-linking reaction. Loss mass is reported as filled symbols, while derivated loss mass is reported as empty symbols.

100

The main difference between these two samples was the water content in the matrix. The cross-linked scaffold did not show any loss of water in this case.

Table 9 suggests in which amount the quantity of water present in the electrospun scaffolds increases with the addition of CNCs and elastin peptide: 3NGP and El8NGP scaffolds showed the maximum percentage of water, 5.1% and 4.6% respectively. This behavior was probably due to the presence of the hydroxyl groups of CNCs and to the hydrophilic regions of the peptide, which can better form hydrogen bonds with water, leading to a higher hydrophilicity of the scaffolds. The finding that all the cross-linked samples showed a smaller presence of water can be explained by the fact that cross-linking induces a decrease of hydrophilic sites and of mobility.

3.3.2 Physical structure

Fig. 34 presents the first heating scans of non-cross-linked electrospun scaffolds (GP, 8NGP and El8NGP).
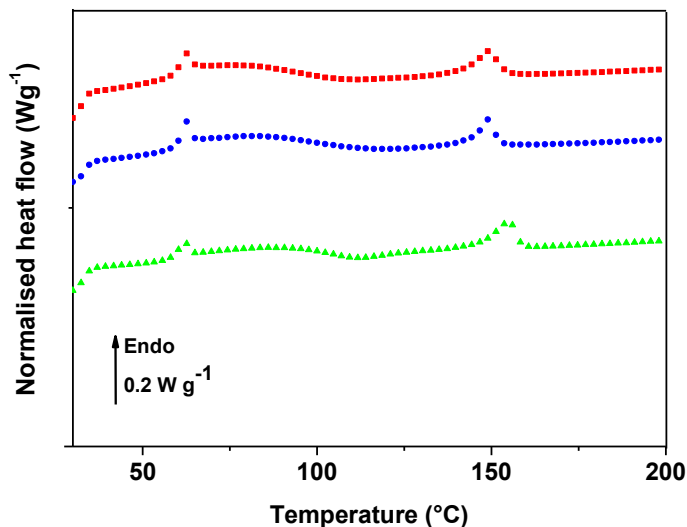
Figure 34: First heating thermograms of non-cross-linked electrospun scaffolds performed at 20 °Cmin^{-1}. Square (red), circle (blue) and up triangle (green), represents GP, 8NGP and El8NGP samples respectively.

The thermal parameters of all samples are reported in table 9.

Table 9: DSC measurements (1st and 2nd refer to first and second heating scan, respectively).

Scaffold	T_g (°C)		T_m (°C)		ΔC_p (J g^{-1} C^{-1})		χ_c (%)
	1st	2nd	1st	2nd	1st	2nd	
GP	56.6	51.7	148.9	/	0.6	0.3	19.6

GPk	61.9	50.7	149.0	/	0.8	0.2	15.9
1NGP	52.9	52.4	155.1	144.7	0.6	0.2	29.1
1NGPk	58.0	53.7	156.3	146.7	0.5	0.3	18.9
3NGP	54.0	53.8	155.3	149.1	0.6	0.2	24.2
3NGPk	54.4	44.6	154.7	/	0.7	0.2	19.0
5NGP	52.3	51.5	155.0	144.1	0.6	0.3	29.5
5NGPk	60.4	50.7	156.9	144.3	0.7	0.3	17.5
8NGP	58.7	53.2	149.0	/	0.8	0.3	13.8
8NGPk	63.3	52.4	156.2	145.7	0.7	0.2	20.0
El8NGP	57.8	54.8	154.9	145.1	0.5	0.3	16.3
El8NGPk	62.8	52.3	156.1	146.3	0.7	0.3	15.6

The scaffolds showed a glass transition temperature, near 56 °C associated with amorphous phase and a peak is superimposed on the heat capacity step attributed to the physical aging. We can note only one T_g, consistent with a good miscibility of the two polymers.

In GE/PLA blends Alippilakkotte noted that the miscibility was achieved when the gelatin was covalently grafted on the PLA surface.[54] Physical aging phenomenon was observed in all samples on the first heating scans and the Tg value was measured between 52.3 °C and 63.3 °C (Table 9).

The presence of interstitial water was confirmed by the broad complex endothermic peak located in a temperature range between 70 °C and 150 °C. At

high temperature, a melting peak was observed at around 149 °C indicative of crystalline phase.

Mukherjee et al obtained T_m values ranging from 102 °C to 104 °C from the analysis of pigskin gelatin.[211]

With the addition of CNCs, the melting temperature was measured between 149°C and 155°C. A similar T_m was registered by Muijca-Garcia et coworkers,[212] which prepared PLA-CNCs nanocomposite fibers via melt-spinning. It interesting to note that the addition of the elastin peptide drives to an analogous T_m value.

In the second heating scans the endothermic event at the glass transition vanishes and the data, listed in Table 9 show a good stability of glass transition temperature with the low level of CNCs, and a decrease of 5°C of T_g in scaffolds with 8% of CNCs or elastin peptide. The melting temperature decreased strongly when it can be measured.

In fig. 35 we compared the 8NGP scaffold first heating scan before and after cross-linking reaction.
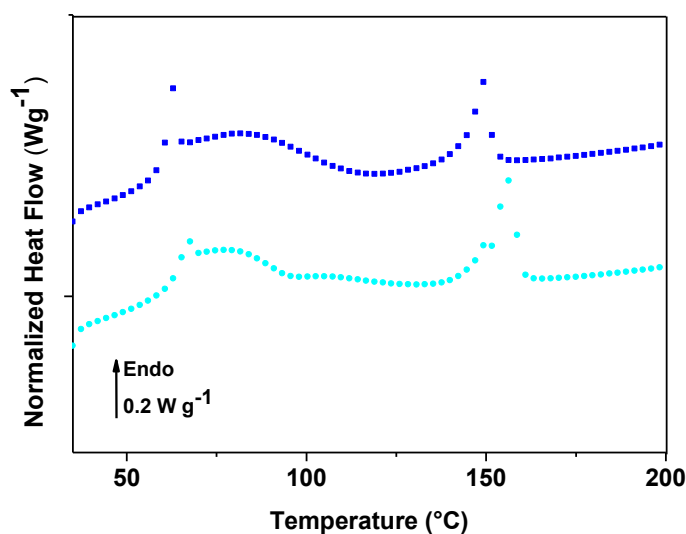
Figure 35: First heating DSC thermograms of 8NGP electrospun scaffolds before (square/blue) and after (circle/cyan) cross-linking reaction.

We can observe an increase of both thermal transitions, glass and melting. The values reported in Table 9 confirm this increase of thermal properties for all the samples. However, the crystalline phase (T_m values) was less affected than amorphous phase (T_g values) by the cross-linking.

In the second heating scans, the glass transition temperature of all the cross-linked scaffolds, decreases until 3NGPk when at higher CNCs concentrations T_g value increases again. This finding suggests that a percolation threshold phenomenon is present at 3 % CNCs (w/w). This phenomenon was observed for example when carbon nanotubes (CNTs) were added in polymeric matrices.[210,213] Finally, T_m value decreases at about 100°C in the second heating scan.

This study shows that the different products used for the scaffold formulation have a good miscibility. In the first heating ramp, we observed the sample fingerprint linked to process and composition. Physical aging phenomenon observed superimposed at the glass transition is due to the electrospinning process, and can make difficult the T_g measurement with good accuracy, this endothermic fingerprint vanishes with thermal cycling.

The addition of CNCs to PDLLA and GE in various ratio formed a hydrogen bonding network, restricting the segmental mobility retarding the cooperative motion of the polymer chains, and leading to the increase of glass transition temperature. A similar T_g behavior was observed by Cai et coworkers,[214] who produced electrospun scaffolds composed of Poly-DL-Lactic acid with a filler different from

CNCs, i.e. nanodiamonds. With elastin peptide the thermal response was unchanged.

A broad endothermic peak superimposed with several transitions [70°C, 150°C] was attributed to the vaporization of bound water.

Cross-linking treatment induces an enhancement of thermal parameters, T_g (excepted 3%) and T_m This result could be due to the effect of the cross-linking reaction of gelatin. In literature, we found analogous results when genipin cross-linked gelatin electrospun scaffolds[215] or with the use of vinyltrimethoxysilane to form cross-linked bonds on PLA electrospun scaffolds.[216] In presence of elastin peptide any specific behavior was not observed.

A second heating scan modifies significantly the thermal behavior of amorphous and crystalline phase of scaffolds, plasticization effect on amorphous phase and smaller crystals thus demonstrating the non-reversible effect of temperature on the electrospinning scaffold.

Adding elastin peptide at the formulation does not modify the thermal properties.

In Table 9 we reported also the electrospun scaffolds crystallinity values, calculated from DSC using the enthalpy of melting of the samples for first heating scan and the theoretical ΔH_m for a 100% crystalline PLA, which is 93 Jg^{-1}.[217,218] GP scaffold presented a crystallinity of 19.6%. An increase of crystallinity was observed with CNCs addition until 5NGP scaffold (29.5%), while, at 8% (w/w) concentration of CNCs and with peptide addition crystallinity decreased, assuming values of 13.8% and 16.3%. This datum suggests that low amount of CNCs could act as nucleating agent for improving the crystallization of PLA molecular chains,[185] and the increase of crystallinity could contribute to the enhancement of the degradation temperature,[219] as found in TGA studies. On the contrary, cross-

linking reaction led to a general decrease of crystallinity except for 8NGPk scaffold.

Differential Scanning Calorimetry at low temperatures was also used in order to analyze the thermal properties of the electrospun scaffolds after conducting the swelling test. The swelling test was done only on the cross-linked scaffolds, because gelatin is water soluble without the cross-linking reaction. The obtained Results are presented in Table 10.

Table 10: Transition temperatures and melting enthalpies of water present in the electrospun scaffolds after swelling test found by using DSC.

Scaffold	T_m H_2O (°C)		ΔH_m (J g^{-1})		Average fibers diameter (μm)
	1st	2nd	1st	2nd	
GPk	10.3	11.3	244.9	241.8	0.9 ± 0.2
1NGPk	7.3	6.6	267.9	231.6	1.6 ± 0.9
3NGPk	8.3	8.0	182.9	173.8	1.7 ± 0.4
5NGPk	5.8	7.4	264.2	260.3	2.2 ± 0.3
8NGPk	10.8	10.3	209.5	205.4	0.8 ± 0.3
El8NGPk	9.2	8.8	178.3	176.9	1.2 ± 0.3

The first heating run brings to the fore the structural melting water (T_m). For GPk scaffold it assumed a value of 10.3 °C and decreased with the addition of CNCs (samples 1NGPk, 3NGPk and 5NGPk), however it became higher in 8NGPk scaffold and decreased with peptide addition to 9.2 °C. The same trend has been found for the second heating scan. Using ImageJ software (Java open source) supplied with the DiameterJ plug-in, average fibers diameters were calculated from SEM images of the electrospun scaffolds and the DSC swelling test values, and listed with their standard deviations, in Table 9. It is interesting to note that seems to be a correlation between the melting temperature of the water and the average fibers diameter of the scaffolds: as a matter of fact, the bigger is the average fibers diameter, the smaller is T_m. This result suggests that during the cooling scan water molecules could rearrange themselves better, leading to a higher crystallinity and a higher T_m water, if the fibers diameter was smaller.

3.3.3 Dynamic Mechanical behavior

Mechanical properties of the scaffolds were analyzed by DMA. In Fig. 36 storage modulus E' and loss modulus E'' are reported as a function of the temperature for GP, 8NGP and El8NGP scaffolds.
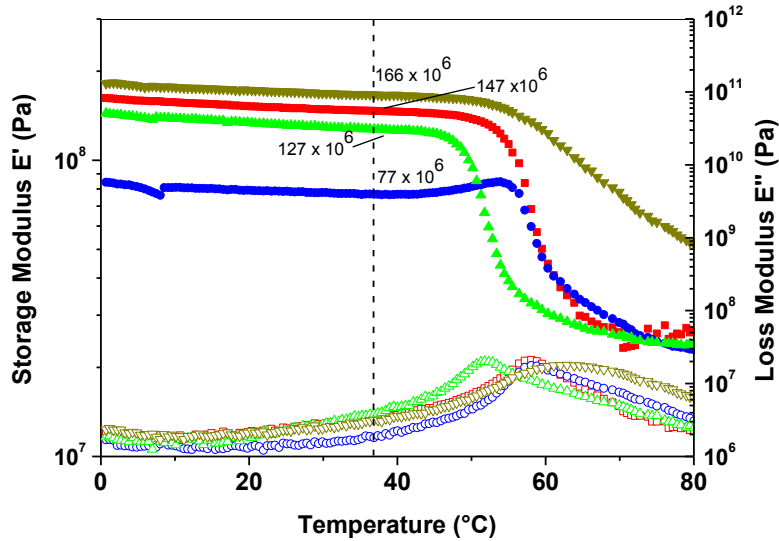
Figure 36: DMA thermograms of GP (square/red), 8NGP (circle/blue), El8NGP (up triangle/green) and 8NGPk (down triangle/dark yellow) electrospun scaffolds. Storage moduli are reported in filled symbols while loss moduli are reported using empty symbols.

In Fig. 36, the viscoelastic step associated with the anelastic manifestation of glass transition, called α mode, is visible on storage modulus. The temperature of α relaxation is consistent with previous calorimetric results.

For 8 % (w/w) CNCs addition the glassy plateau decreases strongly, and the α relaxation is increased. Add elastin peptide at this ratio (El8NGP) enhanced the modulus in the whole temperature range, and shifted α relaxation to a lower temperature. Cross-linking treatment enhanced the glassy and the rubbery plateau and α relaxation at this ratio.

The influence of cellulose nanocrystals added at GP is studied and reported in Fig. 37.
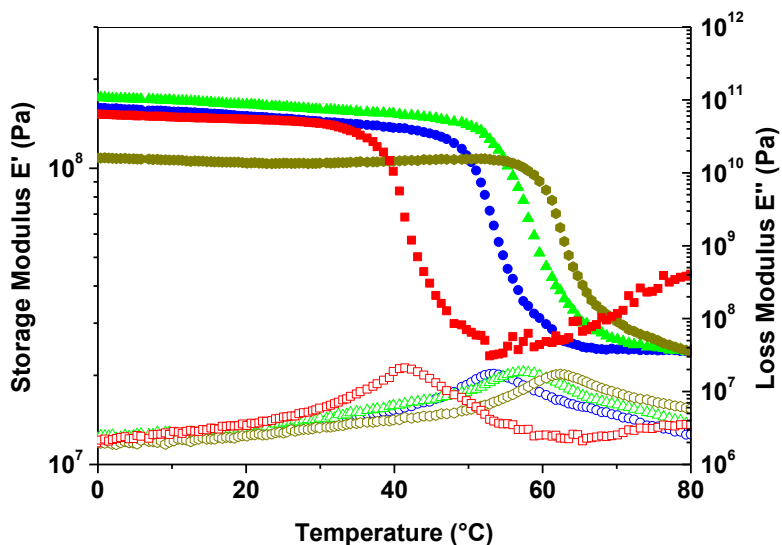
Figure 37: Effect of percentage of cellulose nanocrystals on the DMA behavior of scaffolds: DMA thermograms of GP (square/red), 1NGP (circle/blue), 3NGP (triangle/green) and 5NGP (exagon/dark yellow) electrospun scaffolds. Storage moduli are reported in filled symbols while loss moduli are reported in empty symbols.

We observed that α relaxation increased with increasing the nanocellulose ratio, and the glassy modulus increased until 3% (w/w) of CNCs and decreases strongly for higher ratio. This datum is in agreement with the work of Pirani et al,[154] who studied biodegradable nanocomposites of CNCs and electrospun PLA and found the maximum value of the storage modulus at a CNCs loading level of 3 % (by the weight). An increase of E' has also been observed when CNCs was used as reinforcing agent in electrospun Poly(ε-caprolactone) nanofibers.[152]

Tα values extracted from loss modulus E'' maximum are reported in figure 38.
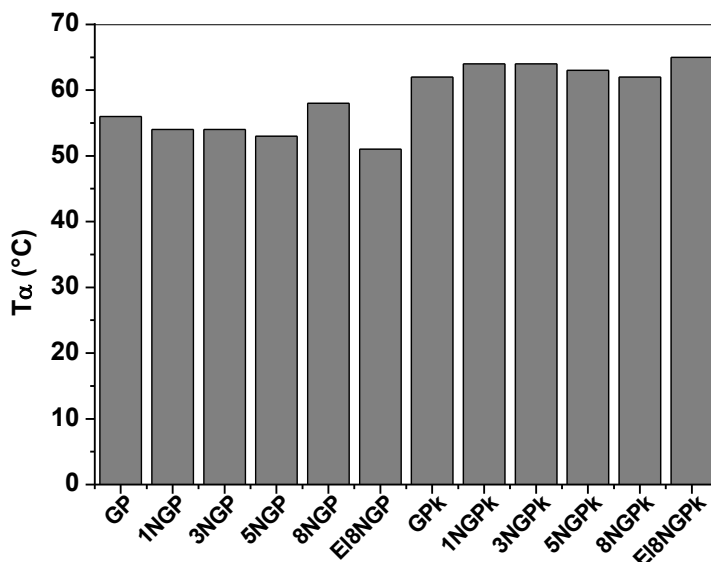
Figure 38: Histogram of Tα values obtained for the scaffolds studied in this work.

We can observe a continuous increase of Tα with increasing CNCs ratio, a decrease of this parameter adding elastin peptide and finally an increase of 10 °C for Tα with the crosslink treatment. This behavior was consistent with calorimetric parameters. It has been associated with the macromolecules mobility loss, and with the increase of the stiffness due to the reticulation. Glassy modulus observed around 150 MPa at low level of CNCs showed an important decrease (around 100 MPa) after 3% of CNCs. This value corresponds at a percolation threshold and can give rise to a modulation of the mechanical properties.

From Dynamic mechanical analysis it can be concluded that the scaffolds are suitable to skin tissue engineering, because natural skin possess tensile modulus

of 15 – 150 MPa.[175,188,219] Furthermore, the properties seem to be tunable through the addition of CNCs or elastin-like peptide with or without cross-linking.

Chapter 4: Industrial activity (LUCART S.p.A in Avigliano Plant)

4.1.1 Brief history of paper

There are many theories about the origin of paper, but the general opinion is that the first to create a documented method to the art of papermaking was a Chinese 2nd-century CE Han court inventor named T'sai Lun, inspired by bees weaving fibers together. At the time in China, due to the difficulty to find small fibers, the paper was made entirely from recycled fibers like rags and cotton, while afterwards innovators learned out how to utilize plants like hemp and bamboo. The Arabs, during the 8th Century, have the merit to improve the quality of paper, adding starch and other additives, which allowed ink to fix on and also increasing the brightness and the strength and also they developed the first industrial paper plant.

Afterwards, the papermaking process was introduced in Europe where was further improved as introducing the so-called *"Hollander Beater" which allowed the extraction of* fibers from plant based materials and de-inking processes. Between 1800 and 1850 trees began to be used for paper production, with the possibility to place industrial plants near the forests and to produce paper pulp from forestry products, while now pulp is mainly produced from a chemical process.[220]

There is no doubt that the paper diffusion has represented a turning point in the development of Western European civilization and has contributed to an increase in the average level of culture and education.

4.1.2 Tissue paper

The standard and most common paper manufacturing process, called "tissue", is obtained by diluting fibrous material in a water suspension to obtain a pulp that, once drained, pressed and dried, is processed in paper machines.

The pulp preparation phase is particularly important for the entire paper production cycle because the mixtures and products used in pulp preparation determine the features of the finished product. Pulp processing is followed by other treatments, either mechanical or chemical, which are carried out according to production requirements.

The raw materials used to produce paper can be distinguished into fibrous and non-fibrous raw materials. Fibrous raw materials form what is known as the body of the product. Coming from conifers and hardwoods, they are mostly made of cellulose. Non-fibrous raw materials, on the other hand, are mostly fillers or adhesives used to give the product the required technological and printability characteristics, such as thickness, permeability, colour and ink stabilisation speed.

Paper is a natural, biodegradable and recyclable product, obtained through the processing of raw materials of vegetable origin. Today, paper is used to make many products that are fundamental to everyday life.

Tissue paper consists in low-grammage sheets, with good dry tensile strength and good absorption, coming from cellulose, but low wet tensile mechanical properties. The main purposes are for domestic and hygienic use as toilet paper, handkerchiefs, napkins, kitchen towels.

4.1.3 Nonwoven definition and airlaid scheme

Airlaid paper is the main product of the Lucart plant in Avigliano (Potenza, Italy) and it can be considered as part of materials called nonwovens.

A definition of nonwoven is given by ISO standard 9092 and CEN EN 29092: "A nonwoven is an engineered fibrous assembly, primarily planar, which has been given a designed level of structural integrity by physical and/or chemical means, excluding weaving, knitting or paper making".

Nonwoven world includes many different kind of processes which differs in web formation and in web bonding as in the following table (Table 11):

Table 11: The three main steps of nonwoven production. The fourth step is the conversion into products.

First step: web formation	Second step: web bonding	Third step: finishing treatment
Drylaid – Carded	Thermal	Mechanical treatment
Drylaid - High loft	- Calendering	Surface modification
(Short Fiber) Airlaid	- Air through	Coating
Wetlaid	Mechanical	
Spunlaid	- Needle punching	
Meltblown	- Hydro-entanglement	
Submicron spinning	- Stichbonding	
	Chemical	

The raw materials used are generally synthetic polymers and the product market applications are many and very different from each other, ranging from hygiene

and personal care to building/roofing, to automotive, to agriculture, filtration and many others.

Airlaid latexbonded is one of the few nonwovens processes that use cellulose and not synthetic fibers as raw material. The final product, usually monoply with medium grammage, has great absorbency, good dry tensile but especially high wet tensile that allows to rinse and reuse the product up to 20 times. Typical applications of the product are kitchen towel, napkins and table top, wipes, substrate for wet wipes.

In the following figure a scheme of a typical airlaid machine is shown:
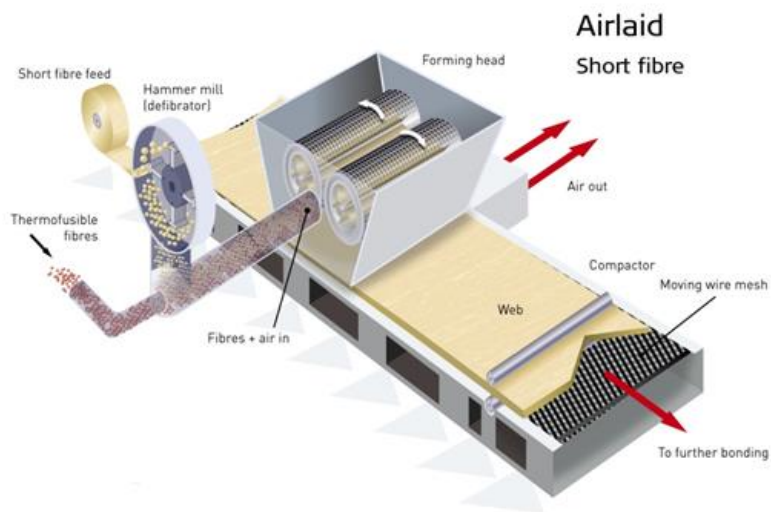
Figure 39: Scheme of a typical airlaid machine.[221]

The mix of the fibers, which are always relatively short, are fed into a forming head, that assures a homogeneous mix of all fibers by an airstream. Then, a

randomly oriented web is formed by depositing a controlled part of the fibers mix on a moving belt, by using air again.

The second step is the web bonding, because the fibers web needs to improve its strength. In particular, chemical bonding refers to the application of a liquid-based bonding agent to the web. In general, three groups of materials are commonly used as binders: vinyl acetate ethylene copolymers, acrylate polymers and copolymers and styrene-butadiene copolymers. The most widely used are water based binder systems but sometimes foam, powdered adhesives and in some cases organic solvent solutions can be found. The binder can be applied in many ways, such as by impregnating, coating or spraying or intermittently.

With the finishing treatments the nonwoven can be tailored or functionalized to meet specific properties.

4.1.4 Lucart SpA and the Avigliano plant

This PhD work, as said in the General Introduction, was carried out in collaboration with the Avigliano plant of Lucart SpA.

Lucart SpA is an Italian multinational leader in the production of paper and it has its headquarters in Porcari, within the Lucca paper district. The history of this group begins in 1953, when the brothers Alessandro, Eliseo, Fernando, Raffaello and Tarcisio Pasquini founded the "Cartiera Lucchese dei F.lli Pasquini" in Villa Basilica (Lucca), starting a long family tradition that still lasts today. During the following decades the company has expanded more and more, improving also from the point of view of technological advancement, with a particular attention to the environmental sustainability.[222]

In particular, Lucart SpA:

✔ was the first Italian company to have developed the de-inking technique of pulp for the production of tissue paper and thin glazed paper for flexible packaging;

✔ Lucart has developed an exclusive technology that allows the cellulose fibers present in beverage cartons such as Tetra Pak® to be recycled to obtain Fiberpack®;

✔ was the first Italian company in the tissue sector to obtain the ecological quality mark for products issued by the European Union: the Ecolabel. Among the first in Europe to obtain UNI EN ISO 9001 quality management systems and UNI EN ISO 14001 environmental certification for the specific product sector of tissue and Yankee paper products;

✔ all the plants of the group have obtained the PEFC and FSC certifications concerning the use of cellulose fibers from sustainably managed forests by

applying strict standards that take into account environmental, social and economic aspects;

✔ all the Italian plants of the Lucart Group have obtained the BS OHSAS 18001 (Occupational Health and Safety Assessment Series) certification and then converted in UNI ISO 45001.

The main business areas of the group can be resumed as follows:

1) B2B: Jumbo coils, tissue and airlaid. Papers intended for other paper industries;

2) Professional: product in tissue and airlaid for the professional sector. They are toilet paper, towels and napkins, consumed by communities, restaurants, industries, cleaning companies, etc. (Away From Home);

3) Consumer: products in tissue and airlaid for the consumer sector, i.e. toilet paper, household paper, napkins and handkerchiefs consumed within the family (At Home).

The main numbers of Lucart SpA are:

- over than 319.000 tons/year of paper produced;

- over than 500.000.000 € of annual revenue;

- 1.600 employees;

- 7 factories;

- 10 Continuous machines;

- 58 converting lines;

- 3 business Units.

One of the factories of Lucart SpA is located at Avigliano (PZ), where there is an airlaid papermachine, the only one in the Lucart group and in Italy, that produces 15.000 tons/year of airlaid paper, and also has 4 converting lines.

The industrial site in Avigliano has about 60000.00 m^2 of surface area and 90 workers are employed.

Figure 40: Image of the Lucart plant located in Avigliano.

In Avigliano site airlaid paper is produced as in the following steps:

1.   Cellulose defiberization

2.   Fibers distribution and belt formation

3.   Compaction and embossing

4.   Binding

5.   Drying

6.   Winding

In the first phase, the cellulose fibers in wrapped rolls (fluff) are unwound by dosing it in hammermills in which the blades, rotating at very high speed, separate fluff into single fibers. Some fans then push the fibers into the dosing systems for the formation phase. The raw material used is only pure bleached virgin cellulose ECF (Elemental Chlorine Free), with no use of synthetic or recycled fibers (Fig. 41).

Figure 41: Image of the fluff of the cellulose.

In the second phase the cellulose fibers are mixed in the formation heads and then efficiently distributed on a conveyor plastic belt by the action of suction hoods that make the cellulose fibers adhere to the belt and allow the cellulose belt to be formed (Fig. 42).

Figure 42: Image of the formation head.

In the third phase, before binding, the cellulose carpet is compacted and, if necessary, calendered, in order to transfer a particular design to the paper.

The fourth phase is the spraying of the vinyl binder. The method of binding the fibers together is to spray a dilute vinyl aqueous binder dispersion, first on the upper side of the belt and then on the bottom one (Fig. 43).

Figure 43: Binder spraying on the surface of the tape.

Each binding phase is followed by a drying phase in an oven with 4 chambers each one at different temperatures from 90 °C until to 200 °C.

During the winding phase, the paper exiting the line is wound in large reels (jumbo) at the winder (Pope, Fig. 44) and subsequently destined for transformation into the finished product in the Converting department or rewound to be sold as a semi-finished product.

Figure 44: Imagine of the winder machine (Pope).

Therefore, although both processes use cellulose as the main raw material, the airlaid papermaking process is completely different from standard tissue papermaking process, as the cellulose fibers are distributed by an air flow and not into an aqueous suspension and also the web binding is different as the airlaid paper is chemically bonded.

In tissue paper, when wet, the hydrogen bonds between fibers are broken, and paper typically loses almost all of its strength, while the high wet tensile strength makes the airlaid paper versatile and reusable: it can be rinsed and reused many times savings costs and storage space.

4.1.5 The vinyl binder cross-linking reaction

The method for binding together the cellulose fibers consists in spraying an aqueous copolymer dispersion with self-crosslinking properties based on vinyl acetate and ethylene (VAE).

VAE polymers binders have been used for many years in paper nonwovens applications and in generally in wood and derived-wood manufacturing industrial processes.

The crosslinking properties are given by the presence of small quantity of *N*-(Hydroxymethyl)-acrylamide (NMA) monomer in the polymer formation. NMA, at the temperature of 130 °C, gives rise to a cross-linking reaction according to the reaction scheme shown in Fig. 45.
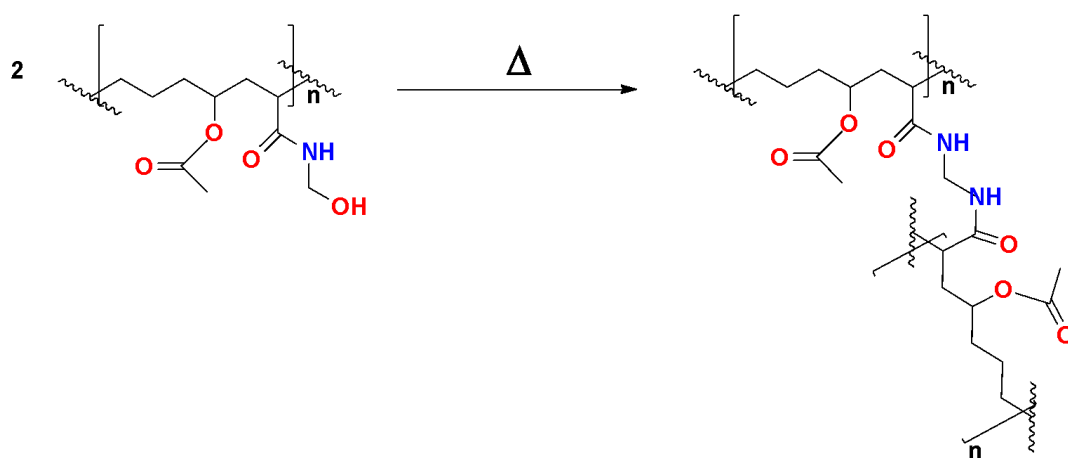

Figure 45: Cross-linking reaction of the vinyl binder used for airlaid paper production.

The cross-linking binder reaction, as shown in Fig. 45, produces, in addition to a new carbon-carbon bond between the polymeric chains, also water vapor and, gaseous formaldehyde as by-products.

The formaldehyde develops inside the ovens from which it is captured and sent to the filtration systems and to the emission points in the atmosphere.

Formaldehyde is a colorless, strong-smelling gas used in making building materials and many household products. It is used in pressed-wood products, such as particleboard, plywood, and fiberboard; glues and adhesives; permanent-press fabrics; paper product coatings; and certain insulation materials. It is also used to make other chemicals so it is normally present at low levels in both indoor and outdoor air.

However, formaldehyde is toxic and health dangerous so, where technically and economically feasible, it must be minimized and, if possible, eliminated or replaced by other materials.

The collaboration between University of Basilicata and Lucart SpA and therefore this Industrial PhD, was signed with the aim of eliminate the already low formaldehyde emission during paper production.

The main producers of consumables, also driven by the European regulations, are directing research and development activities towards products increasingly biodegradable and compostable. Manufacturers of binders, like those of plastics in general, are also working in the same direction.

Although airlaid paper already has these characteristics, being mainly made of cellulose, another goal was added to these research activities: the further increase of the biodegradability and compostability of the paper, substituting partially or totally the small percentage of synthetic raw material (the vinyl binder) with natural or coming from natural sources substances.

In the next chapter the materials and the methods used in this research will be shown.

4.2 Materials and methods

4.2.1 Laboratory-scale simulation method

First step was to understand if it is possible to reproduce the industrial process in a laboratory-scale, in order to obtain data as reliable as possible before conducting an industrial trial. Unfortunately, due to the complexity of the process, especially in the phases of defibration of cellulose and binder spraying, it was not possible to replicate the process in laboratory scale but a good compromise was found adopting a laboratory-scale paper-making method as follow. A monoply tissue roll 24 g/m^2 was taken as substrate, this substrate was submerged in a container with the blend previously prepared (Fig. 46 A) for about 3 s and then put in oven at 150 °C for 10 minutes (Fig. 46 B). We tried to use dispersions with starting concentrations such as to have then concentrations on paper comparable with the airlaid paper ones. Samples so dried are ready to be cut in strips for tensile strength tests.

This lab-scale method does not predict with accuracy the results of the industrial scale but is useful for comparing the results between one trial and another.
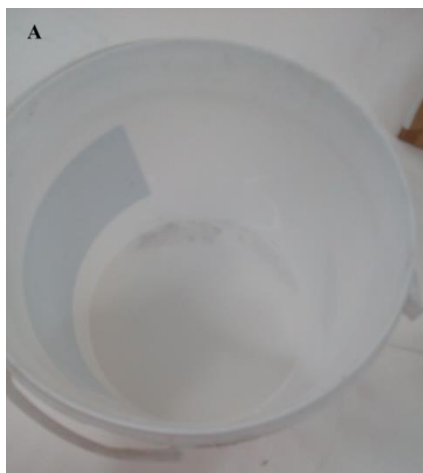
Fig. 46: Images of: (A), the container with the binder and (B), the cut paper in the oven.

4.2.2 Calculation of the percentage of latex on paper

The percentage of binder (which in the following we will also call "latex") present on paper after the thermic treatment in oven was determined in lab scale trials as indicated below. The tissue paper was weighed on a balance (Precisa Instruments AG, Model. XR 205 SM-DR, 8953 Dietikon, Switzerland, 2005) having sensibility ±

0.00001 g, both before and after the immersion in the polymeric dispersion and subsequent heating. The percentage of latex on paper was then determined according to the following equation (eq. 12):

$$\text{Latex (\%)} = \frac{W_f - W_i}{W_f} \text{ x } 100$$

In the above formula used for percentage of latex calculation, W_i is the initial mass of the tissue paper without the binder, while W_f is the final mass, with the presence of the binder.

4.2.3 Paper dry and wet tensile strength and elongation measurement

Tensile and elongation measurements, both dry and wet, are essential for assessing the quality of the paper. These values were calculated according to Edana test WSP 110.4.R4 (12).[223] EDANA is the European leading association and voice of the nonwovens and related industries.

Test specimens of 30 cm of length and 5 cm wide were clamped in a tensile testing machine and a force applied to the specimens until they broke. Values for the breaking force (expressed in cN/5 cm) and elongation (expressed in %) of the test specimen were obtained from the machine. For the wet data, the samples were wet before apply the force. These measurements were carried out using MTS 200/M dynamometer (Adamel Lhomargi, New Castle, Delaware, USA), as shown in Fig. 47.

Figure 47: Image of dynamometer used for determining wet and dry tensile and elongation of the paper.

4.2.4 Determination of the water absorption quantity

Water absorption property, derived from the cellulose hydrophilicity, is also important for the intended use of the paper. The absorption quantity was determined according to Official EDANA test WSP 010.1 R3.

Each sample was immersed in water at room temperature (r.t.) for 2 minutes. Thereafter, the samples were dried on air removing the excess of water for 1 minute and weighed on a balance (Precisa Instruments AG, Model. XR 205 SM-DR, 8953 Dietikon, Switzerland, 2005) having sensibility ±0.00001 g. The water absorbed was calculated according to the following equation (eq. 13):

$$\textbf{Absorption} = \frac{W_w - W_d}{W_d}$$

In the above formula used for absorption quantity, W_w and W_d are the masses (g) of the wet and dry paper, respectively.

4.2.5 Measurement of binders viscosity

Viscosity is the measure of the internal friction of a fluid, that becomes apparent when a layer of fluid is made to move in relation to another layer. The term shear represents the amount of force required to cause this movement, resulting in a higher force to move in high viscous fluids, than less viscous materials.

Isaac Newton defined viscosity considering two parallel planes of fluid of equal area A separated by a distance dx which are moving in the same direction at different velocities V_1 and V_2. He assumed that the force required to maintain this difference in speed was proportional to the difference in speed through the liquid, or the velocity gradient, writing this relation (eq. 14):[224]

$$\frac{F}{A} = \eta \frac{dv}{dx}$$

were η is a constant and is the viscosity of the material and dv/dx is the velocity gradient, also called shear rate (expressed in s^{-1}) and represents the change in speed at which the intermediate layers move with respect to each other. The ratio F/A takes the name of shear stress and indicates the force per unit area required to produce the shearing action and its unit of measurement is dynes per square centimeter (dynes/cm^2).

Therefore, the mathematical definition of viscosity can be rewritten as follows (eq. 15):

$$\eta = \frac{\tau}{\dot{\gamma}}$$

where τ is the shear stress and $\dot{\gamma}$ the shear rate.

The fundamental unit of viscosity measurement is the poise, but in the International System it is expressed in Pascal-seconds (Pa·s) or milli-Pascal-seconds (mPa·s), with one Pascal-second that is equal to ten poise and one milli-Pascal-second equal to one centipoise.

Fluids as water with a viscosity independent of the shear rate at a given temperature are called Newtonian fluids. A significant number of fluids, as polymeric fluids, do not present this behavior, with the ratio $\tau/\dot{\gamma}$ which is not constant, resulting in a change of the viscosity if the shear rate is varied. These fluids are called non-Newtonian.

The viscosity and the torque of the polymeric blends were determined by using a Brokfield DV2T viscometer. The spindle used was the n. 1 and the rotation speed was chosen depending on the characteristics of the mixtures.

Figure 48: Image of the viscometer Brokfield DV2T used for viscosity measurement.

4.2.6 Standardization of a formaldehyde solution

In order to fine tuning a method for the determination of the formaldehyde produced in the latex cross-linking reaction, a formaldehyde solution was standardized.

The reactant used were:

- stock solution of formaldehyde 10% (m/V);

- 920 mg/L formaldehyde solution to be titred;

- 0.05 M iodine solution (0.635 g of I_2 + 1.5 g of KI in 50 mL of H_2O);

- 25% (V/V) sulfuric acid solution;

- 1 M sodium hydroxide solution;

- 1% starch (indicator);

- 0.05 M sodium thiosulfate solution.

8 mL of H_2O (or 8 mL of the formaldehyde solution) were placed in a flask, then, 10 mL of the iodine solution and 4 mL of the NaOH solution were added and the mixture was left 15 minutes at room temperature (the solution took on a light yellow color). Thereafter, 4 mL of sulfuric acid (the solution became dark again) and 2 mL of starch solution were added and titration with thiosulfate until the solution becomes colorless was carried out. The reactions are the following:

$$CH_2O + I_2 \rightarrow CH_2O_2 + 2I^- + I_2 \text{ (excess)}$$

$$I_2(\text{excess}) + 2S_2O_3^{2-} \rightarrow 2I^- + S_4O_6^{2-}$$
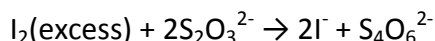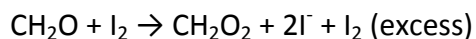
This is a back-titration: the excess of the iodine solution, i.e. the one that has not reacted with formaldehyde, is titrated with thiosulfate.

The concentration of formaldehyde was determined according the following equation (eq. 16):

$$\frac{(V_1 - V_2)mL \; x \; 15 \; gmol^{-1} \; x \; 0.05 \; M \; x \; 1000}{8 \; mL}$$

In the above formula used for the calculation of the concentration of the formaldehyde solution, V_1 and V_2 are the volume of thiosulfate used to titrate the sample containing H_2O and volume of thiosulfate used for the sample containing formaldehyde, respectively.

4.2.7 Determination of the formaldehyde

The formaldehyde released during the cross-linking reaction was determined by using the following method, which involves the reaction with a mixture containing acetylacetone. The composition of the mixture was the following:

- 15% (m/V) ammonium acetate solution;

- 0.3% (V/V) acetic acid solution;

- 0.2% (V/V) acetylacetone solution distilled under pressure (pH 6.4).

500 μL of formaldehyde-containing sample was reacted with 500 μL of reagent and the solution was incubated at 40 °C for 30 minutes.

Formaldehyde reacts with acetylacetone giving a yellow colored product:
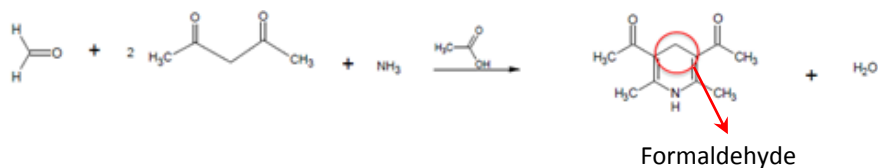
Formaldehyde

The absorbance was then measured at 412 nm.

4.2.8 Determination of the gaseous formaldehyde released from the vinyl binder cross-linking reaction

For the determination of the gaseous formaldehyde released from the cross-linking reaction, 5 ml of 17% (w/w) vinyl binder solution (the concentration used in the Avigliano plant for the airlaid paper production) were heated to 130 °C for 15 minutes and the vapors were collected in 2 mL of distilled water, then the reaction was allowed to proceed for another 30 minutes and the vapors were again collected in another 2 mL of distilled water (Fig. 49 A). Subsequently, the acetylacetone assay was performed on 500 μL of each sample. Moreover, 20 mL of 17% (w/w) latex were heated at 130 °C for 30 minutes and the vapors were collected in 1 mL of acetylacetone at 40 °C, so that the reaction occurred at the same time as the vapor was collected (Fig. 49 B).
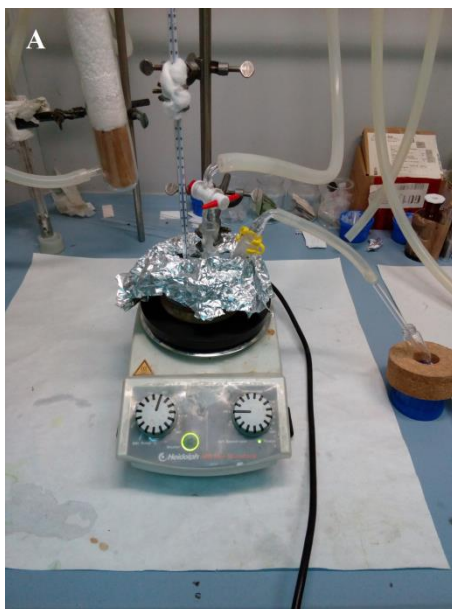
Figure 49: Photographs of the *apparatus* used to determine the gaseous formaldehyde released from the cross-linking: (A) without, (B) with the simultaneous reaction with acetylacetone.

4.2.9 Determination of the residual formaldehyde on lab-scale paper samples

A method for determining the residual formaldehyde on lab scale paper samples, prepared accordingly to the method described in par. 4.2.1, was developed.

Paper samples were placed in different vials, containing distilled water, so as not to let them come into contact with the liquid present, and placed in an oven at 48 °C for 20 hours. The day after the test for the determination of formaldehyde was conducted (as described above), adding the reagent with acetylacetone to the aqueous extracts.

4.2.10 Determination of the formaldehyde on lab-scale paper samples with the official UNI EN 1541: 2002 method (hot method)

The presence of residual formaldehyde on lab-scale paper samples was measured also with the official method UNI EN 1541, in hot conditions: the tissue paper was immersed in 20 mL of water at 80 ° C for 2 hours. Thereafter, the pieces of paper were washed with 5 mL of water and the assay with acetylacetone was carried out.

Since formaldehyde is gaseous and in the industrial process it is directly conveyed inside the ovens towards the filtration and emission points, the quantity detectable on paper is irrelevant and very close to the detection limit of standard methods. For this purpose, a hot method was used, generally not applicable to this type of product, in order to increase the quantity detected on paper and to have more comparable reference parameters.

4.2.11 Materials used

During these three years of the research activity, a many products were evaluated and tested, in co-formulation with the standard vinyl binder or in substitution of it, choosing mixtures and dispersions with low viscosity so that they can easily be used in the spraying process in case of industrial test.

At the beginning the attention was focused on the research of a binder similar to the vinyl one used in the airlaid process, but with no formaldehyde emission. In literature was found the work of Cui et al,[225] which produced a polymer with the same components, i.e. ethylene, vinyl acetate and *N*-(Hydroxymethyl)-acrylamide, but with the addition of urea before the polymerization. The reaction is the following (Fig. 50):
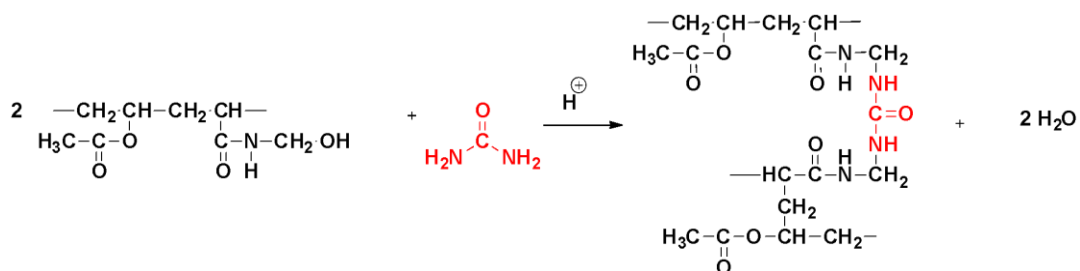
Figure 50: Image of the reaction of polymerization of two chain of a EVAc-NMA binder with an urea molecule.[225]

As shown in Fig. 50, the presence of urea ensures that formaldehyde is not released, because the cross-linking does not happen between two NMA molecules but between two NMA molecules and a bridging urea molecule.

Starting from this work, this polymer was produced according to the procedure described in the work of Cui et al.[225]

Thereafter in order to replicate this new cross-linking reaction, different quantities of urea were added to the vinyl binder used for the production of airlaid paper in

the Lucart S.p.A plant in Avigliano. The formaldehyde present in these papers was detected by using the methods described in paragraphs 4.2.9 and 4.2.10 and, after many laboratory experiments, an industrial trial was carried out.

Urea was purchased from Chimica D'Agostino S.p.A. (70132, Bari, BA, Italy).

Another lab-scale trial concerned the use of mixes of two polymers instead of the traditional vinyl latex: a XBS Binder HCHO free, an aqueous dispersion of styrene-butadiene copolymer with 25 - 30% bio polymer content, and a polyamidoamine-epichlorohydrin (PAE) binder, recommended to improve the wet strengths. Blends of different percentages of these two polymers were prepared and the properties of the paper samples obtained were studied.

Another research strategy undertaken in these three years was the use of the aqueous dispersions of poly(vinyl alcohol), PVA, as substitute of the latex or in co-formulation with it. PVA is water soluble, biodegradable, nontoxic and biocompatible. It is obtained by controlled hydrolysis of poly(vinyl acetate),[14] and, therefore, it can present different molecular weight and hydrolysis degree, which lead to different values of viscosity. Herein, in this PhD work seven different types of PVA dispersions were tested; in particular, their viscosity was measured and the mechanical properties of the tissue paper were analyzed, in order to choose the PVAs which can be used in a possible industrial trial. Aqueous suspensions of PVAs were purchased from Mare S.p.A. (Milano, MI, Italy).

Moreover, a new filler was tested in blends with the vinyl binder in order to increase the biodegradability of the paper. This is a engineered polysaccharide (EP) manufactured using enzymatic polymerization of sucrose, which presents an alpha(1→3) linkage, as shown (Fig. 51):
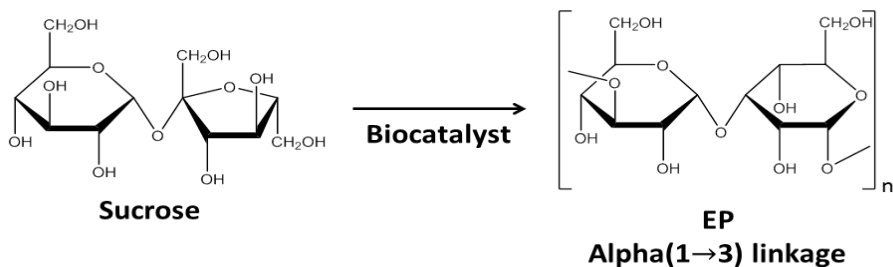
Figure 51: Image of the EP formation reaction starting from sucrose: it presents an alpha(1→3) linkage.

This product is under the form of a water dispersion, white colored, biodegradable, compostable and therefore it can be useful as a filler in nonwoven technology. Also in this case, after many laboratory experiments, an industrial trial was carried out using a mix of vinyl latex-EP.

4.2.12 Scanning Electron Microscopy analysis (SEM)

A theoretical description of scanning electron microscopy and the functioning of the microscope has already been given in the paragraph 2.2.9. The morphology of the airlaid paper with the mix vinyl latex-urea of the industrial trial and the tissue paper with the mix vinyl latex-EP was investigated on Philips, FEI ESEM XL30

instrument. SEM images were acquired with a voltage of 20 kV and different magnifications, after gold sputter coating.

4.2.14 Statistical analysis

Data of absorbance, dry and wet tensile and elongation are reported as mean ± standard deviation and graphs were plotted by using Origin Data Graph software (OriginLab® Corporation, Northampton, MA, USA) and Microsoft^{TM} Excel.

4.3 Results and discussion

The most important results of the activities carried out in collaboration with Lucart S.p.A. are shown in this paragraph.

In detail, are described below:

● The standardization of a formaldehyde solution and its determination by reaction with acetylacetone;

● The method adopted for detection of formaldehyde gas from the cross-linking binder reaction;

● A method to determine the formaldehyde on laboratory scale paper sample with standard binder and with urea addition;

● Analysis on different urea added binder mix for industrial test;

● Lab-Scale test on an innovative XBS Binder HCHO free containing 25-30% bio polymer;

● Tests on different compostable PVA dispersions;

● Lab scale test and industrial test with a blend of standard vinyl binder a new compostable engineered polysaccharide (EP);

4.3.1 Standardization of a formaldehyde solution

Standardization of a formaldehyde solution was carried out according to the method described in par. 4.2.6. The values of V_1, the volume of thiosulfate used to titrate the sample containing H_2O, and V_2, the volume of thiosulfate used for the sample containing formaldehyde, were 17.6 mL and 7.8 mL, respectively. Therefore, eq. 16 takes this form, giving the following value of formaldehyde concentration:

$$\frac{(17.6-7.8)mL \; x \; 15 \; gmol^{-1} \; x \; 0.05 \; M \; x \; 1000}{8 \; mL} = \textbf{918.7 mL}$$

As a consequence, it can be said that the titration of formaldehyde was successful.

4.3.2 Determination of the formaldehyde by reaction with acetylacetone

In order to detect the presence of the formaldehyde, two calibration curves were constructed using various formaldehyde solutions prepared from the previously standardized one (see par. 4.2.6) and the essay with the acetylacetone, described in par. 4.2.7, was carried out. In table 12 A and B results of the two tests are shown.

Table 12: Values of the absorbance found for the formaldehyde solutions at different concentration for A, the first test and B, the second test.

A)

Formaldehyde concentration (mg/L)	Absorbance at 412 nm (A.U.)
0.14	0.018
0.28	0.034
0.57	0.069
1.1	0.14
2.3	0.27
4.6	0.56
9.2	1.1
White sample	0.071

B)

Formaldehyde concentration (μg/L)	Absorbance at 412 nm (A.U.)
57.5	0.0061
115	0.017
230	0.028
460	0.056
920	0.11
White sample	0.071

As a consequence, two calibration curves were built, as shown in Fig. 52 A and B:
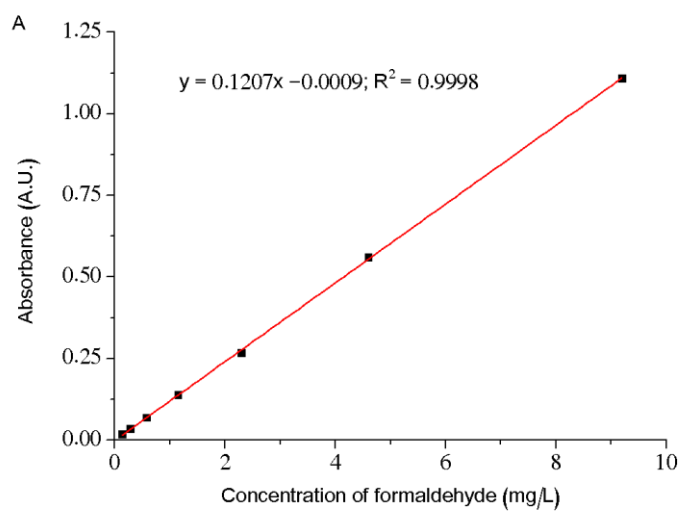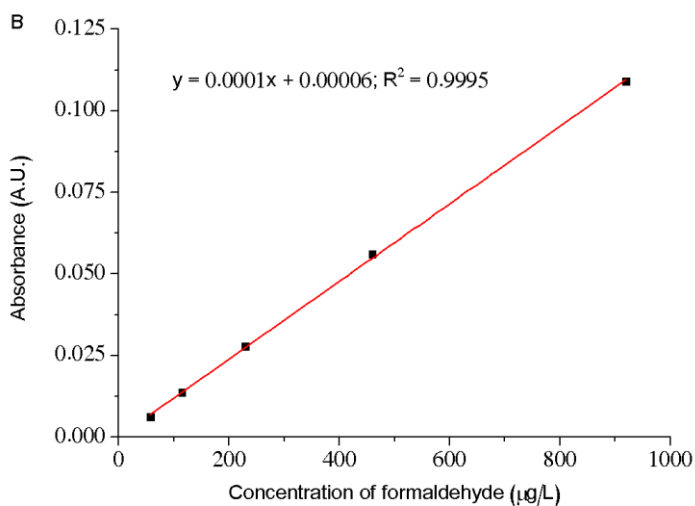
Figure 52: Calibration curves obtained from the formaldehyde solutions at different concentration for A, the first test and B, the second test.

Observing the curves and their equations, it is interesting to note the values of R^2, very close to 1, index of a great linearity of the correlation.

Analyzing the curves, it was possible to determine the limit of detection of this method, equal to 57.2 μg/L of formaldehyde, even if not calculated by using certified reference materials.

4.3.3 Determination of the gaseous formaldehyde from the vinyl binder cross-linking reaction

As described in par. 4.2.8, two methods for the detection of the gaseous formaldehyde released from the vinyl binder cross-linking reaction have been developed, where in the second one the reaction with acetylacetone occurred at the same time as the vapor was collected.

In the first test 5 ml of 17% (w/w) vinyl binder aqueous dispersion were heated to 130 °C for 15 minutes and the vapors were collected in 2 mL of distilled water, then the reaction was allowed to proceed for another 30 minutes, in order to collect as much formaldehyde as possible, giving the following absorbance values:

1) Absorbance at 15 minutes (A.U.): 0.016;

2) Absorbance at 30 minutes (A.U.): 0.05.

As expected, after a longer time, a higher absorbance was found and these values fall into the second calibration curve.

Regarding the second test, in which the vapors were directly collected in 1 mL of acetylacetone at 40 °C, the registered value of absorbance was 0.24, therefore greater than the two previous values, demonstrating that the second collection system was better than the first one.

Simultaneously with these tests, GC-MS (Gas Chromatography – Mass Spectroscopy) analyzes were conducted on both the formaldehyde standards and on a sample obtained by bubbling the gas in the acetylacetone.

In Fig. 1 of appendix GC-MS spectrum of the formaldehyde standard is shown.

Analyzing the chromatogram of the standard solution, the two main peaks represent, respectively, a retention time of 4.948 minutes attributable to an enamine, adducted between the acetylacetone and the ammonium salts present in the solution, and the formaldehyde-acetylacetone adduct, at tr = 10.000 minutes, as shown in the following summary Table 13:

Table 13: Main signals of the mass spectrum of the eluate at tr = 10.000 minutes of the formaldehyde standard.

Signal	m/z
1	32.0
2	43.1
3	63.0
4	77.0
5	106.1
6	133.9
7	176.1
8	191.1

The GC-MS spectrum of one of the experimental samples (Fig. 2 of Appendix), on the other hand, presents a singular characteristic: an eluted species was detected after about 11 minutes, very similar to the adduct between formaldehyde and the reactive with acetylacetone, but with an additional methyl, while the desired species was not found, as shown in table 14:

Table 14: Main signals of the mass spectrum of the eluate at tr ∼ 11.000 minutes of one sample.

Signal	m/z
1	32.1
2	43.1
3	55.1
4	73.0
5	91.0
6	106.1
7	120.1
8	134.1
9	149.0
10	164.2
11	178.1
12	192.1
13	207.1
14	281.1

This would lead us to think that, instead of formaldehyde, acetaldehyde reacted, probably deriving from any vinyl acetate monomers present in the binder. In order to verify that the acetaldehyde-acetylacetone adduct also has a yellow color and presents an absorbance at 412 nm, as well as the formaldehyde-acetylacetone adduct, the essay for the determination of formaldehyde was

carried out using acetaldehyde as standard (density of stock solution = 0.785 g/mL at 25 ° C). Three different solutions were prepared:

Dilution 1: 100 = 7.85 g/L: absorbance = 0.2492

Dilution 1: 200 = 3.925 g/L: absorbance = 0.1475

Dilution 1: 400 = 1.96g/L: absorbance = 0.079

Therefore, it is evident that acetaldehyde interfered with the essay.

4.3.4 Determination of the residual formaldehyde on lab-scale paper samples

According to the method described in par. 4.2.1, four samples of tissue paper (10 cm x 10 cm) were prepared: two of them were immersed in 50% (w/w) vinyl binder (the starting mixture from which the 17% dispersion is produced by dilution), two in 17% (w/w) binder and placed in an oven at 130 °C for 15 minutes. Then the paper samples were placed in four different vials, two containing the reagent with acetylacetone and two distilled water and placed in the oven at 48 °C for 20 hours. The following day the test for the determination of formaldehyde was conducted (as in par. 4.2.7), adding the reagent with acetylacetone to the two samples containing only H_2O: the two samples inserted in the vials containing the acetylacetone reagent took on a yellow color, probably because the acetylacetone evaporated and reacted with the formaldehyde present on the paper. In table 15, the absorbance registered is reported:

Table 15: Paper produced with the absorbance registered.

Paper	Absorbance (A.U.)
With 50% (w/w) binder (acetylacetone reagent)	0.060
With 17% (w/w) binder (acetylacetone reagent)	0.060
With 50% (w/w) binder (water)	2.0 (too high)
With 17% (w/w) binder (water)	0.90

The mixture (composed of H_2O and the reactive) resulting from the reaction with the paper soaked with the 17% (w/w) vinyl binder was then subjected to a GC-MS analysis (Fig. 3 of Appendix).

The chromatogram shows a peak at about 10 minutes which from the mass spectrum can be attributed precisely to the adduct formed by formaldehyde, while the presence of the adduct deriving from the presence of acetaldehyde is not noted, just as in the sample formed by the standard solution of formaldehyde, as shown in Table 16:

Table 16: Main signals of the mass spectrum of the eluate at tr = 10.000 minutes of the paper soaked with the 17% (w/w) vinyl binder.

Signal	m/z
1	43.1
2	61.9
3	77.0
4	106.1
5	134.0
6	149.2
7	176.0
8	191.1

The same applies to the GC-MS spectrum referred to the paper sample soaked in 50% (w/w) glue (Fig. 4 of Appendix and Table 17):

Table 17: Main signals of the mass spectrum of the eluate at tr = 10.000 minutes of the paper sample soaked in 50% (w/w) glue.

Signal	m/z
1	32.1
2	43.1
3	63.1
4	77.0
5	106.1
6	134.0
7	149.2
8	176.1
9	191.1

Therefore, this method seems to be better than the previous one for the detection of formaldehyde.

4.3.5 Determination of the formaldehyde present on tissue paper immersed in the binder with urea

As described in par. 4.2.11, a polymer composed of EVAc-NMA was produced according to the procedure described in the work of Cui et al[225].

The reaction was successfully conducted and tests on paper were carried out.

Paper produced: 6 pieces 8 cm x 8 cm in 17% (w/w) resin, (samples 1 to 6), 4 pieces of paper 8 cm x 8 cm in the binder containing urea (samples 7 to 10).

Table 18: Samples produced with the percentage of the binder on the paper.

Sample N°	Percentage (%) of total binder remained on the paper after immersion
1	29.4
2	30.4
3	29.2
4	28.9
5	31.5
6	34.5
7	41.1
8	42.5
9	38.1
10	44.6

Average of standard binder percentage on paper: 30 ± 2.

Average of standard binder with urea addition: 41 ± 3.

It is interesting to note that the percentage on paper with the binder containing urea is higher than the paper with the vinyl binder.

The acetylacetone essay was carried out on the aqueous extract of the pieces of paper, giving these values of absorbance:

Table 19: Absorbance registered for the produces samples.

Sample	Absorbance (A.U.)
1	0.83
2	0.87
3	0.83
4	0.86
5	0.98
6	1.0
7	0.13

8	0.090
9	0.089
10	0.094

Average absorbance of 17% (w/w) vinyl binder samples = 0.90 ± 0.09. Average absorbance of samples with resin with urea = 0.10 ± 0.02.
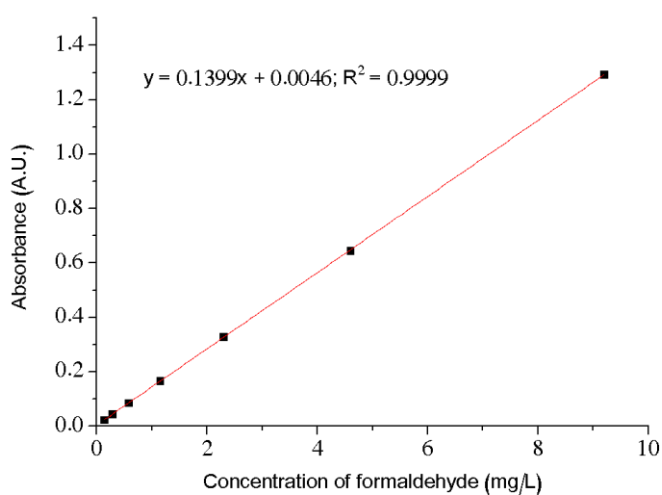
This is the calibration curve obtained (Fig. 53):

Figure 53: Calibration curve obtained from the formaldehyde solutions at different concentrations.

From the calibration curve it was possible to find the concentration of the formaldehyde released from the samples:

- formaldehyde concentration in samples treated with 17% (w/w) vinyl binder = **6.45 mg/L**. The mass spectrum revealed the presence of the formaldehyde/acetylacetone adduct (not shown);

- formaldehyde concentration in the samples treated with the resin with urea = **0.69 mg/L**. The mass spectrum did not reveal the presence of the formaldehyde/acetylacetone adduct (not reported).

Therefore, the urea-containing binder appeared to release much less formaldehyde than the standard vinyl binder; therefore, it was decided to add different quantities of urea.

4.3.6 Addition of urea to the standard vinyl binder

As the binder added with urea seemed to release much less formaldehyde than the standard vinyl binder, different quantities of urea were added to the binder used for the production of airlaid paper I order to identify the best addition for an industrial trial.

To 40 ml of 17% (w/w) vinyl binder 0.088, 0.176, 0.352 and 0.704 g respectively of urea were added, two 8 cm x 8 cm pieces of paper for each urea addition were produced and then the formaldehyde was detected.

Results are shown in table 20.

Table 20: Percentages of binder on paper and absorbance values found for the paper with different amounts of urea.

Sample	Percentage of binder on the paper (%)	Absorbance (A.U.)

1 (without urea)	32.8	0.79
2 (without urea)	29.3	0.71
3 (0.088 g of urea)	33.0	0.73
4 (0.088 g of urea)	31.1	0.68
5 (0.176 g of urea)	36.4	0.64
6 (0.176 g of urea)	38.7	0.55
7 (0.352 g of urea)	32.8	0.35
8 (0.352 g of urea)	29.7	0.37
9 (0.704 g of urea)	33.9	0.38
10 (0.704 g of urea)	30.3	0.39

The absorbance seemed to decrease with the amount of the added urea. It was therefore decided to use larger quantities of urea, in particular 0.704 g and 1.408 g in 40 mL of vinyl resin and the results are shown below:

- Absorbance of samples with 0.704 g of urea = **0.27 ± 0.03** A.U.;

- Absorbance of samples with 1.41 g of urea = **0.3 ± 0.1** A.U.

Again, a decrease in absorbance was found.

In order to identify the quantity of urea to be used in the industrial trial, a test with different quantities of it was conducted in quadruplicate, giving the following results (calibration curve not shown):

Table 21: Concentration of formaldehyde found in the samples with different amounts of urea (n = 4).

Sample % urea (w/V)	Concentration of formaldehyde (mg/Kg)
0.000	21.1 ± 0.4
0.220	25.2 ± 0.9
0.440	13.5 ± 0.9
0.880	7.9 ± 0.1
1.76	4.4 ± 0.5
3.52	2.1 ± 0.3
7.04	2 ± 1
14.1	0.9 ± 0.7
Paper without resin	2.7 ± 0.2
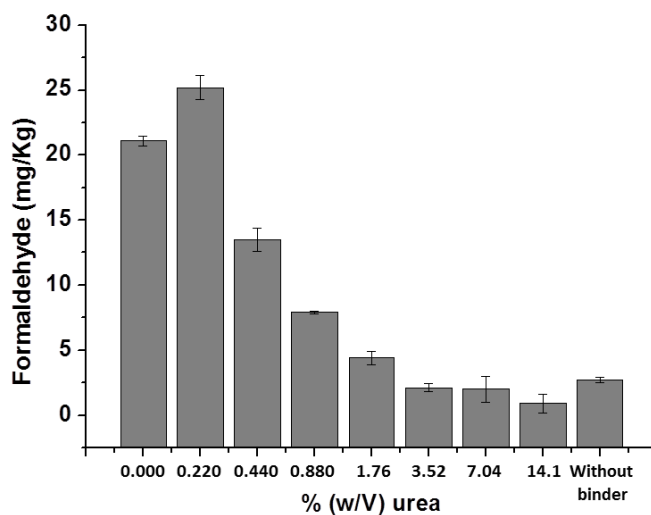
Figure 54: Histogram of formaldehyde found adding different quantities of urea.

The amount of formaldehyde decreased with the amount of urea, presenting a plateau of about 3.52% (w/V) of urea, therefore a subsequent test was conducted using quantities of urea between 1.76% (w/V) and 3.52% (w/V), i.e. 2.2 - 2.64 - 3.08 - 3.52%. A NMA-free vinyl binder was used as a negative control. In the histogram of Fig. 55 results are shown.
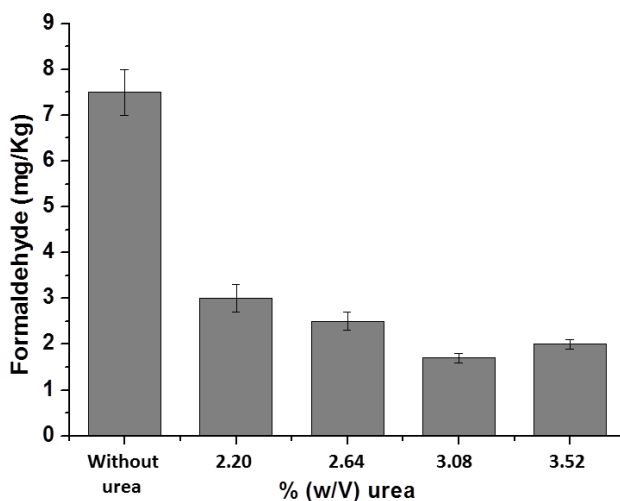

Figure 55: Histogram of formaldehyde found adding different quantities of urea between 3.52% (w/V) and 2.20% (w/V), n = 4.

Observing these data, 3.00% (w/V) urea appeared to be the minimum amount to add to the binder to produce a consistent decrease in formaldehyde.

Before conducting the industrial trial, the concentration of formaldehyde on the aqueous extract of airlaid paper produced at the Lucart plant in Avigliano was

determined either by using the method described in par. 4.2.9 that official UNI EN 1541: 2002 method, described in par. 4.2.10.

Table 22: Concentrations of formaldehyde found in the aqueous extract from airlaid paper and from tissue paper without the vinyl binder with the method described in par. 10.9 and with the official UNI EN 1541: 2002 method (n =4).

	Concentration of formaldehyde (ppm) First method	Concentration of formaldehyde (ppm) UNI EN 1541: 2002 method
Airlaid paper	4.5 ± 0.4	11.1 ± 0.9
Tissue paper	1.9 ± 0.5	7.1 ± 0.6

Observing data in table 22, it can be noted that the official method was able to detect more formaldehyde (11.1 ± 0.9 ppm) than the method used until that moment (4.5 ± 0.4 ppm).

After all these laboratory tests, an industrial trial was carried out at Lucart plant in Avigliano and the following kind of airlaid paper were produced:

1) Vinyl binder without adding urea, temperature 180 °C, line speed of 180 m/min;

2) first test: blend composed of vinyl binder 14.45% (w/w) and urea 2.55% (w/w), temperature 180 °C, line speed of 180 m/min;

3) second test: blend of vinyl binder 14.45% (w/w) and urea 2.55% (w/w), temperature 150 °C, line speed of 180 m/min;

4) third test: blend of vinyl binder 14.45% (w/w) and urea 2.55% (w/w), temperature 180 °C, line speed of 170 m/min.

The properties of the produced papers are summarized in the following table 23:

Table 23: Properties of the papers produced in the industrial trial.

Binder	Resin (% w/w)	Dry longitudinal tensile (cN/5 cm)	Dry transversal tensile (cN/5 cm)	Wet longitudinal tensile (cN/5 cm)	Wet transversal tensile (cN/5 cm)	Absorption
Vinyl	17	1696	1423	1133	828	7.6
First Test	17	1558	1220	923	624	7.6
Second Test	17	1392	1153	470	302	8.1
Third Test	17	1644	1417	1127	886	7.9

Observing these data, it can be noted that the values of dry and wet tensile of the papers produced by using the blend vinyl binder-urea are slightly lower than those found with the mix containing only the vinyl binder, probably because the percentage of it was inferior.

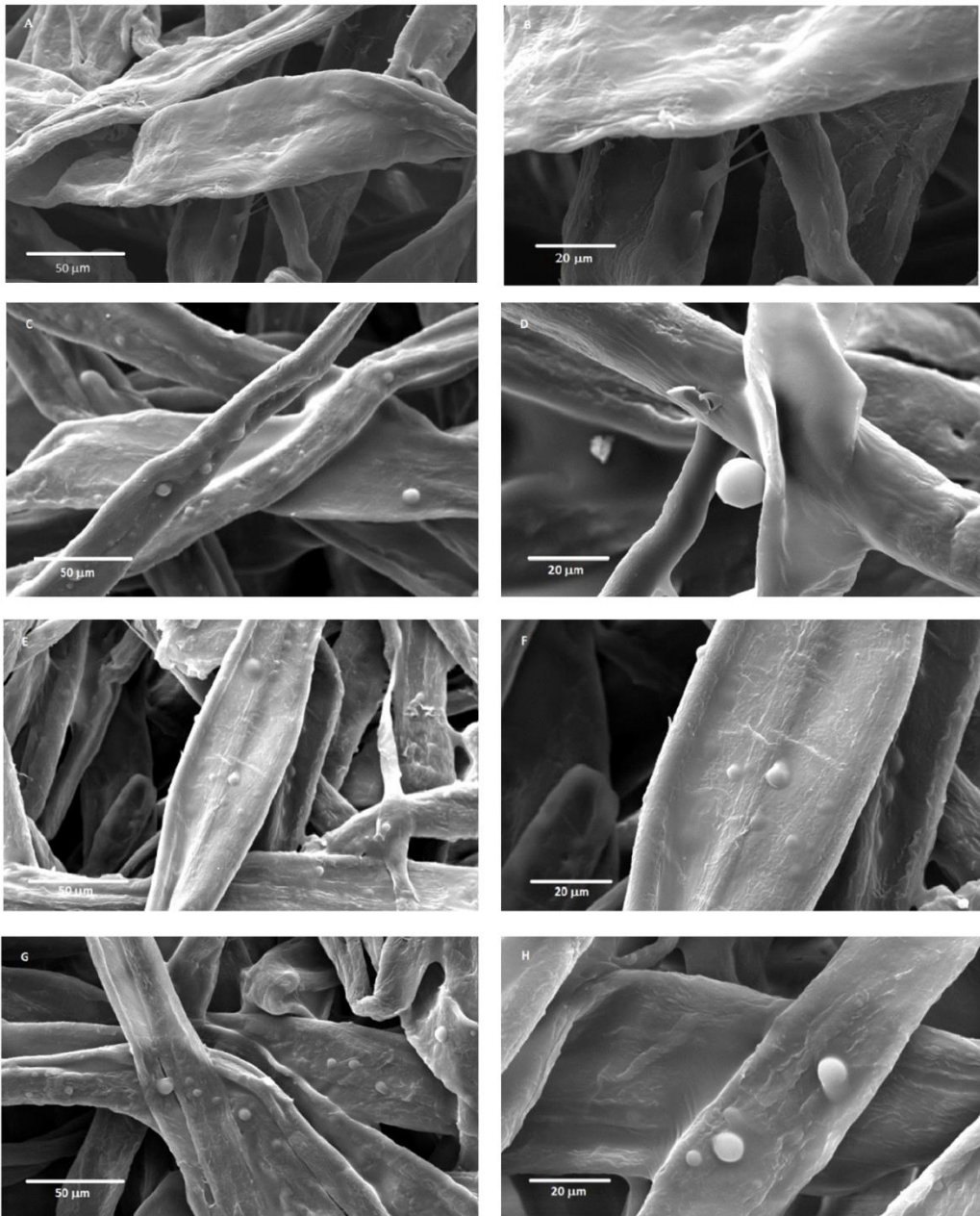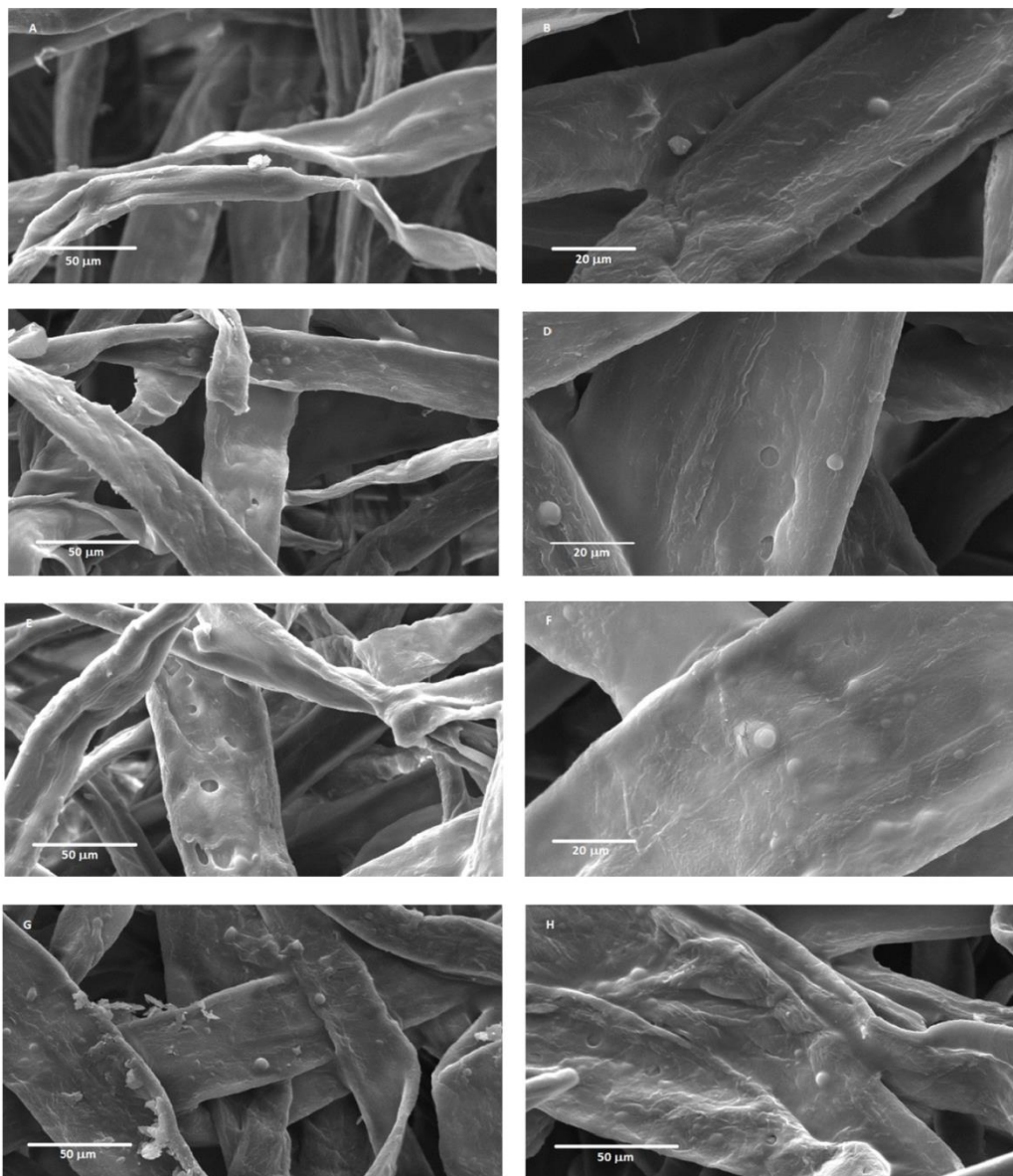SEM analysis was conducted on these papers and in Fig. 56 SEM images are shown.

Fig. 56: SEM images of A – B, airlaid paper without urea, C – D, airlaid paper of the first test, E – F, airlaid paper of the second test and G – H, airlaid paper of the third test.

From the SEM images, it is possible to note the nonwoven structure of the airlaid papers and also, in the images relating to the paper treated with resin containing urea, the presence of small aggregates, which almost look like bubbles and could correspond to water vapor trapped in the glue, or urea crystals, or only lumps of glue. In order to eliminate them, paper was heated to 130 °C for 15 minutes. In Fig. 57 these images are shown:

Figure 57: SEM images of A – B, airlaid paper without urea, C – D, airlaid paper of the first test, E – F, airlaid paper of the second test and G – H, airlaid paper of the third test after the thermal treatment at 130 °C for 15 minutes.

SEM images showed that on all four industrially produced papers there are both bubbles and "traces" attributable to burst bubbles (probably due to the heat treatment). The bubbles are found in all samples quite homogeneously.

On these papers both the essays for the detection of formaldehyde were carried out, with results which are shown in Fig. 58:
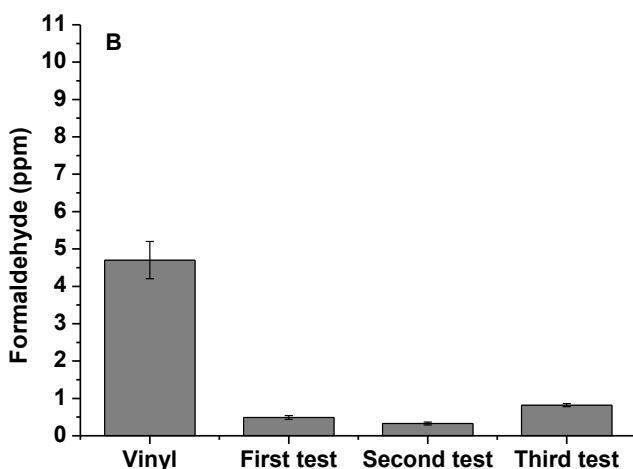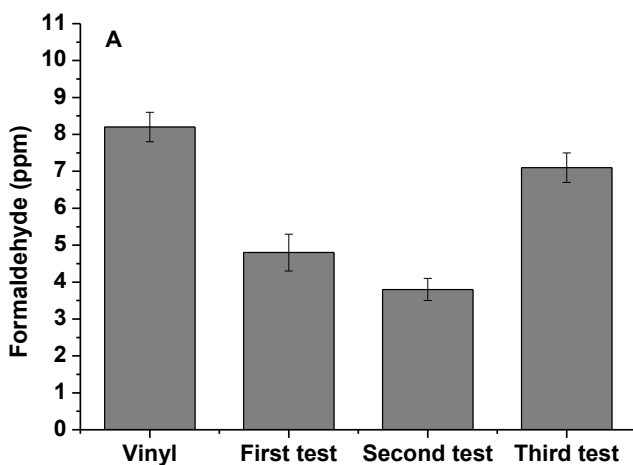
Figure 58: Histograms of the concentration of formaldehyde found A, with the official UNI EN 1541: 2002 method and B, with the first method (n = 10).

As it can be seen, with both the tests carried out in laboratory, a decrease of formaldehyde in the aqueous extract was detected, in particular with the UNI EN 1541: 2002 method, which leads to higher values.

At the same time, the analysis on the paper were also carried out by an accredited external laboratory, "Ecolstudio", which performed the test on the hot aqueous extract, giving the results showed in Table 24:

Table 24: Values of formaldehyde found in the hot aqueous extract by "Ecolstudio" laboratory.

Paper	Concentration of formaldehyde ($\mu g/dm^2$)
Vinyl	4.4
First test	7.0
Second test	5.5
Third test	6.5

Observing these results, a higher value of formaldehyde was found in the papers with the blend vinyl binder-urea. An explanation to these data could be that urea may have interfered with the essay. Furthermore, it is important to keep in mind that in our case urea was added to the vinyl binder, while in the work of Cui et al[225] this molecule was involved in the polymerization of the glue and therefore its effect to the cross-linking may not have been effective. For this reason, since the addition of urea to the vinyl binder did not lead to the desired effects, it was decided to abandon this path.

165

4.3.7 XBS Binder HCHO free and PAE blend

Another research strategy was to test innovative binders offered by the market as the use of the mix composed of XBS Binder HCHO free and PAE, an aqueous dispersion of styrene-butadiene copolymer with 25 - 30 % bio polymer content the first one, while a polyamidoamine-epichlorohydrin resin the second one, instead of the vinyl binder.

The aim was to verify if it can substitute the standard binder, with no HCHO emission and plus a faster biodegradability, while the addition little percentages of PAE was recommended to improve the wet strengths. Tissue paper were prepared using these blends and in the scale laboratory the tensile strengths (both dry and wet) and the other characteristics predictive of the behavior on an industrial scale were measured.

First of all, water was added to dilute XBS Binder from 50% (w/w) down to 17% (w/w) and then the PAE: the effect was the deposit of particles at the bottom as shown in following image (Fig. 59).

Figure 59: Image of the blend composed of XBS Binder HCHO free and PAE, with the deposited particles.

Therefore, it was decided to prepare the blend first adding water into PAE, mixing and then add PAE blend to dilute XBS Binder from TSC 50% down to 17. Following this procedure, the deposit of particles was minor but still present. Thinking in terms of the industrial process, the sedimentation of particles is not acceptable, because it can cause the clog of spray nozzles, in addition to the loss of resin efficiency.
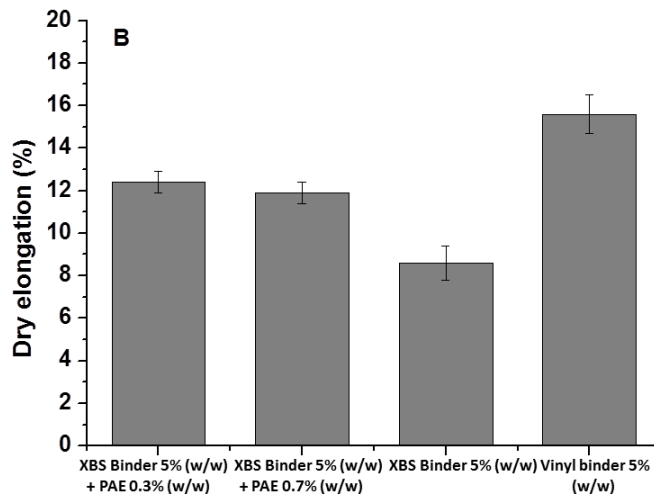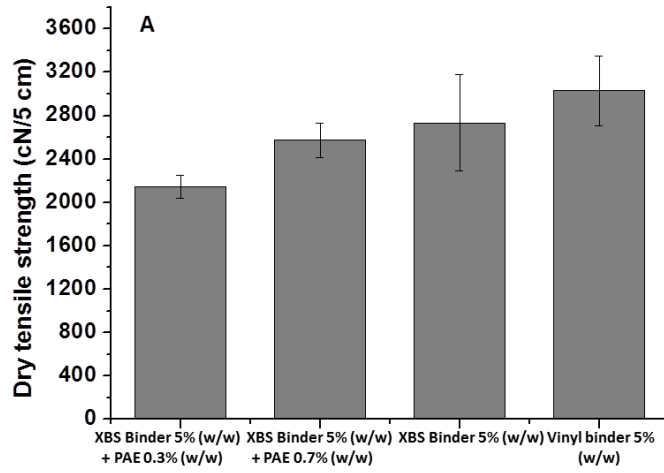
In the following Table 25 the various mixes prepared are shown, together with the percentage of latex on paper found (five replicates for each type of sample):

Table 25: Blends prepared with the average percentages of latex on paper (n = 4).

Samples	Average percentage of latex on paper (%)
XBS Binder 5.0% (w/w)/ PAE 0.3% (w/w)	11.3
XBS Binder 5.0% (w/w)/ PAE 0.7% (w/w)	17.4
XBS Binder 5.0% (w/w)	11.4
Standard Vinyl binder 5.0% (w/w)	13.3

Observing the data in Table 25, we can note that the different percentages of latex on paper were due to the manual submerging method, which not always allowed an optimal repeatability of measurements.

According to the method described in Par. 4.2.3, wet and dry tensile and elongation measurements were carried out and results are shown in Fig. 60:
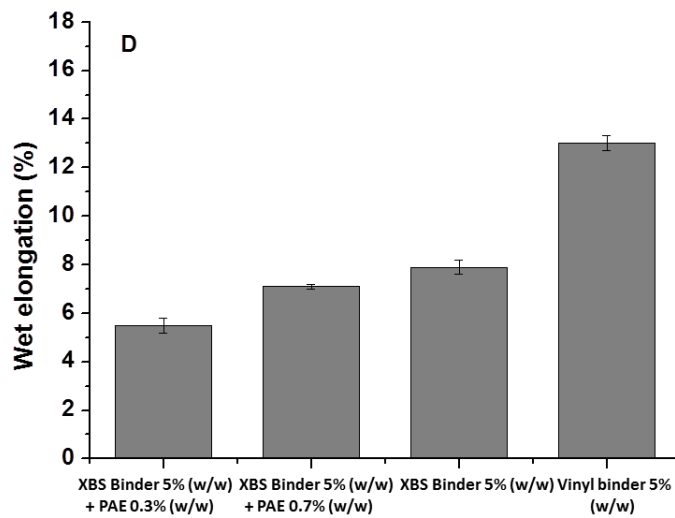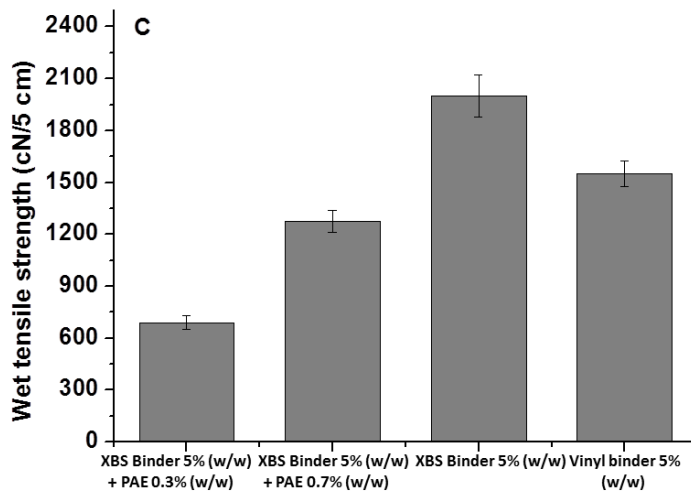
A

Dry tensile strength (cN/5 cm)

XBS Binder 5% (w/w) + PAE 0.3% (w/w) | XBS Binder 5% (w/w) + PAE 0.7% (w/w) | XBS Binder 5% (w/w) | Vinyl binder 5% (w/w)

B

Dry elongation (%)

XBS Binder 5% (w/w) + PAE 0.3% (w/w) | XBS Binder 5% (w/w) + PAE 0.7% (w/w) | XBS Binder 5% (w/w) | Vinyl binder 5% (w/w)

Figure 60: Histograms of A, dry tensile strength, B, dry elongation, C, wet tensile strength and D, wet elongation for the produced samples (n = 10).

Observing the results shown in Fig. 60 A and C, it is possible to note that both dry and wet tensile were lower adding PAE, with values of 2144 ± 103 cN/5 cm, 2576 ± 158 cN/5 cm for dry tensile and 690 ± 38 cN/5 cm and 1277 ± 65 cN/5 cm for wet tensile for the blend with 0.3% (w/w) and 0.7% (w/w) of PAE respectively. This unusual behavior confirmed the polymer sedimentation adding the wet strength agent. Instead, strength values found for XBS Binder (2736 ± 443 cN/5 cm and 2001 ± 120 cN/5 cm for dry and wet tensile respectively) were similar to those of the vinyl resin (3030 ± 321 cN/5 cm and 1550 ± 75 cN/5 cm for dry and wet tensile respectively). Regarding elongation, all the values found were lower than those of the paper with the vinyl binder (Fig. 60 B and D).

Furthermore, the softness of the paper was not evaluable in lab scale due to hard tissue substrate.

Absorption measurements were also carried out on tissue papers, giving the following results (Fig. 61):
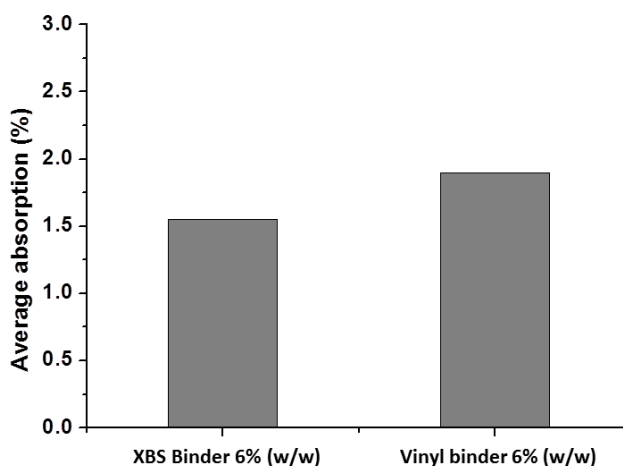
Figure 61: Average absorption values found for the tissue papers.

As shown in Fig. 61, the tissue paper with 6% (w/w) XBS Binder blend presented a lower value of the absorption (1.55 versus 1.90), probably due to a higher hydrophobicity of the polymer: this could also explain the high wet tensile values, with a greater difficulty for water molecules to penetrate the paper.

In conclusion, after the tests conducted in laboratory with the blends composed of XBS Binder HCHO free and PAE, the addition of wet strength agent could not be done due to polymer sedimentation and, in spite of good dry and wet tensile from XBS binder, the absorbency decrease not suitable with final product use did not allow to proceed with the industrial test.

4.3.8 Tests on PVA dispersions

Another pathway of research explored was the use of the aqueous dispersions of PVA, as substitute of the standard binder or in co-formulation with it.

In particular, seven typologies of aqueous dispersions of poly(vinyl alcohol), different from each to other for the initial concentration, pH, hydrolysis degree, viscosity and molecular weight were analyzed. PVA n. 6 is cationic in nature, while the others are anionic, n. 7 is a carboxylated version of n. 4, which makes it more easily dissolvable and more stable over time.

According to par. 4.2.5, for each sample, viscosity was measured and the characteristics of these PVA are listed in table 26:

Table 26: Properties of the seven typologies of PVAs studied.

PVA	Concentration % (w/w)	pH	Density (g/mL)	Hydrolysis degree (%)	Molecular weight (g/mol)	Viscosity (centipoise)	Viscosity 4% (w/w) (centipoise)
1	15.1	5.8	1.03	88.0	40000	/	6.0
2	10.2	6.2	1.03	88.0	150000	/	48.0
3	15.2	6.0	1.03	99.0	40000	/	5.0
4	10.0	6.0	1.03	99.0	100000	/	27.0
5	9.9	5.9	1.03	96.0	124000	600	29.0
6	9.8	5.5	1.03	86.5	85000	2000	20.0
7	9.8	6.8	1.03	98.0	124000	700	30.0

Observing table 26, it is possible to note that the PVAs with a lower viscosity were the ones with lower molecular weight, i.e. PVA number 1, 3 and 6.

Using dispersions at different concentrations, several typologies of tissue paper were prepared in laboratory and the results obtained in the mechanical tests are shown in Fig. 62.
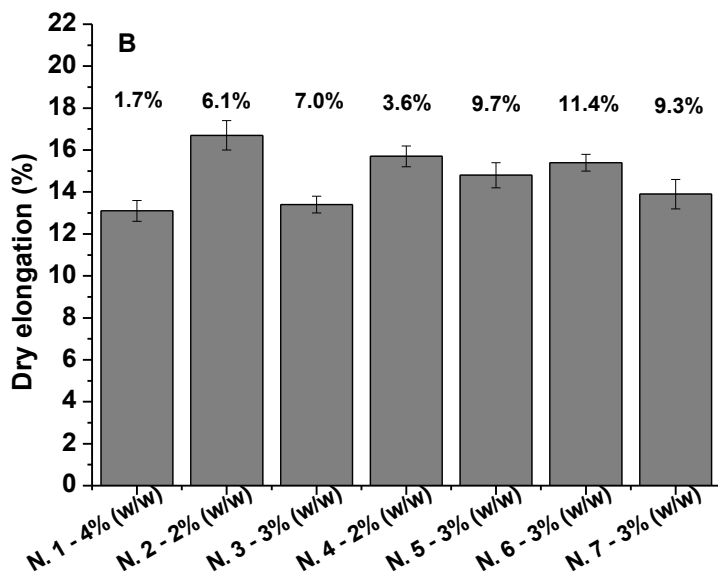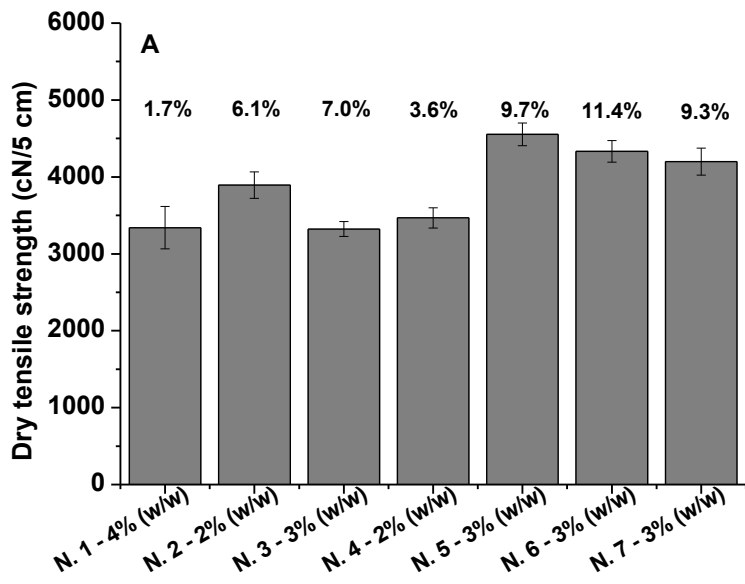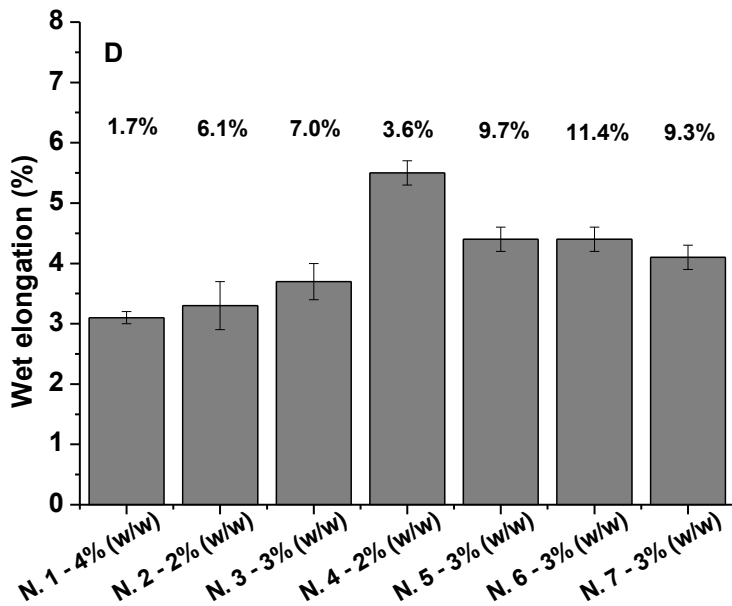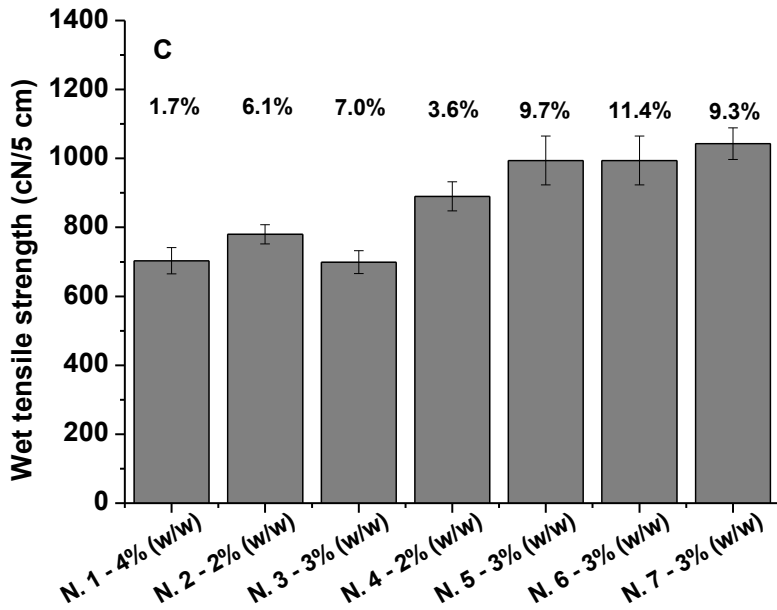
Figure 62: Histograms of A, dry tensile strength, B, dry elongation, C, wet tensile strength and D, wet elongation for the produced samples with the different typologies of PVA. the

labels placed above each column of the histograms represent the values of the percentage of latex on the paper (n = 10).

In Fig. 62 we can see that all the tissue papers presented a different percentage of latex on paper, dependent on the type of PVA used, with the paper with PVA n. 6 which presented the biggest value. These percentages certainly influenced the mechanical properties of the paper. Regarding the dry tensile strength and elongation, the values obtained are quite similar to each other (Fig. 64 A − B), while for the wet tensile strength, the polymers with the highest values are PVA n. 6, and 7, with values of 994 ± 71 cN/5 cm and 1043 ± 46 cN/5 cm respectively (Fig. 62 C). Instead, the paper which presented the highest value of wet elongation was the one with PVA n. 4 (5.5 ± 0.5 %, Fig. 64 D). It is worth of note that all these values are lower than those obtained with the vinyl binder, i.e. 1739 ± 51 cN/5 cm and 11.7 ± 0.1% for wet tensile strength and elongation, respectively.

In conclusion, after the laboratory tests with the PVA it is possible to say that, from the point of view of the viscosity, the best polymers were PVAs n. 1, 3 and 6, while the ones that gave the paper the best wet mechanical properties were n. 4, 6 and 7.

A next step could be to add small quantities of vinyl binder to the PVA, in order to obtain a mix with low viscosity and a paper with better properties and biodegradability.

4.3.9 Blends vinyl binder-EP

An innovative form natural origin binder was tried mixed with the vinyl binder in order to increase the biodegradability and the compostability of the paper. This biodegradable and compostable engineered polysaccharide presents an alpha (1→3) linkage and was obtained by using enzymatic polymerization of sucrose.

The idea was to mix this dispersion with the vinyl binder and analyze the results on tissue paper laboratory scale samples.

According to the usual method, samples with two different blends of vinyl binder-EP were prepared, in particular the mixes tested were two:

1) blend of 6% (w/w) total concentration, with vinyl binder 4.8% (w/w) and EP 1.2% (w/w) (ratio 80:20);

2) blend of 6% (w/w) total concentration, with vinyl binder 4.2% (w/w) and EP 1.8% (w/w) (ratio 70:30).
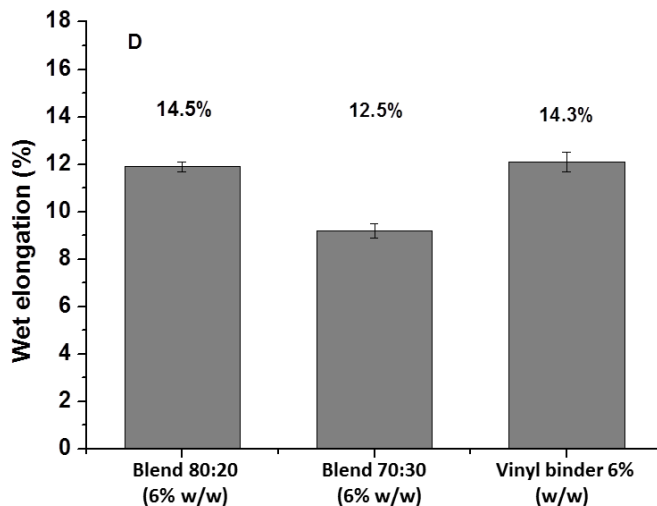
The results obtained are shown in Fig. 63:
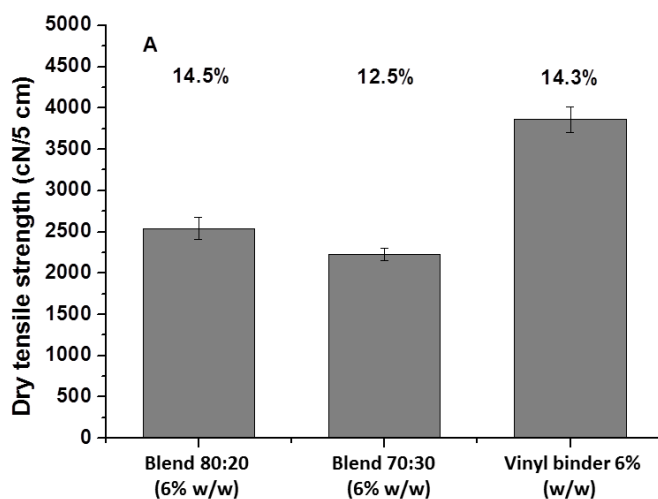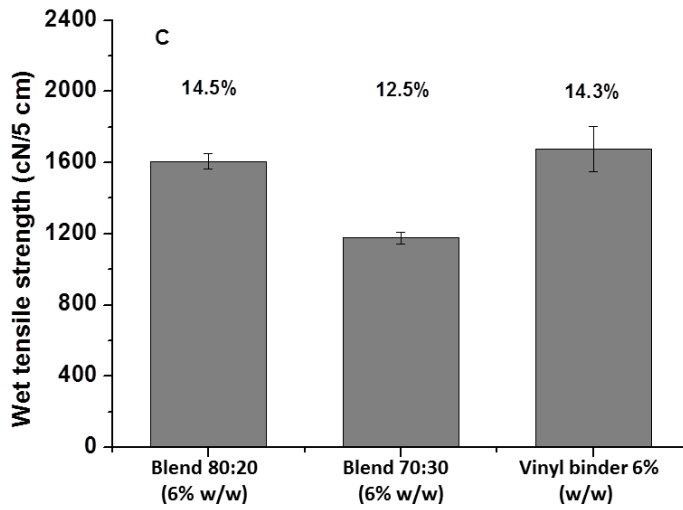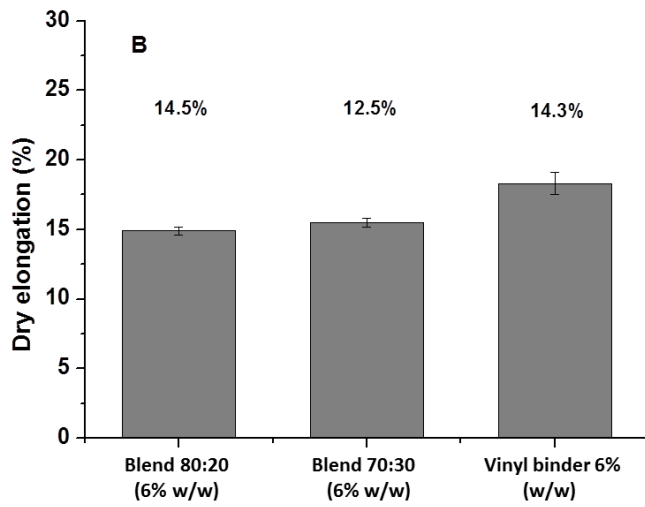
Figure 63: Histograms of A, dry tensile strength, B, dry elongation, C, wet tensile strength and D, wet elongation for the produced samples with the different blends of vinyl binder and EP. The labels placed above each column of the histograms represent the values of the percentage of latex on the paper (n = 10).

Observing Fig. 63, for both the papers with EP dry and wet tensile strength and elongation are lower than the paper with only the vinyl binder, in particular for the paper with a substitution of 30%. As a matter of fact, this paper presented a lower percentage of latex (12.5%).

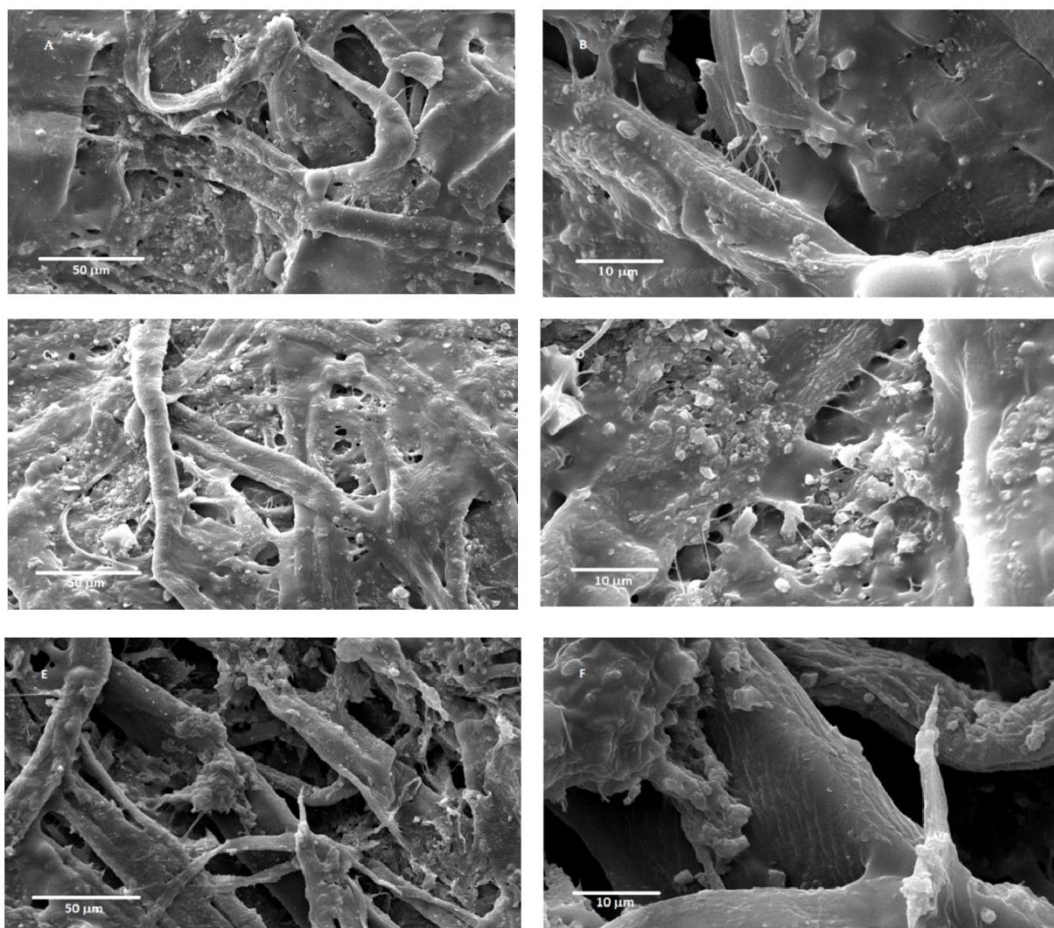In Fig. 64 SEM images of these papers are shown:

Figure 64: SEM images of A – B, tissue paper with the vinyl resin, C – D, tissue paper with 30% substitution of EP and E – F, tissue paper with 20% substitution of EP.

The morphologies of the papers in Fig. 64 are quite similar, with the fibers brought together by the binder and the presence of corpuscular aggregates even in the paper without the EP.

Starting from these laboratory results, an industrial trial was carried out, using a mix with a total concentration of 17% (w/w), 13.6% (w/w) of vinyl binder and 3.4% (w/w) of EP (ratio 80:20).

Before performing the industrial trial, viscosity of the blend used was measured, with the following result:

- viscosity: **12.1 cP**;

- rotational speed: **120 rpm**;

- torque: **24.3%**.

The value obtained were optimal for the production of the airlaid paper.

During the industrial trial no particular technical problems occurred and in the following table the properties of the airlaid papers produced are listed (Table 27):

Table 27: Properties of the airlaid papers produced in the industrial trial.

Trial number	Blend	Latex on paper (%)	Grammage (g/m^2)	Thickness (mm)
1	Vinyl binder	12.33	65.0	1.03
2	Vinyl binder	12.37	64.9	1.11
3	Vinyl binder	12.30	65.1	1.05
4	**Vinyl binder- EP**	**12.53**	**64.0**	**1.11**
5	**Vinyl binder- EP**	**12.63**	**63.7**	**1.07**

In table 27 it is possible to see that properties such as percentage of paper, grammage and thickness are quite similar for all the papers produces, both for those with the EP and for those without.

In the following table 28 mechanical properties of the paper produced during the industrial trial are shown:

Table 28: Results of mechanical tests carried out on the paper produced during the industrial trial.

Latex	Dry tensile strength MD (cN/5 cm)	Dry tensile strength CD (cN/5 cm)	Wet tensile strength MD (cN/5 cm)	Wet tensile strength CD (cN/5 cm)
Average vinyl blend	1567 ± 22	1255 ± 56	898 ± 118	699 ± 76
Average vinyl blend - EP	1778 ± 8	1530 ± 83	725 ± 52	642 ± 7
Difference	**+ 13%**	**+ 22%**	**- 19%**	**-8%**
	+ 18%		**- 14%**	

The results of the industrial trial highlighted, for the paper with the mix vinyl binder - EP a better dry tensile strength (18% higher), probably due to the action of EP as a filler. Regarding the wet tensile strength, there was a decrease of the values, due to the lower quantity of the vinyl binder, but less than expected.

These results encourage to plan new industrial tests at different percentages of substitution of standard binder with the aim of reducing as much as possible the synthetic component and therefore accelerating the biodegradation of the product.

Chapter 5: Conclusions

5.1 Production and characterization of electrospun scaffolds containing 8.0% (w/w) of CNCs

In this work, we produced electrospun scaffolds made of green and nature-inspired polymers. GE, PDLLA, CNCs, and El were carefully chosen as scaffold components because of their complementary properties in terms of hydrophobicity, bioactivity, elasticity, and bioresorbability.[226] The achievement of processing parameters by electrospinning let the production of scaffolds with uniform morphology at a macroscopic level and devoid of any defects or beads at microscopic level. FTIR spectra in the solid state characterized scaffolds at the molecular level. The successful embedding in the scaffolds of crystalline CNCs and of El as well was assessed by XRD and HPLC analysis, respectively. Electrospun scaffolds were cross-linked given the presence of GE and the quantitative degree of cross-linking was evaluated by the TNBS assay. Further insights into the success of the cross-linking reaction were obtained by ATR spectroscopy revealing molecular changes triggered by the cross-linking reaction. One of the main challenges inherent to 3D reticulation of scaffolds is represented by the occlusion of pores. Herein, we demonstrated by SEM that EDC and NHS did not seal the network of interconnected pores. We have characterized the electrospun scaffolds through the investigation of the dimensions of the electrospun fibers, their wettability, elasticity, and resistance to rupture as well. For the first time, we have combined El and nanocellulose in GP electrospun scaffolds. The results were encouraging and the electrospun scaffolds showed good potential. The present study suggests, in the first instance, that CNCs could be used not only as reinforcement but also as a plasticizer for improving the levels of compliance

before failure of the material. Additionally, we demonstrated that brittleness decreases in the swollen state. Last but not least, noncytotoxicity, cell attachment, and proliferation were evaluated for all electrospun scaffolds. Finally, we suggest wound dressing applications as potential use for CNC- and El-containing electrospun membranes.[227]

5.2 Thermal and mechanical characterization at Université Paul Sabatier-Toulouse

During the period spent at Université Paul Sabatier-Toulouse, thermo-mechanical properties of different electrospun scaffolds composed of GE, PDLLA, different percentages of CNCs and the elastin peptide were analyzed. ThermoGravimetric Analysis presented an increase of degradation temperature and hydrophilic properties with addition of CNCs up to 3 % (w/w) and elastin peptide. By using Differential Scanning Calorimetry it was found an increase of the T_g with CNCs addition for the scaffolds series. Furthermore, a correlation between water melting temperature and average fibers diameter, after the swelling test, has been found. Finally, Dynamic Mechanical Analysis showed an important increase of the Tα after the cross-linking and brought to the fore a concentration threshold on storage modulus values.

These results suggest that the electropsun scaffolds show better thermal and mechanical properties than bulk materials and the scaffolds 3NGP and El8NGP have the more interesting parameters for application. Therefore these polymeric blends are useful for the preparation of electrospun scaffolds biocompatible and suitable for applications in the field of tissue engineering.

5.3 Industrial activity (LUCART S.p.A in Avigliano Plant)

This industrial PhD project in collaboration with Lucart SpA mainly consisted in the research of biopolymers and substances of natural origin suitable to be used in the airlaid process in the Avigliano Plant, as cross-linkers in blends or in substitution of the standard vinyl binder.

Airlaid latex-bonded is a Non-Woven process that, while using only cellulose fibers instead of synthetic fibers as in many Non-woven productions, allows to get a high tensile strength product able to be rinsed and reused several times with consequent economic and environmental savings.

A laboratory-scale binder distribution simulation method was developed consisting of a distribution by wetting rather than by spraying as in the industrial plant, but able to compare the results with different binders.

First research efforts were directed to block the development of formaldehyde during the binder crosslinking reaction after checking a scientific publication that obtained this result by adding urea (Cui et al).[225]

The lab-scale method to measure the gaseous formaldehyde was abandoned after verifying the acetaldehyde adduct interference at the same formaldehyde adduct wavelength absorbance.

As the formaldehyde quantity detectable on paper is irrelevant and very close to the detection limit, official UNI EN 1541:2002 aqueous extraction but with hot method was used, generally not applicable to this type of product, but helpful to increase the quantity detected on paper and to have more comparable reference parameters.

Laboratory tests results obtained by adding urea to the standard binder dispersion showed a clear decrease in the production of formaldehyde upon the addition of urea up to a plateau, so, an industrial trial was carried out.

Laboratory scale results was not confirmed in the industrial test as the formaldehyde in the aqueous extract from paper produced adding urea to the binder was even higher than the values coming from standard vinyl binder. In the publication of Cui the result was achieved by adding urea in the polymer preparation phase, the post adduction of urea at commercial binder before using in the industrial process did not show the same cross-linking.

The second path was to collaborate with the Company in the Research and Development of alternative sustainable binders, trying to substitute, partially or totally, the residual synthetic part (the vinyl binder) with substances of natural origin, without compromising the final product properties in terms of tensile strength and physical characteristics (absorbency, softness, color, smell).

Lucart is active from many years in the research for green binders and bio binders, collaborating in the development with the most important producers in the world.

All binders or polymer blends dispersions tested was first verified on a laboratory scale in accordance with the methodology previously adopted, included the viscosity measurement in such a way to be possibly used in the process after lab-scale promising results.

A laboratory test was performed on an innovative XBS Binder, HCHO free and containing 25 - 30 % bio polymer, added with a PAE based wet strength agent: in the scale lab test the addition of wet strength agent could not be done due to
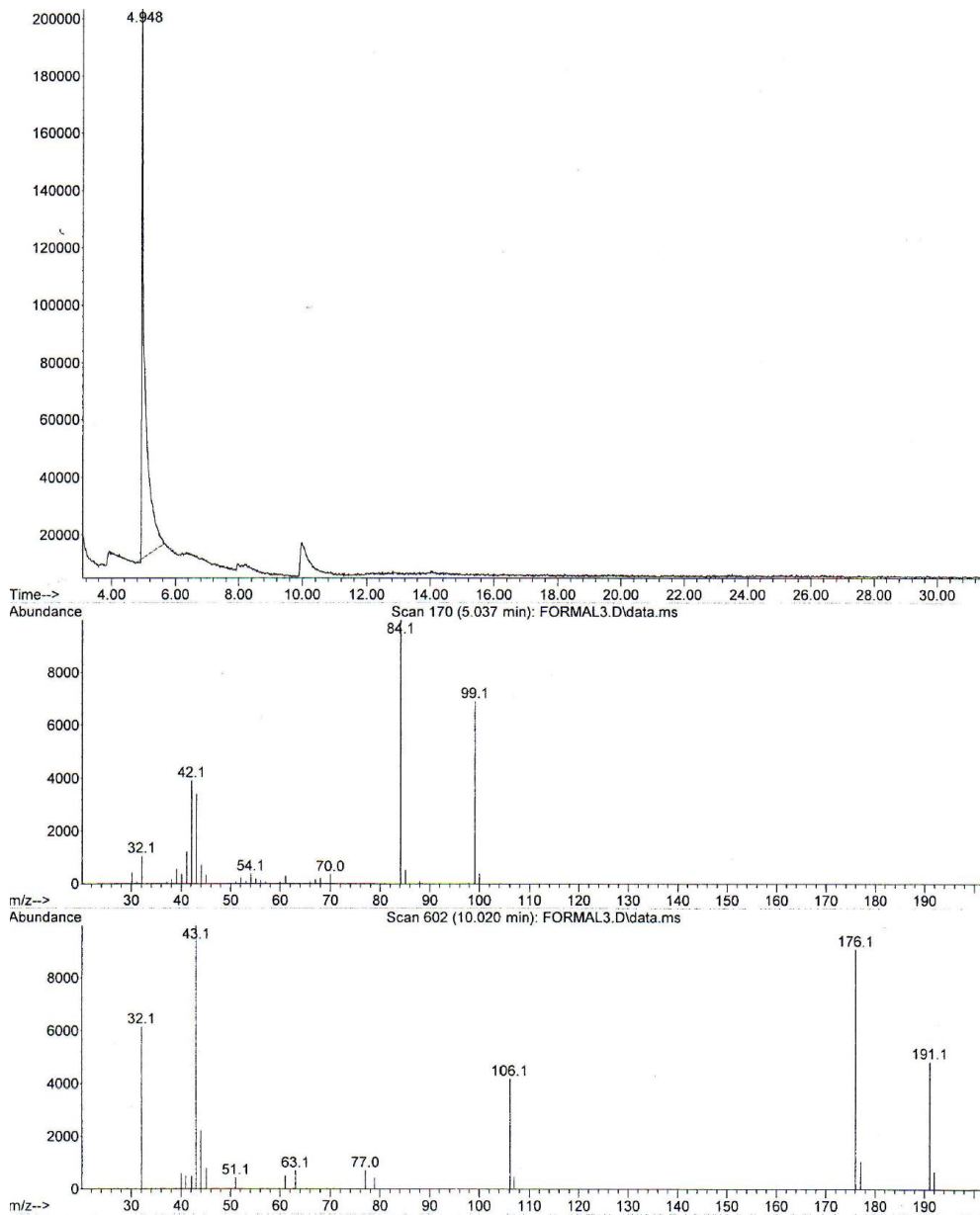
polymer sedimentation. The absorbency of the paper sample with only XBS Binder showed an important absorbency decrease due to a higher hydrophobicity of the polymer and therefore not suitable with final product use.

Many laboratory test was conducted on different PVAs dispersions grades measuring the polymer viscosity and Tensile Dry and Wet Strength on the lab-scale paper prepared, both with PVA only and with the blend PVA-standard vinyl binder. Polyvinyl alcohol (PVA) is a water-soluble synthetic resin employed principally in the treating of textiles and also in a variety of medical applications because of its biocompatibility and its biodegradable & compostable properties. The current cost of PVA does not make it usable in low-cost applications but it is foreseeable that the growing demand of the market will expand its range in the coming years. Laboratory test demonstrated that, due high viscosity values, the stand-alone PVA using cannot be used but a blend with standard binder, although results in a reduction of wet tensile, could be eventually tested in a future industrial trial.

Finally, an innovative binder, a biodegradable and compostable alpha(1→3) linkage engineered polysaccharide was tested. Due to high viscosity and absence of cross-linking properties able to provide wet tensile strenght, the EP was added to the vinyl binder with a substitution of 20%, with the aim of speeding up the final product compostability. Also first industrial trial was performed confirming the reduction of wet tensile anticipated by laboratory test.
New industrial tests at higher percentage of polysaccharide in the blend polymer binder dispersion will be planned in the future.
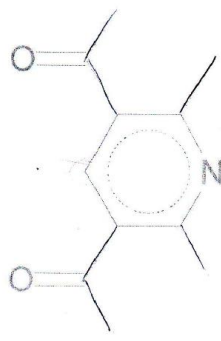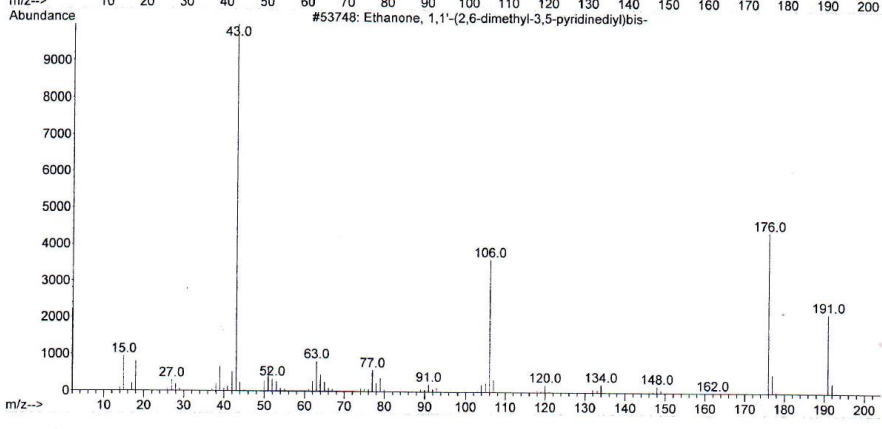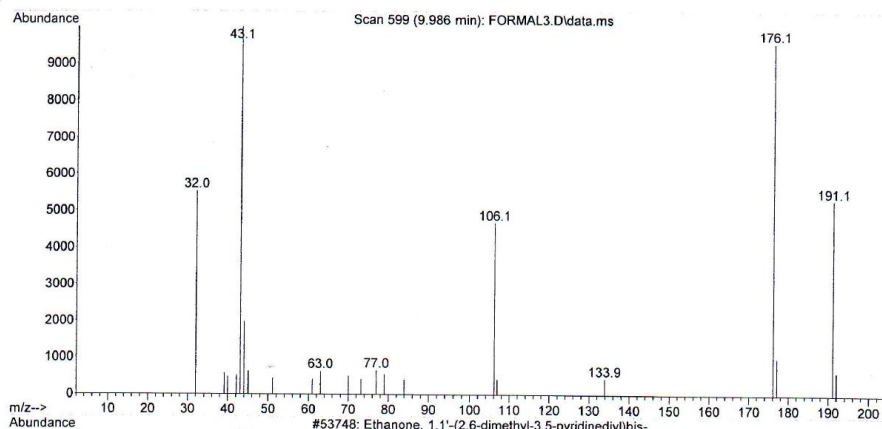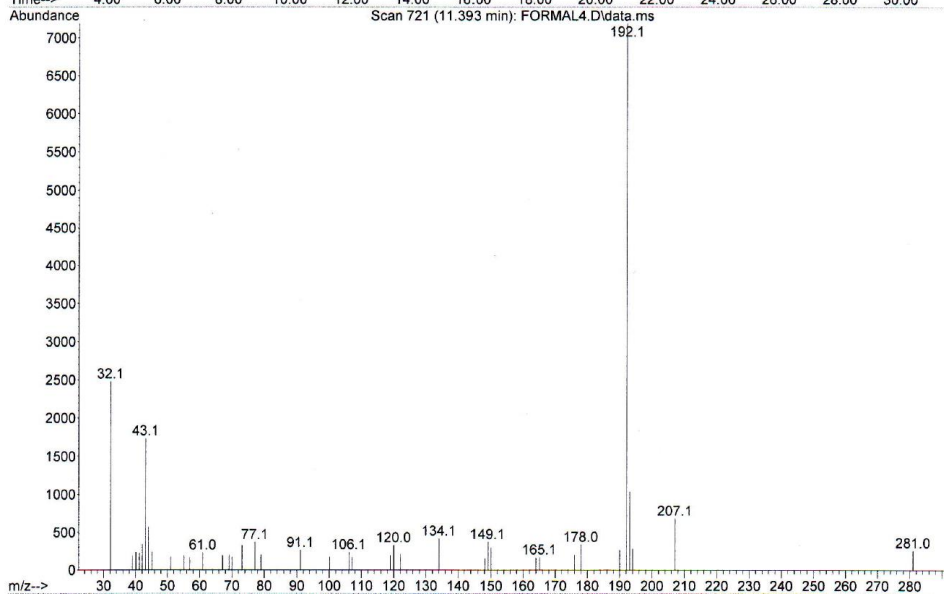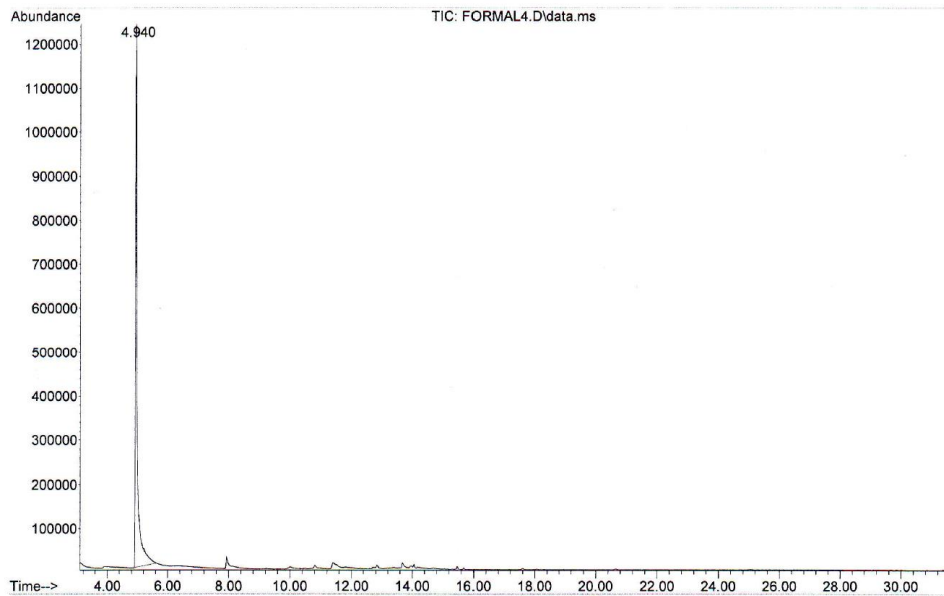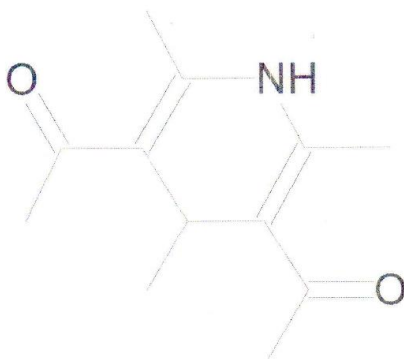
Appendix

Figure 1: GC-MS spectrum of the formaldehyde standard.

TIC: FORMAL4.D\data.ms

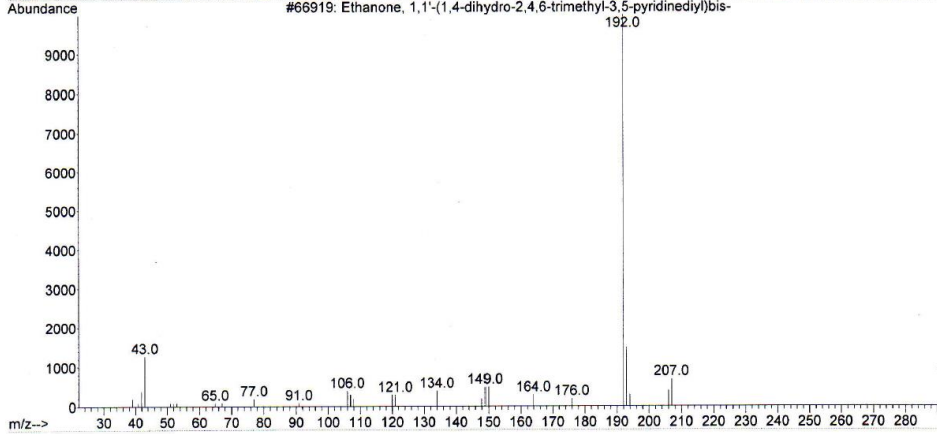Scan 721 (11.393 min): FORMAL4.D\data.ms
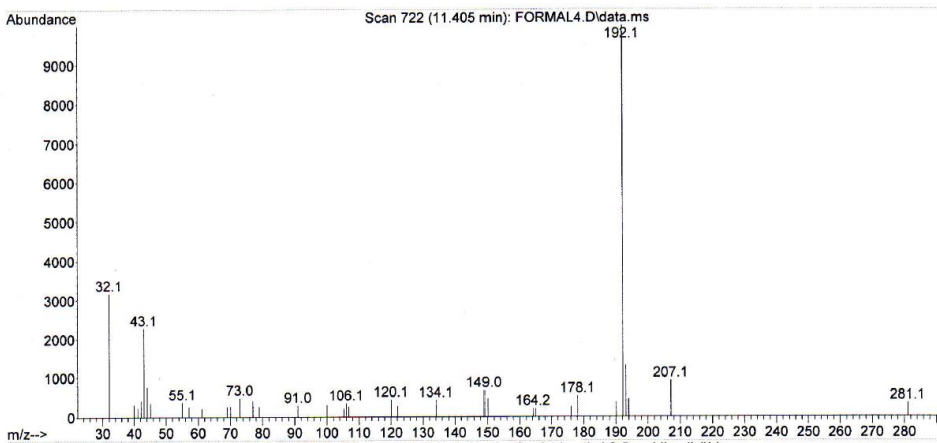
Figure 2: GC-MS spectrum of one sample.

TIC: FORMAL7.D\data.ms

Abundance

Time-->

Scan 587 (9.847 min): FORMAL7.D\data.ms (-575) (-)

Abundance

m/z-->

191
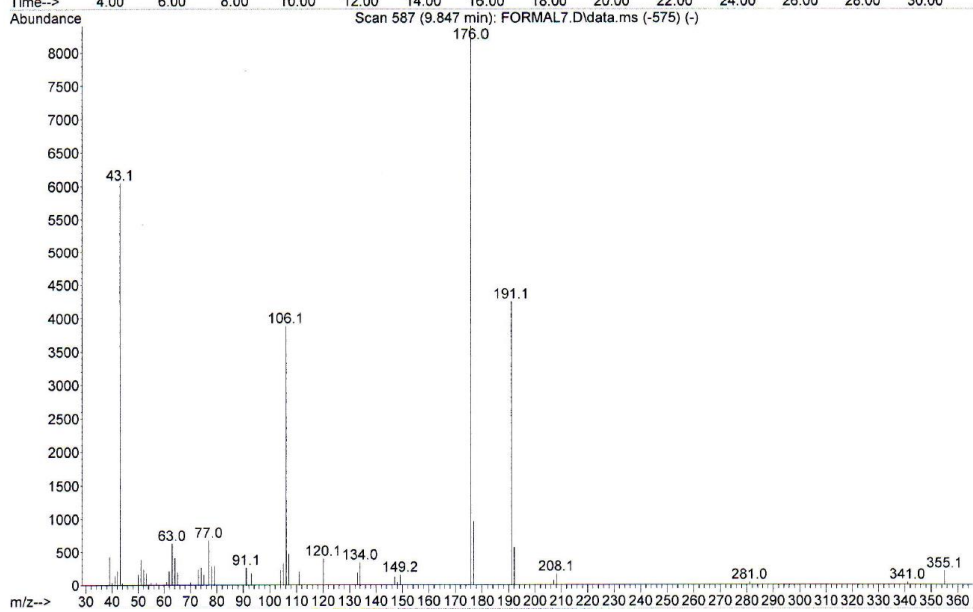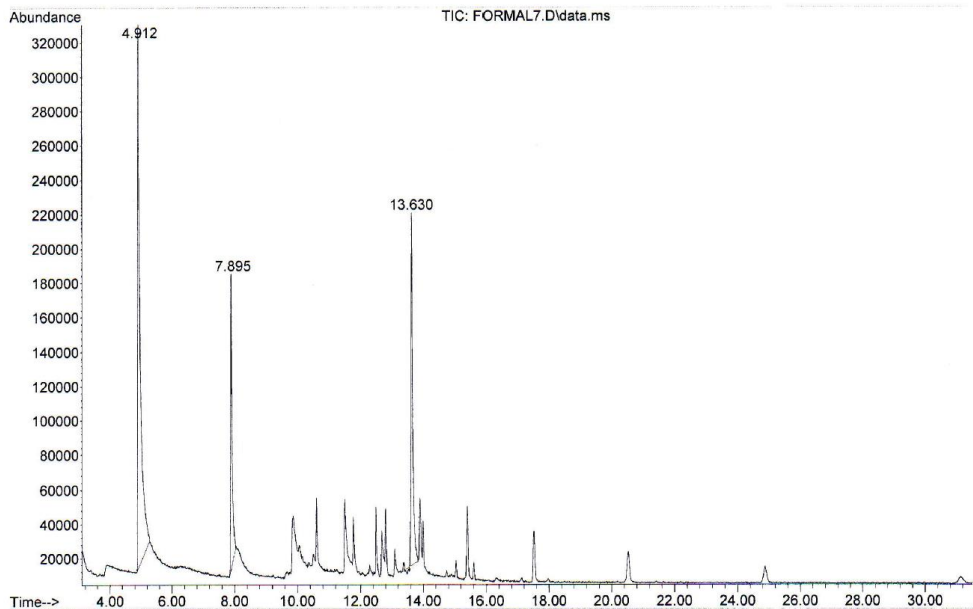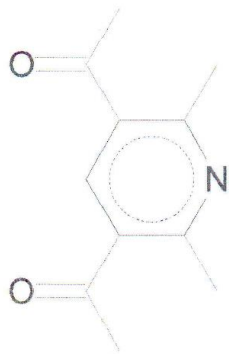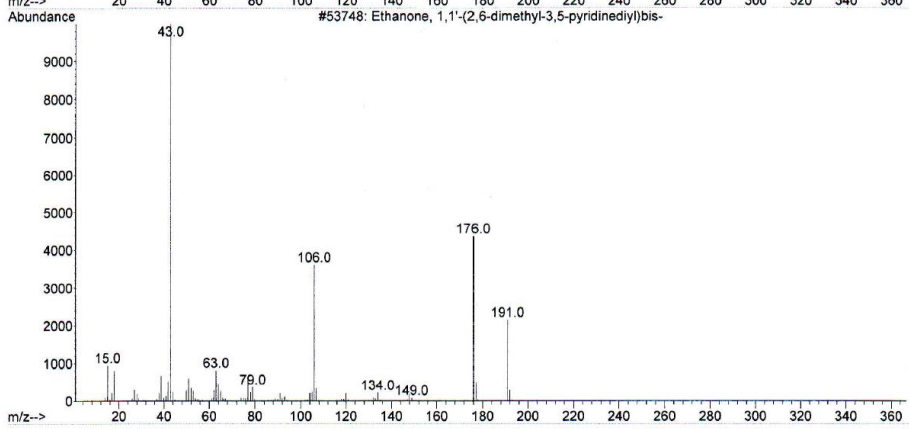
Figure 3: GC-MS spectrum of the paper soaked with the 17% (w/w) vinyl binder.

TIC: FORMAL8.D\data.ms

Scan 161 (4.933 min): FORMAL8.D\data.ms
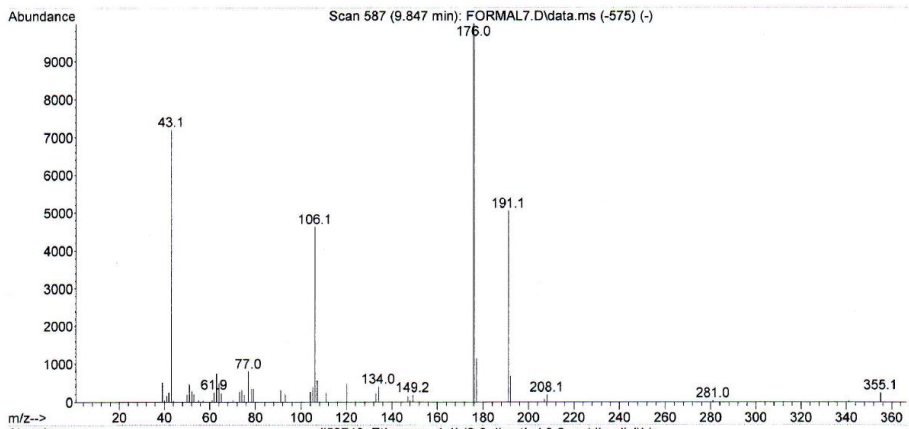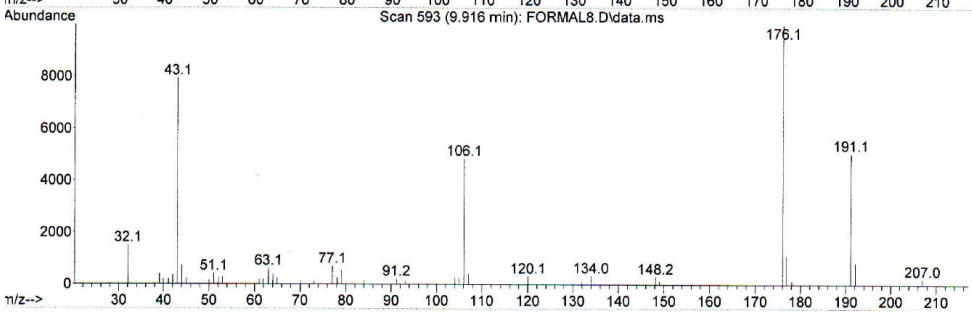
Scan 593 (9.916 min): FORMAL8.D\data.ms

193
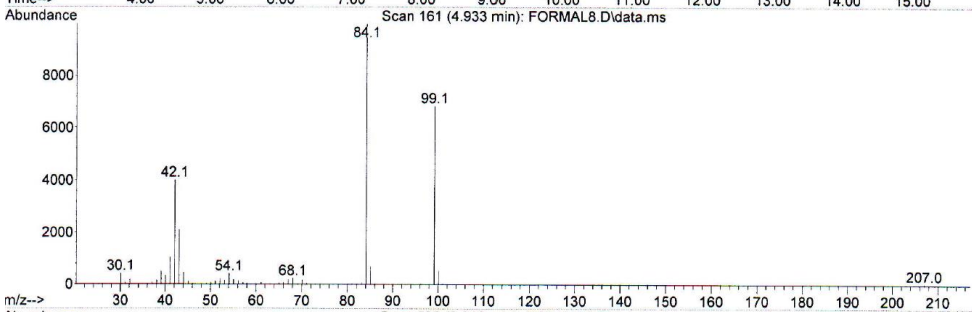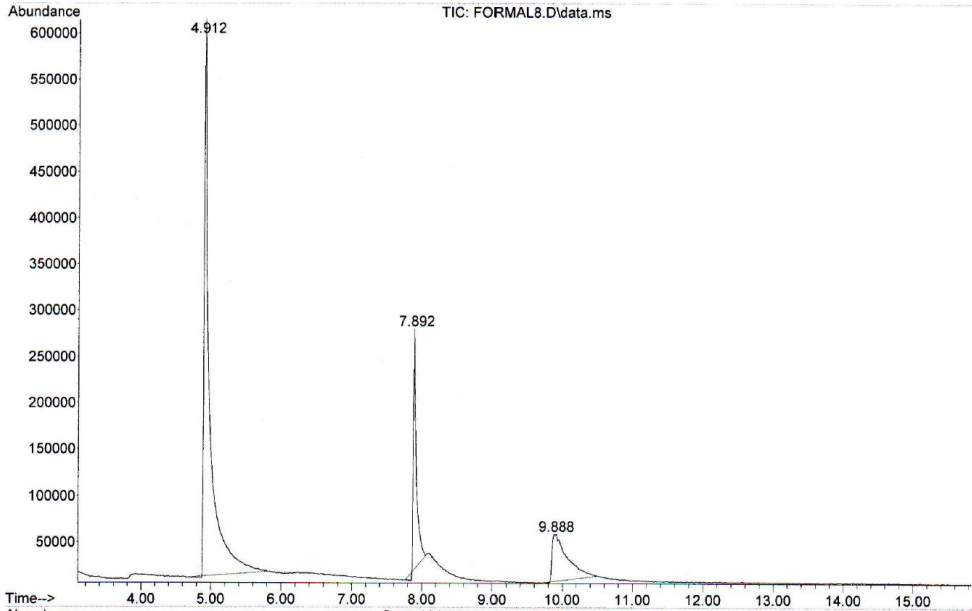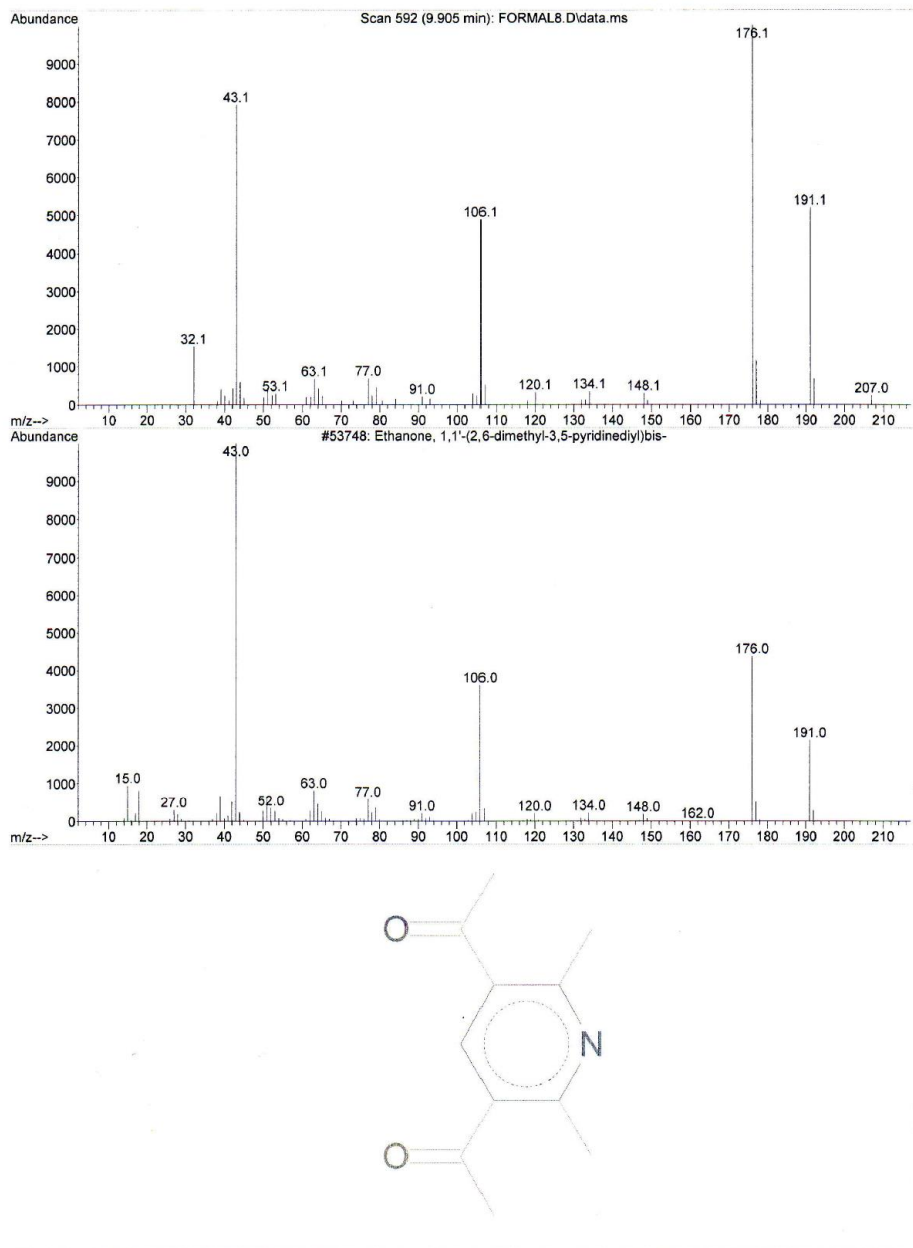
Figure 4: GC-MS spectrum of the paper soaked with the 50% (w/w) resin.

Bibliography

1 P. T. Anastas and J. C. Warner, in *Green Chemistry: Theory and Practice*, Oxford University Press, New York, 1998.

2 I. Horvath and P. T. Anastas, *Chem. Rev.*, 2007, **107**, 2167.

3 P. T. Anastas and N. Eghbali, *Chem. Soc. Rev.,* 2010, **39**, 301-312.

4 S. Ravichandran, *Int. J. Chemtec Res.*, 2011, **3**, (3), 1046-1049.

5 R. Verma, L. Kumar and V. B. Kurba, *Int. J. Phar. Res.*, 2014, **4**, (1), 1-3.

6 L. M. Gilbertson, J. B. Zimmermann, D. L. Plata, J. E. Hutchison and P. T. Anastas, *Chem. Soc. Rev.*, 2015, 1-55.

7 P. T. Anastas, L. B. Bartlett, M. M. Kirchhoff and T. C. Williamson, *Catal. Today*, 2000, **55**, 11-22.

8 M. Koel and M. Kaljurand, *Pure Appl. Chem.*, 2006, **78**, (11), 1993-2002.

9 M. a. Dubé and S. Salehpour, *Macromol. React. Eng.*, 2014, **8**, 7-28.

10 S. D. Dage, *IJRPC*, 2013, **3**, 518-520.

11 V. M. Kolb, *Sustainability,* 2010, **2**, 1624-1631.

12 J. H. song, R. J. Murphy, R. Narayan and G. B. H. Davies, *Phil. Trans. R. Soc. B*, 2009, **364**, 2127-2139.

13 G. Kale, T. Kijchavengkul, R. Auras, M. Rubino, S. E. Selke and S. P. Singh, *Macromol. Biosci.*, 2007, **7**, 255-277.

14 M. S. Peresin, Y. Habibi, J. O. Zoppe, J. J. Pawlak and O. J. Rojas, *Biomacromolecules*, 2010, **11**, 674-681.

15 M. Labet and W. Thielemans, *Chem. Soc. Rev.*, 2009, **38**, 3484-3504.

16 E. Rudnik, in *Compostable Polymer materials*, Elsevier, Amsterdam, 2019.

17 F. De Santis, R. Pantani and G. Titomanlio, *Thermochim. Acta*, 2011, **522**, 128-134.

18 C. S. K. Reddy, R. Ghai, Rashmi and V. C. Kalia, *Bioresour.*, 2003, **87**, 137-146.

19 F. Xie, P. Luckman, J. Milne, L. McDonald, C. Young, C. Y. Tu, T. Di Pasquale, R. Faveere and P. J. Halley, *J. Renew. Mater.*, 2014, **2**, 95-106.

20 M. H. Periayah, A. S. Halim and A. Z. M. Saad, *Pharmacogn. Rev.*, 2016, **10**, (19), 39-42.

21 F. Asghari, M. Samiei, K. Adibkia, A. Akbarzadeh and S. Davaran, *Artif. Cell. Nanomed. B.*, 2017, **45**, (2), 185-192.

22 T. L. Jenkins, *Regen. Med*. 2019, **4**, (1), 15.

23 S. Hinderer, S. L.Layland and K. Schenke-Layland, *Adv. Drug. Deliv. Rev.*, 2016, **97**, 260–269.

24 E. Nyilas and T. H. Chiu, *Bioresorbable polyesters and polyester composites*, U.S. Patent WO 4481353, October 7, 1983.

25 Y.-E. Miao and T. Liu, Electrospun Nanofiber Electrodes: *A Promising Platform for Supercapacitor Applications. In Electrospinning: Nanofabrication and Applications*, B. Ding, X. Wang, J. Yu, Eds. Elsevier: Amsterdam, Netherlands, 2019, 641–669.

26 P. Lu, S. Murray and M. Zhu, *Electrospun Nanofibers for Catalysts. In Electrospinning: Nanofabrication and Applications*, B. Ding, X. Wang and J. Yu, Eds. Elsevier: Amsterdam, Netherlands, 2019; 695–717.

27 S. S. Sankar, S. R. Ede, S. Anantharaj, K. Karthick, K. Sangeetha and S. Kundu, *Catal. Sci.*, 2019, **9**, 1847–1856.

28 Y. Sun, S. Cheng, W. Lu, Y. Wang, P. Zhang and Q. Yao, *RSC Adv.*, 2019, **9**, 25712–25729.

29 J. Xue, Y. Niu, M. Gong, R. Shi, D. Chen, L. Zhang and Y. Lvov, *ACS Nano*, 2015, **9**, 1600–1612.

30 W. Cui, Y. Zhou and J. Chang, *Sci. Technol. Adv. Mater.*, 2010, **11**, 014108.

31 S. Agarwal, J. H. Wendorff and A. Greiner, *Adv. Mater.*, 2009, **21**, 3343–3351.

32 K. D. Patel, H. W. Kim, J. C. Knowles and A. Poma, *Adv. Funct. Mater.*, 2020, **30**, 2001955–2001970.

33 W. Chen, X. Tian, W. He, J. Li, Y. Feng and G. Pan, *BMC Mater.*, 2020, **2**, 1.

34 T. L. Jenkins and D. Little, *npj Regener. Med.*, 2019, **4**, 15–28.

35 S. Hinderer, S. L. Layland and K. Schenke-Layland, *Adv. Drug Delivery Rev.*, 2016, **97**, 260–269.

36 G. Sandri, S. Rossi, M. C. Bonferoni, C. Caramella and F. Ferrari, *Electrospinning Technologies in Wound Dressing Applications.* In *Therapeutic Dressings and Wound Healing Applications*; J. Boateng, Ed. John Wiley & Sons, Inc.: Hoboken, NJ, 2020, 315–336.

37 E. Nyilas and T. H. Chiu, Bioresorbable Polyesters and Polyester Composites. U.S. Patent 4,481,353 A, October 7, 1983.

38 X. Gao, S. Han, R. Zhang, G. Liu and J. Wu, *J. Mater. Chem. B*, 2019, **7**, 7075–7089.

39 M. S. Singhvi, S. S. Zinjarde and D. V. Gokhale, *J. Appl. Microbiol.*, 2019, **127**, 1612–1626.

40 B. Gupta, N. Revagade and J. Hilborn, *Prog. Polym. Sci.*, 2007, **32**, 455–482.

41 L. Fambri, A. Pegoretti, R. Fenner, S. D. Incardona and C. Migliaresi, Polymers, 1997, **38**, 79–85.

42 G. Reddy, M. Altaf, B. J. Naveena, M. Venkateshwar and E. V. Kumar *Biotechnol. Adv.*, 2008, **26**, 22–34.

43 K. Fukushima, K. Sogo, S. Miura and Y. Kimura, *Macromol. Biosci.* 2004, **4**, 1021–1027.

44 J. R. Dorgan, H. Lehermeier and M. Mang, *J. Polym. Environ.*, 2000, **8**, 1–9.

45 B. Desguin, P. Soumillion, R. P. Hausinger and P. Hols, *FEMS Microbiol. Rev.*, 2017, **41**, S71–S83.

46 S. Salminen, A. V. Wright and A. Ouwehand, *Lactic Acid Bacteria: Microbiological and Functional Aspects, 3rd ed., Revised and Expanded*, Marcel Dekker, Inc.: New York, NY, 2004.

47 P. Goffin, M. Deghorain, J.-L. Mainardi, I. Tytgat, M.-C. Champomier- Vergés, M. Kleerebezem and P. Hols, *J. Bacteriol.*, 2005, **187**, 6750–6761.

48 K. O. Stetter and O. Kandler, *Arch. Mikrobiol.*, 1973, **94**, 221–247.

49 T. Hiyama, S. Fukui and K. Kitahara, *J. Biochem.* 1968, 64, 99–107.

50 T. Casalini, F. Rossi, A. Castrovinci and G. Perale, *Front. Bioeng. Biotechnol.*, 2019, **7**, 259–274.

51 K. Madhavan Nampoothiri, N. R. Nair and R. P. John, *Bioresour. Technol.*, 2010, **101**, 8493–8501.

52 S. Inkinen, M. Hakkarainen, A.-C. Albertsson and A. Södergård, *Biomacromolecules*, 2011, 12, 523–532.

53 B. Bochicchio, K. Barbaro, A. De Bonis, J. V. Rau and A. Pepe, *J. Biomed. Mater. Res. A*, 2020, **108**, 1064–1076.

54 S. Alippilakkotte and L. Sreejith, *J. Appl. Polym. Sci.*, 2018, **135**, 46056–46068.

55 A. Eskandarinia, A. Kefayat, M. Agheb, M. Rafienia, M. A. Baghbadorani, S. Navid, K. Ebrahimpour, D. Khodabakhshi and F. Ghahremani, *Sci. Rep.* 2020, **10**, 3063–3077.

56 G. C. Yeo, B. Aghaei-Ghareh-Bolagh, E. P. Brackenreg, M. A. Hiob, P. Lee and A. S. Weiss, *Adv. Healthcare Mater.* 2015, **4**, 2530–2556.

57 A. M.Tamburro, A. Pepe and B. Bochicchio, *Biochemistry*, 2006, **45**, 9518–9530.

58 S. Natarajan, K. Harini, G. P. Gajula, B. Sarmento, M. T. Neves-Petersen and V. Thiagarajan, *BMC Mater.*, 2019, **1**, 2.

59 C. Liu, X. Xu, J. Zhou, J. Yan, D. Wang and H. Zhang, *BMC Mater.*, 2020, **2**, (7).

60 S. Liu, S. Qin, M. He, D. Zhou, Q. Qin and H. Wang, *Composites B*, 2020, **199**, 108238–108262.

61 R. Hashaikeh, P. Krishnamachari and Y. A. Samad, *Nanomanifestation of Cellulose: Applications for Bio-degradable Composites.* In *Handbook of Polymer Nanocomposites Processing, Performance and Application: Volume C: Polymer Nanocomposites of Cellulose Nanoparticles*, J. K. Pandey and H. Takagi, A. N. Nakagaito, H.-J. Kim, Eds. Springer: New York, NY, 2015; 229–248.

62 Y. Habibi, L. A. Lucia and O. J. Rojas, *Chem. Rev.*, 2010, **110**, 3479–3500.

63 S. Beck-Candanedo, M. Roman and D. G. Gray, *Biomacromolecules*, 2005, **6**, 1048–1054.

64 I. Sakurada, Y. Nukushina and T. Ito, *J.Polym. Sci.*, 1962, **57**, 651–660.

65 H.-Y. Yu, C. Wang and S. Y. H. Abdalkarim, *Cellulose*, 2017, **24**, 4461–4477.

66 T. Ben Shalom, Y. Nevo, D. Leibler, Z. Shtein, C. Azerraf, S. Lapidot and O. Shoseyov, *Macromol. Biosci.* 2019, **19**, 1800347.

67 Z. Fan, B. Liu, J. Wang, S. Zhang, Q. Lin, P. Gong, L. Ma and S. Yang, *Adv. Funct. Mater.*, 2014, **24**, 3933–3943.

68 N. Bhardwaj and S. C. Kundu, *Biotechnol. Adv.* 2010, **28**, 325–347.

69 J. Stanger, N. Tucker and M. Staiger, *Rapra Rev. Rep.*, 2005, **16**, 10.

70 J. F. Cooley, *Apparatus for electrical dispersing fluids*, U. S. Patent 692631, 1902.

71 A. Formhals, *Process and Apparatus for Preparing Artificial Threads*, U. S. Patent 1975504, 1934.

72 G. I. Taylor, *R. Soc. Lond. Proc. Ser. A Math. Phys. Sci.*, 1964, **280**, 1382.

73 G. I. Taylor, *R. Soc. Lond. Proc. Ser. A Math. Phys. Sci.*, 1965, **291**, 1425.

74 G. I. Taylor, *R. Soc. Lond. Proc. Ser. A Math. Phys. Sci.*, 1969, **313**, 1515.

75 J. Doshi and D.H. Reneker, *J. Electrostat.*, 1995, **35**, 2-3, 151.

76 S. Thenmozhi, N. Dharmaraj, K. Kadirvelu and Hak Yong Kim, *Mater. Sci. Eng. B*, 2017, **207**, 36-48.

77 I. Sas, R. E. Gorga, J. A. Joines and K. A. Thoney, *J. Polym. Sci. Pol. Phis.*, 2012, **50**, 824-845.

78 H.S. Wang, G.D. Fu and X.S. Li, *Recent Pat. Nanotech.,* 2009, **3**, (1), 21-31.

79 D.H. Reneker, A.L. Yarin, E.Zussman and H. Xu, *Adv. Appl. Mech.,* 2007, **41**, 43-19.

80 H. Karakaş, *MDT "Electrospinning",* 2015, 2-35.

81 D. H. Reneker and I. Chun, *Nanotechnology*, 1996, **7**, 216-223.

82 M. Cloupeau, and B. Prunet-Foch, *J. of Electrostatics*, 1990, **25**, 165.

83 A. L. Yarin, S. Koombhongse and D. H. Reneker, *J. Appl. Phys.*, 2001, **89**, 3018-3025.

84 T. Subbiah, G. S. Bhat, R. W. Tock, S. Parameswaran and S. S. Ramkumar, *J. Appl. Polym. Sci.*, 2005, **96**, 557-569.

85 Y. M. Shin, M. M. Hohman, M. P. Brenner and G. C. Rutledge, *Appl. Phys. Lett.*, 2001, **78**, 1149-1151.

86 A. K. Haghi and M. Akbari, *Phys. Stat. Sol. A*, 2007, **204**, 1830-1834.

87 B. Bera, *I.J.I.R.*, 2016, **2**, (8), 972-984.

88 Z. Li and C. Wang, *One Dimensional Nanostructures, Electrospinning Technique and Unique Nanofibers*, 2013.

89 X. Zong, K. Kim, D. Fang, S. Ran, B.S. Hsiao and B. Chu, *Polymer*, 2002, **439**, 4403–4412.

90 S. Ramakrishna, K. Fujikara, W.E. Teo, T.C. Lim and Zuwel. Ma, *An Introduction to Electrospinning and Nanofibers*, World Scientific Publishing Pvt. Ltd., 2005.

91 Buchko C.J., Chen L.C., Shen Yu and D.C. Martin, *Polymer*, 1999, **40**, 7397–7407.

92 C. Zhang, X. Yuan, L. Wu, Y. Han and J. Shang, *Eur. Polym. J.*, 2005, **41**, 423–432.

93 C. Su, C. Lu, H. Cao, F. Gao, J. Chang, Y. Li and C. He, *Materials Letters*, 2017, **204**, 8-11.

94 G. C. Rutledge and S. V. Fridrikh, *Adv. Drug. Deliv. Rev.* 2007, **59**, 1384-1391.

95 B. Robb and B. Lennox, *Electrospinning for Tissue Engineering*, Woodhead Publishing in Materials, 2011.

96 J. Venugopal, Sharon Low, Aw Tar Choon and S. Ramakrishna, *J. Biomed. Mater. Res. B*, 2007, **84B**, 1, 34-48.

97 X. Geng, O. H. Kwon and J. Jang, *Biomaterials*, 2005, **26**, 5427–5432.

98 C. S. Ki, D. H. Baek, K. D. Gang, K. H. Lee, I. C. Um and Y. H. Park, *Polymer*, 2005, **46**, 5094–5102.

99 C. L. Casper, J. S. Stephens, N. G. Tassi, D. B. Chase and J. F. Rabolt, *Macromolecules*, 2004, **37**, 573–578.

100 H. S. SalehHudina , E. N. Mohamada, W. N. L. Mahadib, and A. M. Afifi, *Mater. Manuf. Proc*ess. 2018, **33**, (5), 479-498.

101 C. Wang, H. S. Chien, C. H. Hsu, Y. C. Wang, C. T. Wang and H. A. Lu, *Macromolecules*, 2007, **40**, (22), 7973–7983.

102 D. Rodoplu and M. Mutlu, *J. Eng. Fibers Fabr.*, 2012, **7**, (2), 118–123.

103 C.H. Kim, Y.H. Jung, H.Y. Kim, D.R. Lee, N. Dharmaraj and K.E. Choi, *Macromol. Res.*, 2006, **14**, 59–65.

104 K. Ohkawa, H. Kim, K. Lee and H. Yamamoto, *Macromol. Symp.*, 2004, **216**, 301–306.

105 C. Lee and S. Hong, *Mod. Chem. Appl. 2*, 2014, **144**, 1-5.

106 L. Avérous, in *Monomers, Polymers and* Composites, ed A. Gandini, M. N. Belgacem, Elsevier, 2008, 433-450.

107 C. H. Hong, S. H. Kim, J. Y. Seo and D. S. Han, *ISRN Polymer Science*, 2012, 1-6.

108 D. R. Witzke, *Introduction to Properties, Engineering, and Prospects of Polylactide Polymers*, in *Chemical Engineering*. 1997, Michigan State University: East Lansing, Michigan, 1997, 32-72.

109 K. Madhavan Nampoothiri, N. R. Nair and R. P. John, *Bioresour. Technol.* 2010, **101**, 22, 8493-8501.

110 S. Inkinen, M. Hakkarainen, A. C. Albertsson and A. Sodergard, *Biomacromolecules*, 2011, **12**, 3, 523-532.

111 W.Hoogsten, A. R. Postema, A. J. Pennings, G. t. Brinke and P. Zugenmair, *Macromolecules*, 1990, **23**, 634.

112 M. Savioli Lopes, A. L. Jardini and R. Maciel Filho, *Procedia Eng.*, 2012, **42**, 1402-1413.

113 A. Gandini, *Green Chem.*, 2011, **13**, 1061-1083.

114 A. Gandini and T. M. Lacerda, *Prog. Polym. Sci.*, 2015, **48**, 1-39.

115 T. Mohan, S. Hribernik, R. Kargl and K. Stana-Kleinschek, in *Cellulose - Fundamental Aspects and Current Trends*, 2015.

116 D. Klemm, F. Kramer, S. Moritz, T. Lindström, M. Ankerfors, D. Gray and A. Dorris, *Angew. Chem. Int.*, 2011, **50**, 5438–5466.

117 M. Roman and W. T. Winter, *Biomacromolecules*, 2004, **5**, 1671-1677.

118 N. Wang, E. Ding and R. Cheng, *Polymer*, 2007, **48**, 3486-3493.

119 N. Wang, E. Ding and R. Cheng, *Langmuir*, 2008, **24**, 5-8.

120 N. Lin, J. Huang and A. Dufresne, *Nanoscale*, 2012, **4**, 3274-3294.

121 K. Hofman, B. Hall, H. Cleaver and S. Marshall, *Anal. Biochem.*, 2011, **417**, 289-291.

122 S. Farris, J. Song and Q. Huang, *J. Agric. Food Chem.*, 2009, **58**, 998-1003.

123 http://jennifermojica.com/2016/05/31/do-you-know-the-most-abundant-protein-in-the-human-body/.

124 A. A. Mariod and H. F. Adam, *Acta Sci. Pol., Technol. Aliment.*, 2013, **12**, (2), 135-147.

125 F. A. Johnston-Banks, *Gelatin*, in *Food gels.*, ed. P. Harris. Elsevier Appl. Sci., London, 1990, 233-289.

126 L. Debelle and A. M. Tamburro, *Int. J. Biochem. Cell Biol.*, 1999, **31**, 261-272.

127 A. C. Weihermann, M. Lorencini, C. A. Brohem and C. M. De Carvalho, *Int. J. Cosmet. Sci.*, 2017, 39, 241-247.

128 M. J. Fazio, M. G. Mattei, E. Passage, M. L. Chu, D. Black, E. Solomon, J. M. Davidson and J. Uitto, *A. J. Hum. Genet.*, 1991, **48**, 696-703.

129 *Swiss Prot. AccessionnumberP15502.*

130 F. C. M. Smits, B. C. Buddingh, M. B. Van Eldijk and J. C. M. Van Hest, *Macomol Biosci.*, 2015, **15**, 36-51.

131 L. D. Muiznieks, A. S. Weiss and F. W. Keeley, *Biochem. Cell Biol.*, 2010, **88**, 239-250.

132 M. I. Chung, M. Miao, R. J. Stahl, E. Chan, J. Parkinson, and F. W. Keeley, *Matrix Biol.*, 2006, **25**, (8), 492–504.

133 B. Vrhovski and A. S. Weiss, *Eur. J. Biochem.*, 1998, **258**, 1-18.

134 V. Samouillan, C. Andre, J. Dandurand and C. Lacabanne, *Biomacromolecules*, 2004, **5**, 958-964.

135 S. Sawant and R. Shegokar, *Bone scaffolds: What's new in nanoparticle drug delivery research?*, in *Nanobiomaterials in Hard Tissue Engineering Applications of Nanobiomaterials Volume 4*, Elsevier, Amsterdam, 2016, 155-187.

136 S. L. Martin, B. Vrhovski and A. S. Weiss, *Gene*, 1995, **154**, (2), 159-166.

137 B. Vrhovski, S. Jensen and A. S. Weiss, *Eur. J. Biochem.*, 1997, **250**, 92-98.

138 L. Debelle, A. J. P. Alix, S. M. Wei, M. P. Jacob, J. P. Huvenne, M. Berjot and P. Legrand, *Eur. J. Biochem.*, 1998, **258**, 533-539.

139 N. Davidenko, J. J. Campbell, E. S. Thien, C. J. Watson and R. E. Cameron, *Acta Biomater*. 2010, **6**, 3957-3968.

140 C. M. Ofner and W. A. Bubnis, *Pharm. Res.*, 1996, **13**, (12), 1821-1827.

141 L. V. Azároff, R. Kaplow, N. Kato and R. J. Weiss, A. J. C. Wilson, *X-Ray Diffraction*, 1974.

142 P. A. Jacobson, L. G. Rosa, C. M. Othon, K. L. Kraemer, A. V. Sorokin, S. Ducharme and P. A. Dowben, *Appl. Phys. Lett.*, 2004, **88**, (1), 88-90.

143 D. P. Subedi, *The Himalayan Phisycs*, 2011, **2**, 1-4.

144 K. Srinivas, *Advan. SES*, 2017.

145 V. Kuete, O. Karaosmanoğlu and H. Sivas, *Anticancer Activities of African Medicinal Spices and Vegetables*, in Medicinal spices and vegetables from Africa, 2017, Cambridge, Massachusetts, USA.

146 N. Saadatkhah, A. Carillo Garcia, S. Ackermann, P. Leclerc, M. Latifi, S. Samih, G. S. Patience and J. Chaouki*, Can. J. Chem. Eng.* 2020, **98**, 34–43.

147 D. Annis, A. Bornat, R. O. Edwards, A. Higham, B. Loveday, and J. Wilson, *Trans. Am. Soc. Artif. Intern. Organs*, 1978, **24**, 209–214.

148 M. Li, M. J. Mondrinos, X. Chen, M. R. Gandhi, F. K. Ko and P. I. Lelkes, *J. Biomed. Mater. Res. A*, 2006, **79**, 963–973.

149 S. G. Kumbar, S. P. Nukavarapu, R. James, L. S. Nair and C. T. Laurencin, *Biomaterials*, 2008, **29**, 4100–4107.

150 J. Rnjak-Kovacina, S. G. Wise, Z. Li, P. K. M. Maitz, C. J. Young, Y. Wang and A. S. Weiss, *Acta Biomater.*, 2012, **8**, 3714–3722.

151 B. S. Lalia, E. Guillen, H. A. Arafat and R. Hashaikeh, *Desalination*, 2014, **332**, 134–141.

152 J. O. Zoppe, M. S. Peresin, Y. Habibi, R. A. Venditti and O. J. Rojas, *ACS Appl. Mater. Interfaces*, 2009, **1**, 1996–2004.

153 K. Paulett, W. A. Brayer, K. Hatch, T. Kalous, J. Sewell, T. Liavitskaya, S. Vyazovkin, F. Liu, D. Lukáš and A. Stanishevsky, *J. Appl. Polym. Sci.*, 2018, **135**, 45772.

154 S. Pirani, H. M. N. Abushammala and R. Hashaikeh, *J. Appl. Polym. Sci.*, 2013, **130**, 3345–3354.

155 G. Piccirillo, M. V. Ditaranto, N. F. S. Feuerer, D. A. Carvajal Berrio, E. M. Brauchle, A. Pepe, B. Bochicchio, K. Schenke-Layland and S. Hinderer, *J. Mater. Chem. B*, 2018, **6**, 6399–6412.

156 I. Colomer, A. Chamberlain, M. Haughey and T. Donohoe, *Nat. Rev. Chem.*, 2017, **1**, 0088.

157 L. Eberson, M. P. Hartshorn, O. Persson and F. Radner, *Chem. Commu.*, 1996, **18**, 2105–2112.

158 W. Song, D. D. Veiga, C. A. Custódio and J. F. Mano, *Adv. Mater.*, 2009, **21**, 1830–1834.

159 S. Wang, K. Liu, X. Yao, L. Jiang**,** *Chem. Rev.* 2015, **115**, 8230–8293.

160 L. P. Novo, J. Bras, A. García, N. Belgacem and A. A. S. Curvelo, *ACS Sustainable Chem. Eng.* 2015, **3**, 2839–2846.

161 K. Sisson, C. Zhang, M. C. Farach-Carson, D. B. Chase and J. F. Rabolt, *Biomacromolecules* 2009, **10**, 1675–1680.

162 R. Auras, B. Harte and S. Selke, *Macromol. Biosci.* 2004, **4**, 835–864.

163 A. L. Daniel-da-Silva, A. M. Salgueiro and T. Trindade, *Gold Bull.* 2013, **46**, 25–33.

164 A. Barth, *Prog. Biophys. Mol. Biol.*, 2000, **74**, 141–173.

165 H.-W. Kim, H.-S. Yu and H.-H. Lee, *J. Biomed. Mater. Res. A*, 2008, **87**, 25–32.

166 C. R. Cammarata, M. E. Hughes and C. M. Ofner, *Gelatin. Mol. Pharm.*, 2015, **12**, 783–793.

167 L. Mengyan, M. J. Mondrinos, C. Xuesi and P. I. Lelkes, *200IEEE Engineering in Medicine and Biology 27th Annual Conference,* Shanghai, China, September, 2005.

168 J. Lee, G. Tae, Y. H. Kim, I. S. Park, S.-H. Kim and S. H. Kim, *Biomaterials* 2008, **29**, 1872–1879.

169 B. Han, J. Jaurequi, B. W. Tang and M. E. Nimni, *J. Biomed. Mater. Res. A*, 2003, **65**, 118–124.

170 B. Jia, Y. Li, B. Yang, D. Xiao, S. Zhang, A. V. Rajulu, T. Kondo, L. Zhang and J. Zhou, *Cellulose*, 2013, **20**, 1911–1923.

171 J. Han, P. Lazarovici, C. Pomerantz, X. Chen, Y. Wei and P. I. Lelkes, *Biomacromolecules*, 2011, **12**, 399–408.

172 S. B. M. Heydarkhan-Hagvall, K. Schenke-Layland, A. P. Dhanasopon, F. Rofail, H. Smith, Wu, R. Shemin, R. E. Beygui and W. R. MacLellan, *Biomaterials*, 2008, **29**, 2907–2914.

173 E. Mele, *J. Mat. Chem. B* 2016, **4**, 4801–4812.

174 S. Thenmozhi, N. Dharmaraj, K. Kadirvelu and H. Y. Kim, *Mater. Sci. Eng. B* 2017, **217**, 36–48.

175 Y. Mo, R. Guo, J. Liu, Y. Lan, Y. Zhang, W. Xue and Y.Zhang, *Colloids Surf. B*, 2015, **132**, 177–184.

176 S. Changsarn, J. D. Mendez, K. Shanmuganathan, E. J. Foster, C. Weder and P. Supaphol, *Macromol. Rapid Commun.*, 2011, **32**, 1367–1372.

177 C. Zhou, R. Chu, R. Wu and Q. Wu, *Biomacromolecules*, 2011, **12**, 2617–2625.

178 K. E. Swindle-Reilly, C. S. Paranjape and C. A. Miller, *Prog. Biomater.*, 2014, **3**, 20.

179 J. Rnjak-Kovacina and A. S. Weiss, *Tissue Eng. B*, 2011, **17**, 365–372.

180 J. M. Ameer, A. K. Pr and N. Kasoju, *J. Funct. Biomater.*, 2019, **10**, 30.

181 A. K. Jaiswal, S. S. Kadam, V. P. Soni and J. R. Bellare, *Appl. Surf. Sci.*, 2013, **268**, 477–488.

182 S. Boral, A. N. Gupta and H. B. Bohidar, *Int. J. Biol. Macromol.*, 2006, **39**, 240–249.

183 O. Elishav, V. Beilin, O. Rozent, G. E. Shter and G. S. Grader, *J. Polym. Sci. B: Polym. Phys.*, 2018, **56**, 248–254.

184 A. Saarai, V. Kasparkova, T. Sedlacek and P. Saha, *Biomedicine*, 2011, 384–389.

185 Q. Shi, C. Zhou, Y. Yue, W. Guo, Y. Wu and Q.Wu, *Carbohydr. Polym.*, 2012, **90**, 301–308.

186 C. Zhou, Q. Shi, W. Guo, L. Terrell, A. T. Qureshi, D. J. Hayes and Q. Wu, *ACS Appl. Mater. Interfaces*, 2013, **5**, 3847–3854.

187 D. Bagheriasl, P. J. Carreau, B. Riedl, C. Dubois and W. Hamad, *Cellulose*, 2016, **23**, 1885–1897.

188 G. Kim, S. Ahn, Y. Kim, Y. Cho and W. Chun, *J. Mater. Chem.*, 2011, **21**, 6165–6172.

189 C. Megret, A. Lamure, M. T. Pieraggi, C. Lacabanne, V. Guantieri and A. M. Tamburro, *Int. J. Biol. Macromol.*, 1993, **15**, 305–312.

190 H. Lim and S. W. Hoag, *AAPS PharmSciTech*, 2013, **14**, 903–910.

191 M. A. Hubble, A. Ferrer, P. Tyagi, Y. Yin, C. Salas, L. Pal and O. J. Rojas, *Bioresources* 2017, **12**, 2143–2233.

192 J. F. Mano, R. A. Sousa, L. F. Boesel, N. M. Neves and R. L. Reis, *Compos. Sci. Technol.*, 2004, **64**, 789–817.

193 P. J. Kluger, R. Wyrwa, J. Weisser, J. Maierle, M. Votteler, C. Rode, M. Schnabelrauch, H. Walles and K. Schenke-Layland, *J. Mater. Sci.: Mater. Med.*, 2010, **21**, 2665–2671.

194 Y. Mo, R. Guo, J. Liu, Y. Lan, Y. Zhang, W. Xue and Y. Zhang, *Colloids Surf. B*, 2015, **132**, 177–184.

195 T. Abudula, U. Saeed, A. Memic, K. Gauthaman, M. A. Hussain and H. Al-Turaif, *J. Polym. Res.*, 2019, **26**, 110.

196 M. Rahmat, M. Karrabi, I. Ghasemi, M. Zandi and H. Azizi, *Mater. Sci. Eng. C*, 2016, **68**, 397–405.

197 K. M. Z. Hossain, M. S. Hasan, D. Boyd, C. D. Rudd, I. Ahmed and W. Thielemans, *Biomacromolecules*, 2014, **15**, 1498–1506.

198 M. M. Pereira, N. R. B. Raposo, R. Brayner, E. M. Teixeira, V. Oliveira, C. C. R. Quintão, L. S. A. Camargo, L. H. C. Mattoso and H. M. Brandão, *Nanotechnology*, 2013, **24**, 075103.

199 R. Machado, A. Da Costa, V. Sencadas, C. Garcia-Arévalo, C. M. Costa, J. Padrão, A. Gomes, S. Lanceros-Méndez, J. C. Rodríguez-Cabello and M. Casal, *Biomed. Mater.*, 2013, **8**, 065009.

200 N. Hong, Z. Siquan, W. Jing, C. Xiangrong, L. Tao, W. Weiyang, Z. Weijuan and C. Yun, *Biomed. Mater. Eng.*, 2012, **22**, 121–127.

201 P. Koegler, P. Pasic, J. Gardiner, V. Glattauer, P. Kingshott and H. Thissen, *Biomacromolecules*, 2014, **15**, 2265–2273.

202 T. Niamsap, N. T. Lam and P. Sukyai, *Carbohydr. Polym.*, 2019, **205**, 159–166.

203 F. A. Bastos and M. Tubino, *J. Braz. Chem. Soc.*, 2016, **00**, (00), 1-9.

204 *Dynamic Mechanical Analysis (DMA), a Beginner's Guide*, PerkinElmer, 2013, Waltham, Massachusetts, USA.

205 K. P. Menard and N. R. Menard, *Dynamic Mechanical Analysis in the analysis of polymers and rubbers*, in Encyclopedia of Polymer Science and Technology, 2015, John Wiley & Sons, Hoboken, New Jersey, USA.

206 D. M. Correia, J. Padrão, L. R. Rodrigues, F. Dourado, S. Lanceroz-Méndez and V. Sencadas, *Polym. Test.*, 2013, **32**, 995–1000.

207 A. Hivechi, S. H. Bahrami and R. A. Siegel, *Int. J. Biol. Macromol.*, 2019, **124**, 411–417.

208 R. Liepins and E. M.Pearce, *Environ. Health Perspect.*, 1976, **17**, 55–63.

209 A. Lonjon, S. Barrau, E. Dantras, P. Demont and C. Lacabanne, *Eur. J. Electr. Eng.*, 2009, **12**, 423–431.

210 I. Mukherjee and M. Rosolen, *J. Thermal Anal. Calorim.*, 2013, **114**, 1161-1166.

211 A. Muijca-Garcia, Hooshmand, M. Skrifvars. J. M. Kenny, K. Oksman and L. Peponi, *RSC Adv.*, 2016, **6**, 9221–9231.

212 D. Carponcin, E. Dantras, J. Dadurand, G. Aridon, F. Levallois, L. Cadiergues and C. Lacabanne, *J. Non-Cryst. Solids*, 2014, **19 – 25**, 392-393.

213 N. Cai, Q. Dai, Z. E. Wang, X. Luo, Y. Xue and F. Yu, *Fiber Polym.*, 2014, **15**, 2544–2552.

214 S. Baiguera, C. Del Gaudio, E. Lucatelli, E. Kuevda, M. Boieri, B. Mazzanti, A. Bianco and P. Macchiarini, *Biomaterials*, 2014, **35**, 1205–1214.

215 M. Rahmat, M. Karrabi, I. Ghasemi, M. Zandi and H. Azizi, *Mater Sci. Eng. C*, 2016, **68**, 397–405.

216 E. W. Fisher, H. J. Sterzel and G. Wegner, *Kolloid- Z. Z.Polym.*, 1973, **251**, 980–990.

217 H. Simmons, P. Tiwary, J. E. Colwell and M. Kontopoulou, *Polym. Degrad. Stab.*, 2019, **166**, 248–257.

218 A. P. Kumar, D. Depan, N. S. Tomer and R. P. Singh, *Prog. Polym. Sci.*, 2009, **34**, 479–515.

219 W. Li, C. T. Laurencin, E. J. Caterson, R. S. Tuan and F. K. Ko, *J. Biomed. Mater. Res.*, 2002, **60**, 613-621.

220 https://www.caseyprinting.com/blog/how-is-paper-made.

221 https://www.edana.org/nw-related-industry/how-are-nonwovens-made.

222 https://www.lucartgroup.com/gruppo/la-nostra-storia/.

223   https://ipstesting.com/find-a-test/nwsp-test-methods/wsp-110-4-tensile-strip-method/.

224   https://www.brookfieldengineering.com/learning-center/learn-about-viscosity/what-is-viscosity.

225 H. - W. Cui, Q. Fang and G. – B. Du, *Wood. Sci. Technol.*, 2014, **48**, 1123–1137.

226 B. Bochicchio, G. C. Yeo, P. Lee, D. Emul, A. Pepe, A. Laezza, N. Ciarfaglia, D. Quaglino and A. S. Weiss, https://doi.org/10.1111/febs.15702, 2021.

227 N. Ciarfaglia, A. Pepe, G. Piccirillo, A. Laezza, R. Daum, K. Schenke-Layland, and B. Bochicchio, *ACS Appl. Polym. Mater.*, 2020, **2**, 4836–4847.